Technical Report

TR-09-14

Modelling of temperature in deep boreholes and evaluation of geothermal heat flow at Forsmark and Laxemar

Jan Sundberg, Pär-Erik Back, Märta Ländell, Anders Sundberg
GEO INNOVA AB

May 2009

Svensk Kärnbränslehantering AB
Swedish Nuclear Fuel
and Waste Management Co

Box 250, SE-101 24 Stockholm
Phone +46 8 459 84 00

SKB

Modelling of temperature in deep boreholes and evaluation of geothermal heat flow at Forsmark and Laxemar

Jan Sundberg, Pär-Erik Back, Märta Ländell, Anders Sundberg
GEO INNOVA AB

May 2009

Preface

This document contains information on bedrock temperature and geothermal heat flow in Forsmark and Laxemar, to be used in the safety assessment SR-Site. The information will be used in e.g. the report “Climate and climate-related issues for the safety assessment SR-Site”.

Stockholm, May 2009

Jens-Ove Näslund

Person in charge of the SKB climate programme

Summary

This report presents modelling of temperature and temperature gradients in boreholes in Laxemar and Forsmark and fitting to measured temperature data. The modelling is performed with an analytical expression including thermal conductivity, thermal diffusivity, heat flow, internal heat generation and climate events in the past. As a result of the fitting procedure it is also possible to evaluate local heat flow values for the two sites. However, since there is no independent evaluation of the heat flow, uncertainties in for example thermal conductivity, diffusivity and the palaeoclimate temperature curve are transferred into uncertainties in the heat flow.

Both for Forsmark and Laxemar, reasonably good fits were achieved between models and data on borehole temperatures. However, none of the general models achieved a fit within the 95% confidence intervals of the measurements. This was achieved in some cases for the additional optimised models.

Several of the model parameters are uncertain. A good model fit does not automatically imply that "correct" values have been used for these parameters. Similar model fits can be expected with different sets of parameter values.

The palaeoclimatically corrected surface mean heat flow at Forsmark and Laxemar is suggested to be 61 and 56 mW/m^2 respectively. If all uncertainties are combined, including data uncertainties, the total uncertainty in the heat flow determination is judged to be within +12% to –14% for both sites. The corrections for palaeoclimate are quite large and verify the need of site-specific climate descriptions.

Estimations of the current ground surface temperature have been made by extrapolations from measured temperature logging. The mean extrapolated ground surface temperature in Forsmark and Laxemar is estimated to 6.5° and 7.3°C respectively. This is approximately 1.7°C higher for Forsmark, and 1.6°C higher for Laxemar compared to data in /SKB 2006/. Comparison with air temperature measurements shows that the extrapolated ground temperature is also higher, 1–1.5°C for Forsmark, and 0.9°C for Laxemar. The difference between the air temperature and the extrapolated values is probably due to factors such as local climate conditions, heat contact resistance, and freezing processes near the ground surface. The results differ slightly from calculations made in /SKB 2006/.

The parameters that seem to have the greatest impact on the calculated temperature gradient and temperature profiles are heat flow, thermal conductivity and current ground surface temperature. The calculated temperature gradient and temperature profiles are also very sensitive to the modelling of the climate (surface ground temperature) during the last 10 kyrs. Another conclusion is that the calculated temperature gradient profile is affected by palaeoclimate temperatures more than 240 kyrs back in time, even though the influence from the early part of this period is quite small.

Contents

1 Introduction 7
1.1 Background 7
1.2 Scope and objectives 7
1.3 Method 7

2 Theory 9
2.1 Heat flow, geothermal gradient and thermal conductivity 9
2.2 Influences and disturbances 10
2.2.1 Pressure influence on thermal conductivity 10
2.2.2 Temperature influence on thermal conductivity and heat capacity 10
2.2.3 Surface temperature variations 10
2.2.4 Ground water movement 11
2.2.5 Drilling 11
2.3 Influence on geothermal temperature and gradient 12

3 Data overview 15
3.1 Geothermal heat flow 15
3.2 Radiogenic heat production 15
3.3 Thermal conductivity and thermal diffusivity 15
3.4 Temperature and geothermal gradient data 15
3.5 Palaeoclimate data 15
3.6 Data availability 15

4 General sensitivity analysis 17
4.1 Introduction 17
4.2 Influence of heat flow, thermal conductivity and internal heat production 17
4.2.1 Sensitivity to heat flow 17
4.2.2 Sensitivity to thermal conductivity 17
4.2.3 Sensitivity to internal heat generation 17
4.2.4 Sensitivity for thermal conductivity in superficial rock 17
4.3 Influence of climate changes and thermal diffusivity 20
4.3.1 Sensitivity to length of modelled climate period 20
4.3.2 Sensitivity to thermal diffusivity 20
4.3.3 Sensitivity to a step change in temperature 20
4.3.4 Sensitivity to ground surface temperature in climate data 23
4.4 Sensitivity analysis conclusions 23

5 Climate models 25
5.1 Climate models in SR-Can 25
5.2 Modified climate models in present study 26

6 Geothermal calculations – Forsmark 29
6.1 Thermal data 29
6.1.1 Geothermal gradient and temperature 29
6.1.2 Ground surface temperature 31
6.1.3 Thermal conductivity, diffusivity and internal heat generation 32
6.2 Model calculations 34
6.2.1 Introduction 34
6.2.2 General models 35
6.2.3 Additional models 41

7 Geothermal calculations – Laxemar 43
7.1 Thermal data 43
7.1.1 Geothermal gradient and temperature 43
7.1.2 Current surface temperature 46
7.1.3 Thermal conductivity, diffusivity and internal heat generation 46

7.2 Model calculations 47
7.2.1 Introduction 47
7.2.2 General models 48
7.2.3 Additional models 54

8 Discussion 57
8.1 Discussion from a heat flow perspective 57
8.2 Surface temperature and heat generation 59

9 Conclusions 61
9.1 Overall conclusions 61
9.2 Specific model conclusions for Forsmark 62
9.3 Specific model conclusions for Laxemar 62
9.4 Conclusions for KLX02 in Laxemar 63

Acknowledgements 65

References 67

Appendix 1 Calculation model 69

Appendix 2 Extended depth graphs – Forsmark 71

Appendix 3 Extended depth graphs – Laxemar 77

Appendix 4 Location of boreholes 83

Appendix 5 Reconstruction of the Eemian period of the palaeotemperature record 85

Appendix 6 Modelling of KLX02 87

1 Introduction

1.1 Background

SKB (Svensk Kärnbränslehantering AB) is responsible for the management of spent nuclear fuel and radioactive waste generated within Sweden. Site investigations for a deep geological repository for spent nuclear fuel have been performed in two municipalities located along the Baltic Sea coast in eastern Sweden. Within a few years, SKB will submit an application to build a deep geological repository at one of these sites. An important document in the application is an assessment of long-term repository safety. In this assessment, a range of climate evolutions form the basis for a number of safety assessment scenarios. Large site investigation programmes have been performed at the Forsmark and Laxemar sites, located along the Swedish Baltic coast.

In the site investigations at Forsmark and Laxemar, the usage of temperature data from deep boreholes has been limited to determining the temperature at repository depth and to verifying water flow from hydraulic tests /SKB 2008, 2009/. However, the temperature development towards depth contains a lot more information that can be used to investigate:

1. spatial variability of the thermal conductivity at a larger scale (approx. proportional to the temperature gradient),
2. assessment of historical changes in climate (these influence the temperature data),
3. assessment of the magnitude of the geothermal heat flow.

In this report, borehole temperature measurements are used to evaluate the latter two of the above-mentioned issues.

1.2 Scope and objectives

The main objective of this report is to evaluate how the temperature and temperature gradient is influenced by different parameters, such as historical surface temperature data, heat production in the rock mass, heat flow and thermal conductivity. Special emphasis is put on comparison between measured temperature and gradient profiles in the Forsmark and Laxemar areas with calculated temperature and gradient profiles, and how potential differences may be explained. A secondary objective is to evaluate the heat flow at the two investigations sites, Forsmark and Laxemar.

1.3 Method

Temperature loggings in boreholes are used to produce temperature profiles and temperature gradient profiles that are compared to calculated model profiles. The model profiles are based on an analytical expression including thermal parameters such as conductivity, diffusivity, heat flow and radiogenic heat production. They are also dependent on the palaeoclimate temperature. A sensitivity analysis can be made concerning variations of these different parameters. When a reasonable fit between the model and the measured data is achieved, the input parameters can be compared to the original parameters, and a reliability assessment can be performed. This is the approach applied in the current report.

2 Theory

2.1 Heat flow, geothermal gradient and thermal conductivity

The relation between heat flow, temperature gradient and thermal conductivity is as follows (the heat flow in Equation 2-1 is uncorrected for the influence of historical climate changes; see Section 2.2.3):

$$Q_0 = \frac{\delta T}{\delta z} \cdot \lambda \qquad \text{Equation 2-1}$$

where

Q_0 vertical surface heat flow (W/m^2)

$\frac{\delta T}{\delta z}$ geothermal gradient (K/m)

λ thermal conductivity (W/(m·K))

z vertical depth (m)

However, the vertical heat flow involves two components, the heat flow from large depth and heat generation within the rock due to radiogenic decay of mainly uranium, thorium and potassium. In Equation 2-2 these parameters have been included.

$$Q_d = \left(Q_0 - \int_0^d A(z)dz \right) = \left[\frac{\delta T}{\delta z} \right]_d \cdot \lambda_d \qquad \text{Equation 2-2}$$

where

Q_0 surface heat flow (W/m^2)

Q_d heat flow at depth d (W/m^2)

$\int_0^d A(z)dz$ integral of volumetric heat generation (A) from surface to depth d (W/m^3)

$\left[\frac{\delta T}{\delta z} \right]_d$ geothermal gradient at depth d (K/m)

λ_d thermal conductivity at depth d (W/(m·K))

z vertical depth (m)

Thermal gradient is normally calculated from temperature determined by fluid temperature loggings, according to Equation 2-3:

$$\frac{\delta T}{\delta z} = \frac{(n\Sigma z_L T - \Sigma z_L \Sigma T)}{\left(n\Sigma {z_L}^2 - (\Sigma z_L)^2 \right) \cdot \sin\varphi} \qquad \text{Equation 2-3}$$

where

z_L borehole length

T measured temperature (K)

φ angle between the borehole and a horizontal plane (°)

n number of temperature measurements used for each calculation of gradient

However, the gradient is also influenced by historical climate changes; see Section 2.2.3.

Heat flow is contributed by the primordial heat from the forming of the Earth and by radiogenic sources in the mantle and crust. The heat flow originates mainly from the mantle and the crust.

Heat generation in the outer crust originates mainly from decay of radioactive isotopes, but also from friction of intraplate strain and plate motions, and heat from exothermic metamorphic and diagenetic processes /Beardsmore and Cull 2001/. These heat sources are of different importance in different areas. For example, the radioactive elements are more common in younger granites and such areas have often an anomalous geothermal gradient.

The radioactive decay is not the only heat source transporting heat to the rock at the investigated sites, but it is the dominating one. Decay of thorium, uranium and potassium is the source of about 98% of the heat generated by decay of unstable isotopes. Because of this, only these three are used in the calculation. This can be seen in Equation 2-4 /Beardsmore and Cull 2001, Balling et al. 1981/:

$$A = \rho \times \left(96.7\times10^{-6}\cdot c_U + 26.3\times10^{-6}\cdot c_{Th} + 3.5\times10^{-9}\cdot c_K\right) \qquad \text{Equation 2-4}$$

where

A radiogenic heat production (W/m^3)
ρ rock density (kg/m^3)
c_U concentration of uranium, ^{238}U (ppm)
c_{Th} concentration of thorium, ^{232}Th (ppm)
c_K concentration of potassium, ^{40}K (%)

2.2 Influences and disturbances

2.2.1 Pressure influence on thermal conductivity

The effect of pressure on thermal conductivity is small in water saturated crystalline rock /Walsh and Decker 1966/. Therefore pressure can usually be ignored, and is not further discussed here.

2.2.2 Temperature influence on thermal conductivity and heat capacity

Temperature has a significant effect on thermal conductivity and heat capacity. Studies of the temperature dependence of thermal conductivity of common rocks presented in the literature have shown a decrease in thermal conductivity with increasing temperature. The decrease may be in the order of 5–15% per 100°C /Sibbit et al. 1979/. In Laxemar there is no pronounced temperature effect on thermal conductivity in the dominating rock types /Sundberg et al. 2008b/. In Forsmark, the temperature effect on thermal conductivity is about 10% decrease in per 100°C for the main rock type and somewhat smaller for secondary rock type /Sundberg et al. 2008a/.

An increase of the heat capacity with increasing temperature has been reported in the literature /Sibbit et al. 1979/. Data from the site investigations indicates an increase in heat capacity in the order of 25% per 100°C for the two sites Forsmark and Laxemar /Sundberg et al. 2008ab/.

2.2.3 Surface temperature variations

Variations in air temperature affect the temperature in the rock. The temperature fluctuations propagate into the crust and decays exponentially with depth. Cyclic variations in air temperature, such as diurnal variations, only affect the ground temperature to one or a few m depth. In crystalline rock, the wavelength of the annual wave might be up to 30–50 m. Climate changes, including the formation and decay of ice sheets, periods of submerged conditions, the land elevation above sea level, affect the temperature and the thermal gradient to a deeper level. The depth depends on the magnitude of the temperature change, the length of the temperature change, time since the change, and the thermal diffusivity of the rock (thermal conductivity divided by volumetric heat capacity). The change in thermal gradient at a specified depth can be calculated by approximation of the Earth as a half space, according to Equation 2-5 /Jaeger 1965, Balling et al. 1981/:

$$\Delta\frac{\delta T}{\delta z}(z,t) = -\Delta T\cdot(\pi\kappa t)^{-1/2}\cdot e^{-z^2/4\kappa t} \qquad \text{Equation 2-5}$$

where

$\Delta\frac{\delta T}{\delta z}(z,T)$	change in temperature gradient (K/m)
ΔT	step change in ground surface temperature (K)
κ	thermal diffusivity (m^2/s) ($\kappa=\lambda/C$, where C=heat capacity ($J/m^3 \cdot K$))
t	time since the step change (s)

It is possible to superimpose the effect of different step changes of the ground surface temperature and use Equation 2-5 to simulate long term effects in the bedrock. A number of factors cause the ground temperature to deviate from the air temperature. The local topography of the surface, radiation, thermal contact resistance between ground and air, presence of vegetation and snow cover, as well as the degree of saturation and processes in soils such as freezing and thawing have an impact on the ground surface temperature and the geothermal gradient. These factors are however only indirectly considered in this report. It is possible to estimate the current ground surface temperature by calculations /SKB 2006/ and from extrapolation of borehole temperature loggings.

2.2.4 Ground water movement

In crystalline rocks, groundwater migrates in fractures and fracture zones. The fractures make it possible for the groundwater to enter the borehole at one level and leave the borehole at a different level, thereby affecting the borehole temperature by advection of heat. Some pathways to and from the boreholes are natural and some were opened during the drilling of the borehole. Large ground water flow in permeable features in the rock may also effect changes in the gradient. The effect of ground water perturbations has been discussed in for example /Drury and Jessop 1982, Kukkonen 1988, Sundberg 1993/.

2.2.5 Drilling

The drilling of a borehole is also affecting the temperature in the borehole and the surroundings. There are two reasons for this: (1) heat is generated during the drilling, and (2) the media used for flushing (water or air) can be either cooling or heating. The time for the borehole to regain pre-drilling conditions can be rather long, and depends mainly on the drilling time, the temperature of the water or air used for flushing and on the thermal properties of the rock. This can be calculated according to Equation 2-6:

$$T = q/(4\pi\lambda)\cdot(E_1(r^2/(4\kappa t)) - E_2(r^2/4\kappa(t-t_0))) \qquad \text{Equation 2-6}$$

where

T	temperature (°C)
q	heat generation in borehole due to drilling (W/m)
r	radius of borehole (m)
t	time from start of drilling (s)
t_0	time when drilling is completed (s)
E_1, E_2	exponential integrals

However, the equation can only be used to give an idea of the magnitude and time for the disturbance since the heat (source or sink) generated, and the time of drilling, is not constant along the borehole.

The time needed for the temperature to stabilise after drilling is exemplified in Table 2-1. In the calculations, different drilling times and different degrees of recovery in terms of dimensionless temperature have been used. The stabilising times in Table 2-1 give only of an estimation of the real conditions. In reality the disturbance is not the same in the whole borehole or in different boreholes. However, the times in the table give an indication of the long stabilising times needed for deep boreholes in order to obtain high quality temperature measurements. This has been used in the approving procedure for temperature logging results in both Forsmark and Laxemar /Sundberg et al. 2008ab/ and is not further discussed in this report.

Table 2-1. Time needed for the temperature to stabilize after drilling. Recovery status expressed as dimensionless temperature. T_{max} – temperature at completed drilling.

Drilling time	$1-T/T_{max}$		
t_0	0.9	0.99	0.999
24 h	1.3 days	18 days	6 months
1 week	6 days	13 weeks	3 years
1 month	21 days	11 months	9.4 years
6 months	96 days	4.5 years	47 years

2.3 Influence on geothermal temperature and gradient

Equation 2-2 and Equation 2-5 are combined in Equation 2-7:

$$\left[\frac{\delta T}{\delta z}\right]_d = \frac{\left(Q_0 - \int_0^d A(z)dz\right)}{\lambda} - \Delta T \times (\pi\kappa t)^{-1/2} \cdot e^{-z^2/4\kappa t} \qquad \text{Equation 2-7}$$

where

$\left[\frac{\delta T}{\delta z}\right]_d$ Calculated geothermal gradient at depth d

Q_0 Surface heat flow (W/m^2)

$\int_0^d A(z)dz$ Integral of heat generation A (W/m^3) from surface to depth d (m)

λ_d Rock thermal conductivity at depth z=d (W/(m·K))

ΔT Step change in surface temperature (K)

κ Rock thermal diffusivity (m^2/s)

t Time since the step change (s)

With Equation 2-7, it is possible to calculate the geothermal gradient and compare it with the measured gradient.

The above equation determines the temperature gradient profile vs. depth. With the current surface temperature and temperature gradient at different depths, the temperature at those depths can be calculated; see Equation 2-8:

$$Tx = T_0 + G_1 \cdot dz + G_2 \cdot dz + ...+ G_x \cdot dz \qquad \text{Equation 2-8}$$

Where

x Depth index (0 at ground surface)

T_x Temperature at depth index x (T_0 = temperature at ground surface)

G_x Gradient at depth index x

dz Length of depth index interval

Depth Calculated from dz·x

The presented Equation 2-7 has a number of limitations, the most important ones being:

- No spatial variability of thermal properties in the rock mass is considered, i.e. constant values are assumed for thermal conductivity and thermal diffusivity.
- No temperature influence on thermal conductivity and thermal diffusivity considered.
- The model is only capable of handling linear or step changes in surface temperature (only step change is described above).

The different influencing parameters discussed earlier are affecting each other, see Equation 2-7, and independent determinations of them are not always available. This means that there are uncertainties related to for example the determination of heat flow in Equation 2-7. Heat flow maps in the literature can be based on geothermal gradients but may have large uncertainties in thermal conductivity and the influence on the gradient from recent or historical climate variations. The effects of different influences on the temperature and temperature gradient are exemplified and analysed by sensitivity analysis in coming chapters.

3 Data overview

3.1 Geothermal heat flow

The distribution of heat flow data in Scandinavia has been investigated by e.g. /Balling 1995/, /Landström et al. 1979/ and /Näslund et al. 2005/. There are also several published heat flow atlases. The heat flow consists of two components, heat produced in the core and the mantle and heat produced in the lithosphere as radiogenic heat production. In this report, heat flow refers to surface heat flow. The site-specific heat flow is evaluated in Chapter 6 and 7 for Forsmark and Laxemar respectively, and discussed further in Chapter 8.

3.2 Radiogenic heat production

The heat production is calculated from Equation 2-4. Data on U, Th and K for different rock types is taken from the Sicada database at SKB, if available.

3.3 Thermal conductivity and thermal diffusivity

Site-specific data on thermal conductivity and thermal diffusivity at rock domain level is obtained from the site descriptive models for Forsmark and Laxemar respectively /Back et al. 2007, Sundberg et al. 2008ab/. The thermal diffusivity is calculated from the mean thermal conductivity and heat capacity for each domain.

3.4 Temperature and geothermal gradient data

Temperature and gradient data is derived from approved fluid temperature loggings in investigation boreholes /Sundberg et al. 2008ab/.

3.5 Palaeoclimate data

Site-specific estimates on ground surface temperature data were presented in /SKB 2006/ (Figure 3-50) for the past 120 kyrs (120,000 years). /SKB 2006/ compiled information on climate related issues relevant for the long-term safety of a repository and supported the safety assessment SR-Can. The extended climate models in the present study are presented in Chapter 5. The ground surface temperature data set for Forsmark has been used for sensitivity studies in Chapter 4. In the temperature modelling for Forsmark and Laxemar in Chapter 6 and 7 respectively, modified ground temperature models have been used.

3. 6 Data availability

Input and output data from the calculations are available in a database at SKB (Excel-files).

4 General sensitivity analysis

4.1 Introduction

Knowledge of how the different parameters of Equation 2-7 affect the temperature and temperature gradient is useful in the modelling described in Chapter 6 and 7. The following sensitivity analysis was made with settings valid for the situation at Forsmark; see Table 4-1. The parameters are set to be independent of depth, i.e. to a constant value. The geothermal gradient and temperature are modelled by Equation 2-7. Concerning Section 4.3, "Influence of climate changes and thermal diffusivity", the climate model in Figure 4-6 is used. The analysis should be regarded as general and therefore, applicable to the thermal parameters and climate for both the Forsmark and Laxemar sites.

4.2 Influence of heat flow, thermal conductivity and internal heat production

4.2.1 Sensitivity to heat flow

In Figure 4-1 the impact of the heat flow parameter is investigated. The internal heat generation is assumed to be zero. The influence on the gradient of changing the heat flow parameter is merely a parallel movement of a straight line (the second part of Equation 2-7 is set to zero). In the following figures, the models in black represent the reference values from /SKB 2006/, whereas the blue and red models represent the uncertainty in the reference value, usually based on max/min values if available.

4.2.2 Sensitivity to thermal conductivity

In Figure 4-2 it can be seen that the effects of variations in thermal conductivity on the geothermal gradient and temperature are similar to the influence from heat flow.

4.2.3 Sensitivity to internal heat generation

In Figure 4-3 the impact of internal heat production of radiogenic origin is analyzed. The influence of radiogenic heat production is small compared to the influence of heat flow and thermal conductivity. The impact of 1 $\mu W/m^3$ is a change of the surface heat flow by only 1 mW/m^2 for 1,000 m rock.

4.2.4 Sensitivity for thermal conductivity in superficial rock

In Figure 4-4 theoretical changes in the apparent thermal conductivity in the superficial rock (representing e.g. potential convective effects) is illustrated. The models represented by the black curves illustrate the case where the thermal conductivity is constant with depth. The red and blue models illustrate alternative cases where the apparent thermal conductivity increases linearly from depth 300 m up to the ground surface. The increase is 0.05 W/(m·K) per 100 m (red) and 0.1 W/(m·K) per 100 m (blue).

Table 4-1. Heat flow, heat production and thermal conductivity data used in the sensitive analysis based on Forsmark data /SKB 2006/.

Thermal property	Reference	Min	Max
Surface geothermal heat flow (mW/m^2)	59	48	65
Radiogenic heat production ($\mu W/m^3$)	2.5	1.0	3.0
Thermal conductivity (W/(m·K))	3.6	3.2	4.0
Thermal diffusivity (mm^2/s)	1.57	1.28	1.9

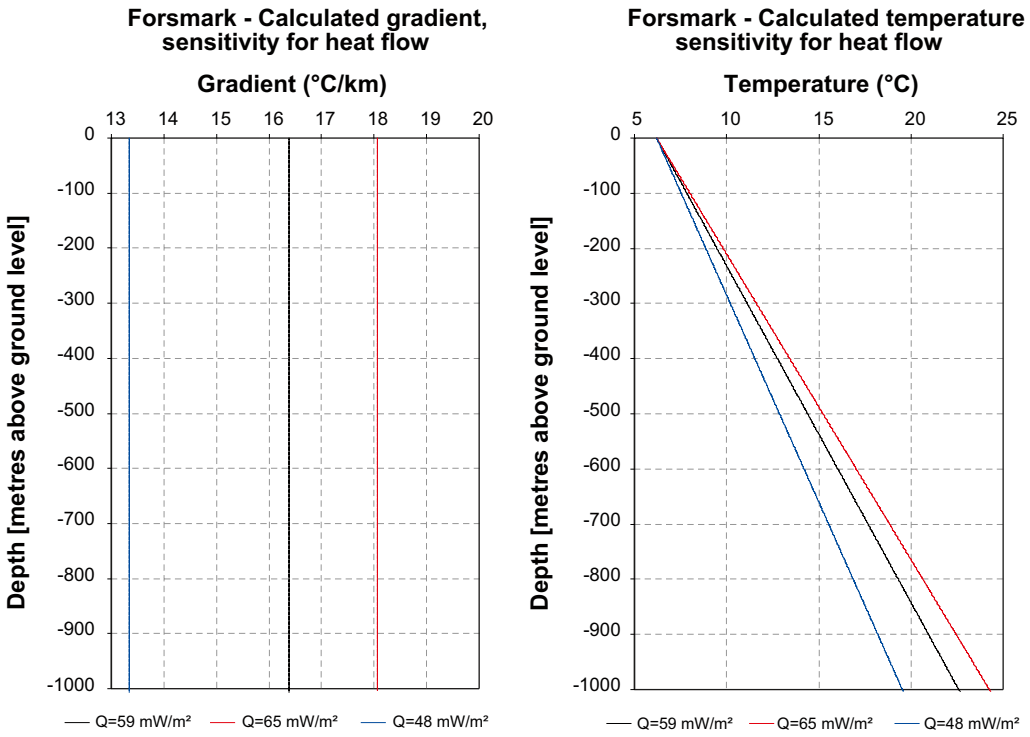

Figure 4-1. *Modelled temperature gradient (left) and temperature (right) at Forsmark, illustrating the sensitivity to heat flow (constant heat flow is used). The black models are based on the reference value in /SKB 2006/. The red and blue models illustrate the corresponding uncertainty interval.*

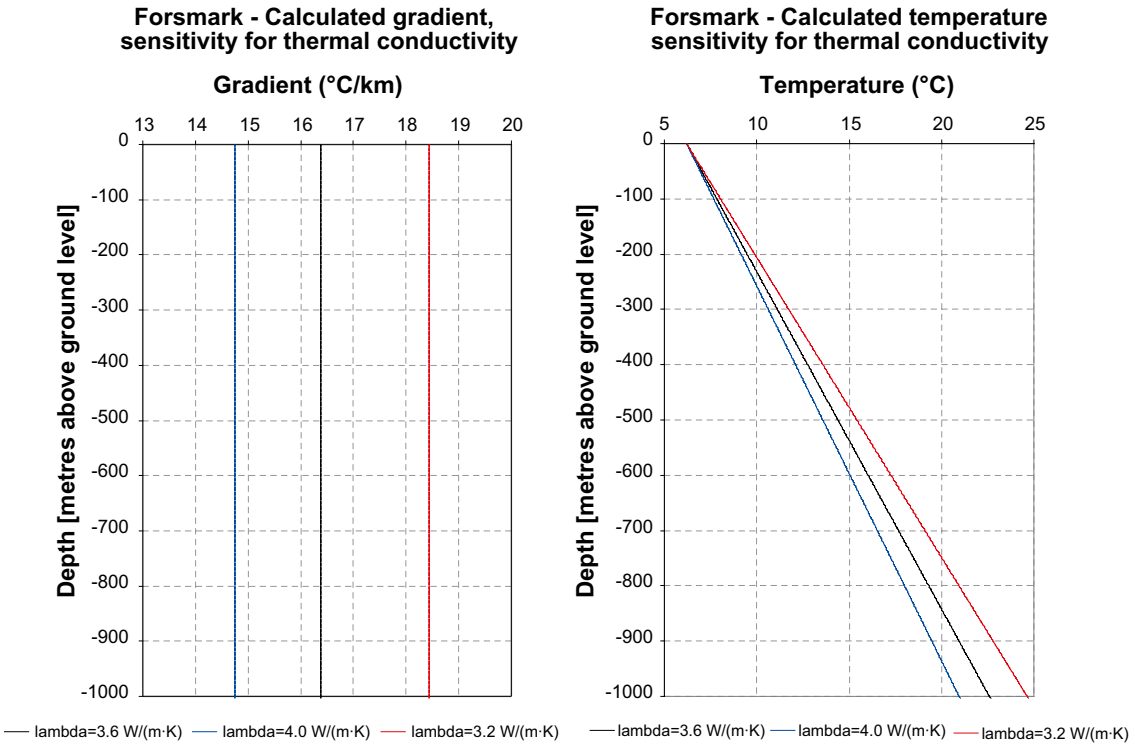

Figure 4-2. *Modelled temperature gradient (left) and temperature (right) at Forsmark, illustrating the sensitivity to thermal conductivity (constant thermal conductivity with depth is used).*

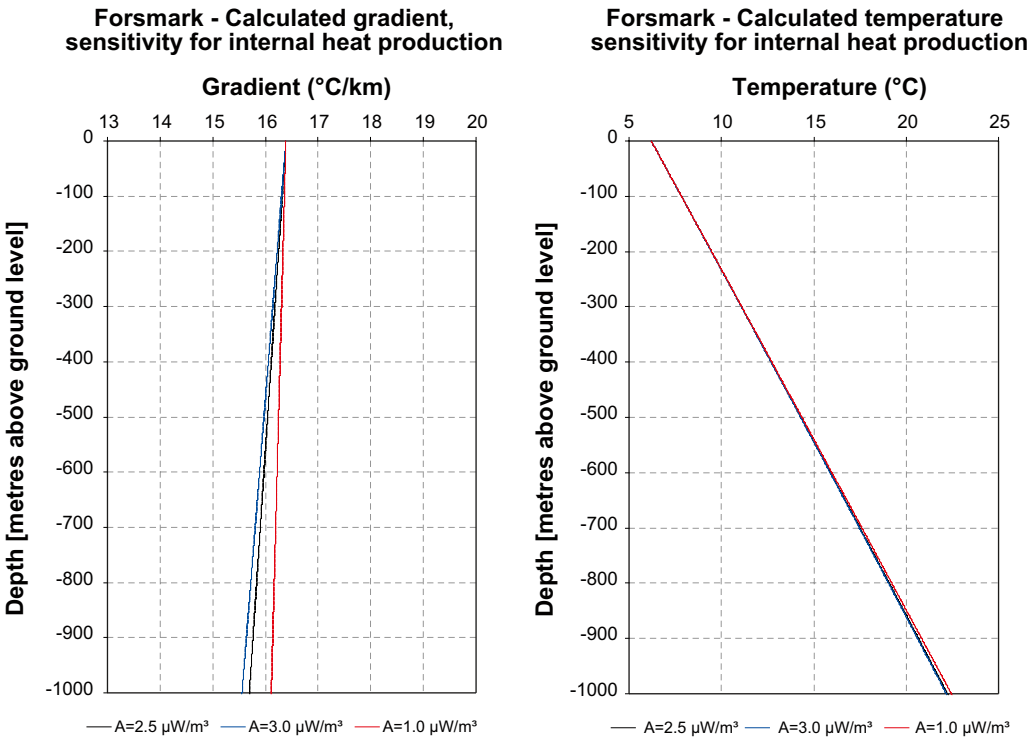

Figure 4-3. *Modelled temperature gradient (left) and temperature (right) at Forsmark, illustrating the sensitivity to internal heat production.*

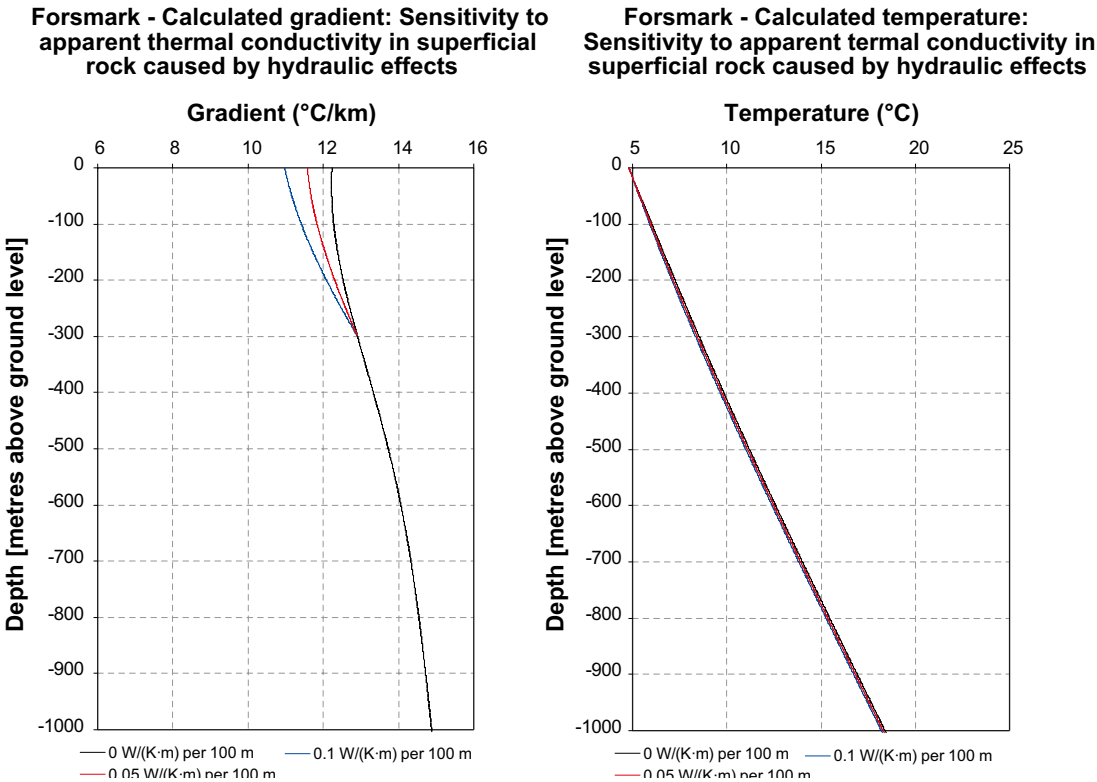

Figure 4-4. *Modelled temperature gradient (left) and temperature (right) at Forsmark, illustrating the sensitivity to higher apparent thermal conductivity in the upper part of the rock mass. The black models illustrate the scenario where the thermal conductivity is constant with depth. The red and blue models illustrate alternative scenarios where the apparent thermal conductivity increases linearly from depth 300 m up to the ground surface. The increase is 0.05 W/(m·K) per 100 m (red) and 0.1 W/(m·K) per 100 m (blue). The models consider both internal heat production and past climate variations. However, the diffusivity is held constant.*

4.3 Influence of climate changes and thermal diffusivity

4.3.1 Sensitivity to length of modelled climate period

It was investigated whether an increase in the length of the modelled climate period would affect the result; see Figure 4-5. A 120 k year climate model was thus compared with a 240 k and a 360 k year model. The 240 k and 360 k climate models consist of the 120 k year model (Figure 4-6) re-used subsequently, i.e. the climate for the period 240–120 kyrs ago is set to be identical to the climate for the period 120 k – 0 years ago, and the same is done for the 360 k year period. This is however a very crude model, and should not be seen as historically realistic.

This analysis shows that climate data older than 120 kyrs ago clearly affects the temperature gradient. The effect is relatively small but consistent. The difference in gradient effect between using a 120 kyrs and a 240 kyrs climate model is larger (approximately twice) than the difference in gradient effect between using a 240 kyrs and a 360 kyrs climate model.

4.3.2 Sensitivity to thermal diffusivity

In Figure 4-7, the impact of diffusivity is analyzed. The models in black represent the reference values from /SKB 2006/, whereas the blue and red models represent the uncertainty in the reference value, usually based on max/min values.

4.3.3 Sensitivity to a step change in temperature

It is interesting to analyse how deep different lengths of a step change in surface ground temperature penetrate the rock. In Figure 4-8 and Figure 4-9, a step change of 1 K has been applied at the ground surface. Recent 1 K step changes in climate (100 years ago) are visible down to about 300 m and episodes 1,000 years ago penetrate down to about 700 m. The thermal diffusivity is important for the penetration depth and is analysed below.

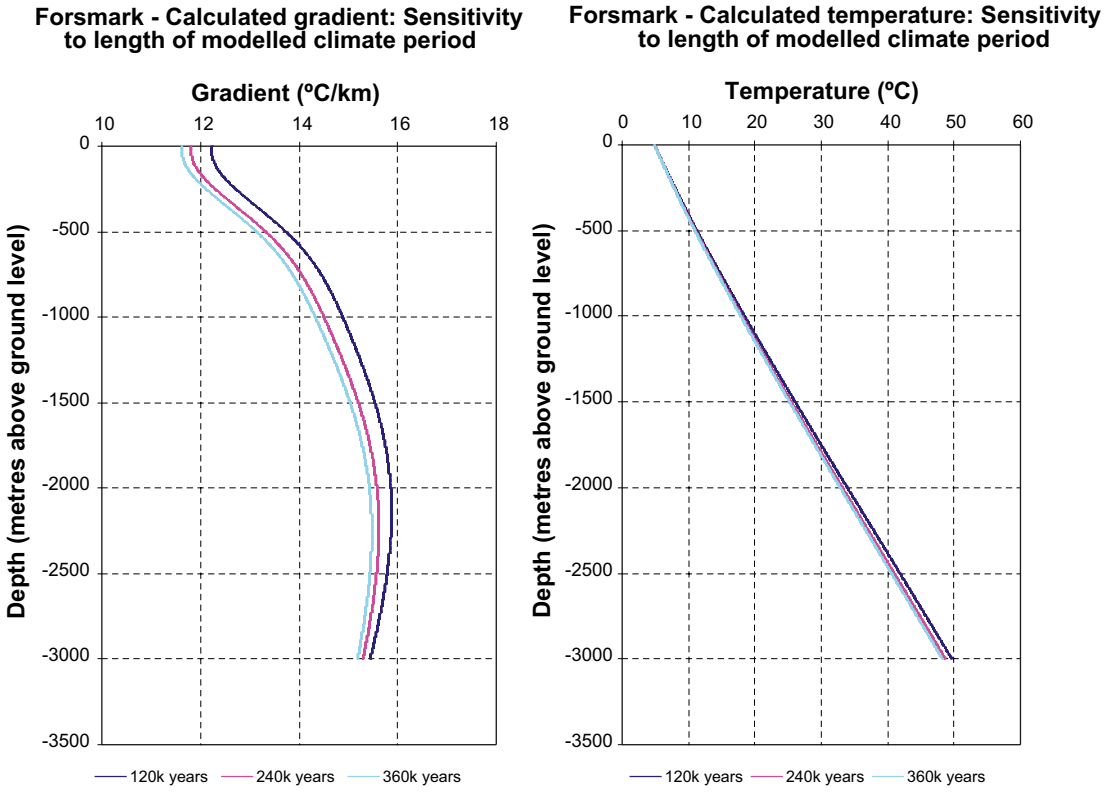

Figure 4-5. *The left graph shows how the change in modelled climate period length affects the temperature gradient, while the right graph shows how the temperature is affected.*

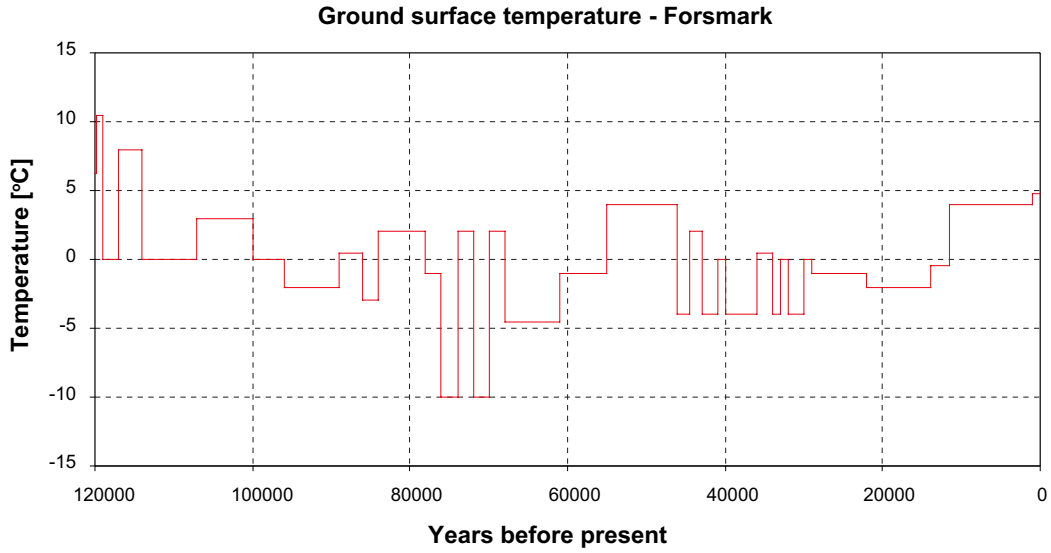

Figure 4-6. *Ground surface temperature model for Forsmark spanning 120 kyrs. The temperature model is a simplified version of the palaeotemperature model for the last glacial cycle used in SR-Can safety assessment /SKB 2006/.*

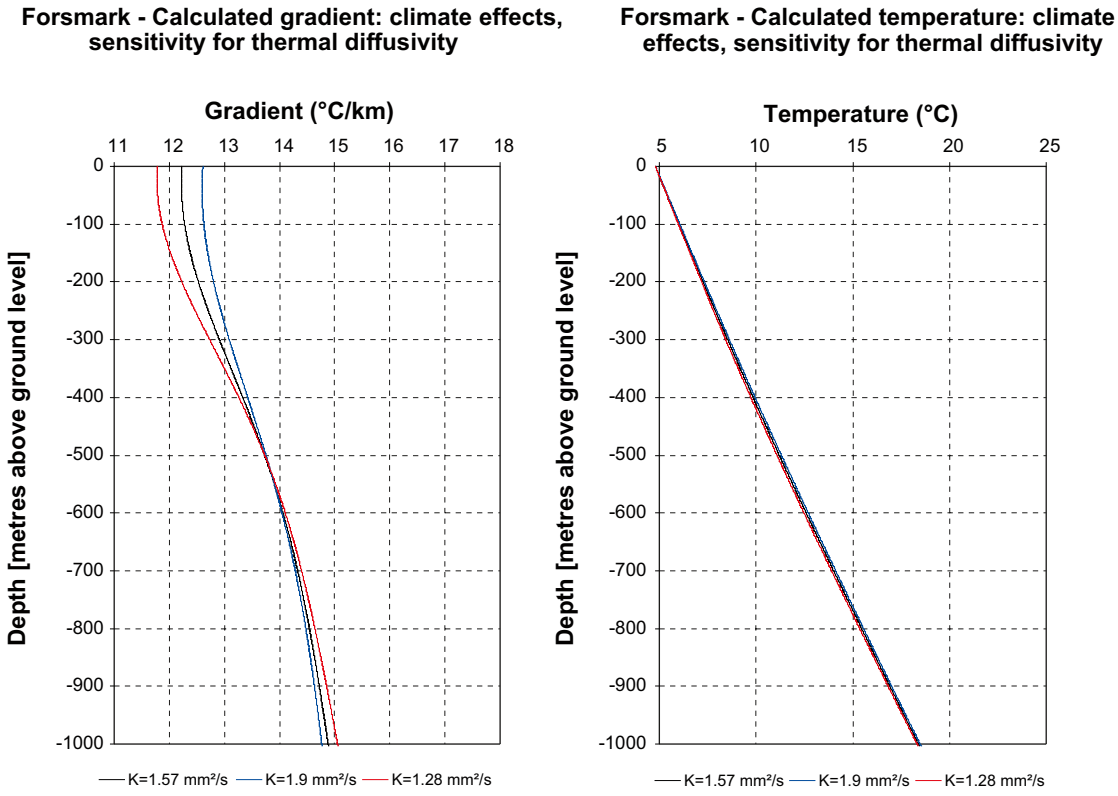

Figure 4-7. *Modelled temperature gradient (left) and temperature (right) at Forsmark, illustrating the sensitivity to thermal diffusivity (constant thermal diffusivity with depth is used). The black models are based on the reference value in /SKB 2006/. The red and blue models illustrate the corresponding uncertainty interval. The models consider both internal heat production and estimated past climate variations during the last glacial cycle.*

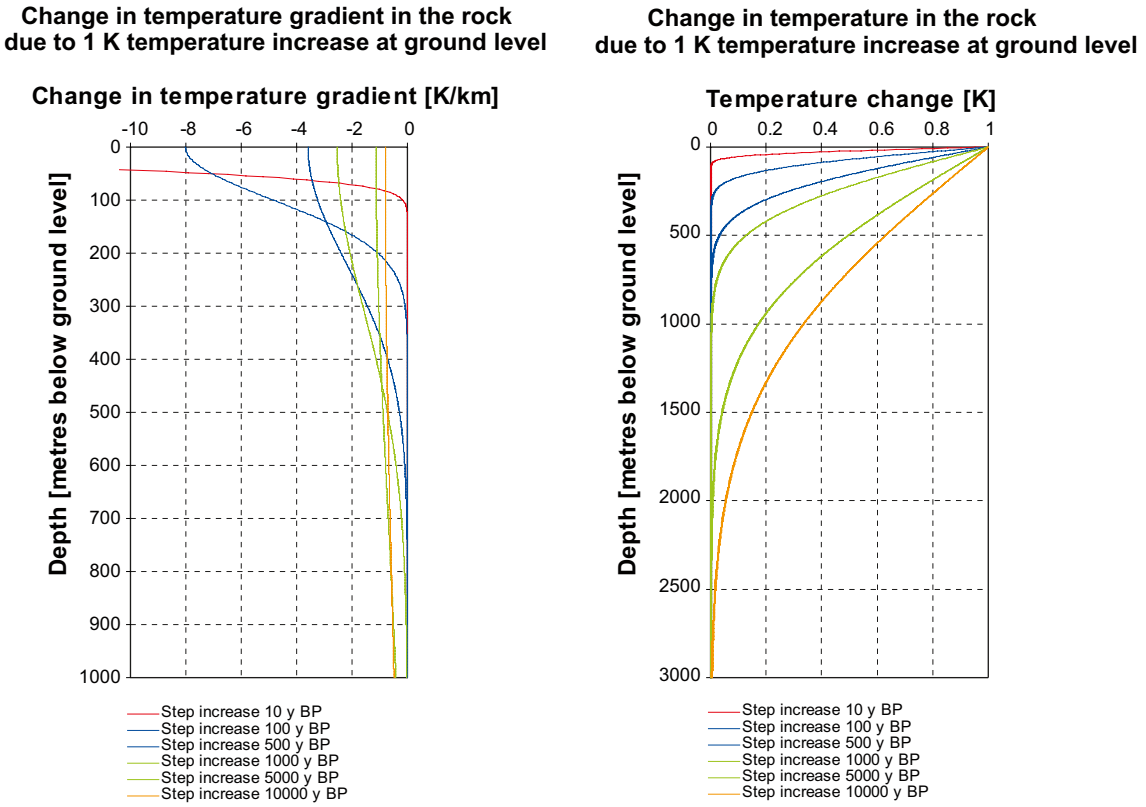

Figure 4-8. *The effect on temperature gradient (left) and temperature (right) in the rock when the ground surface temperature is increased by 1 K (step increase). Gradient in K/km. Thermal diffusivity=1.57·10⁻⁶ m²/s. Compare with Figure 4-9 where depth is increased and the times for step change of temperature are different.*

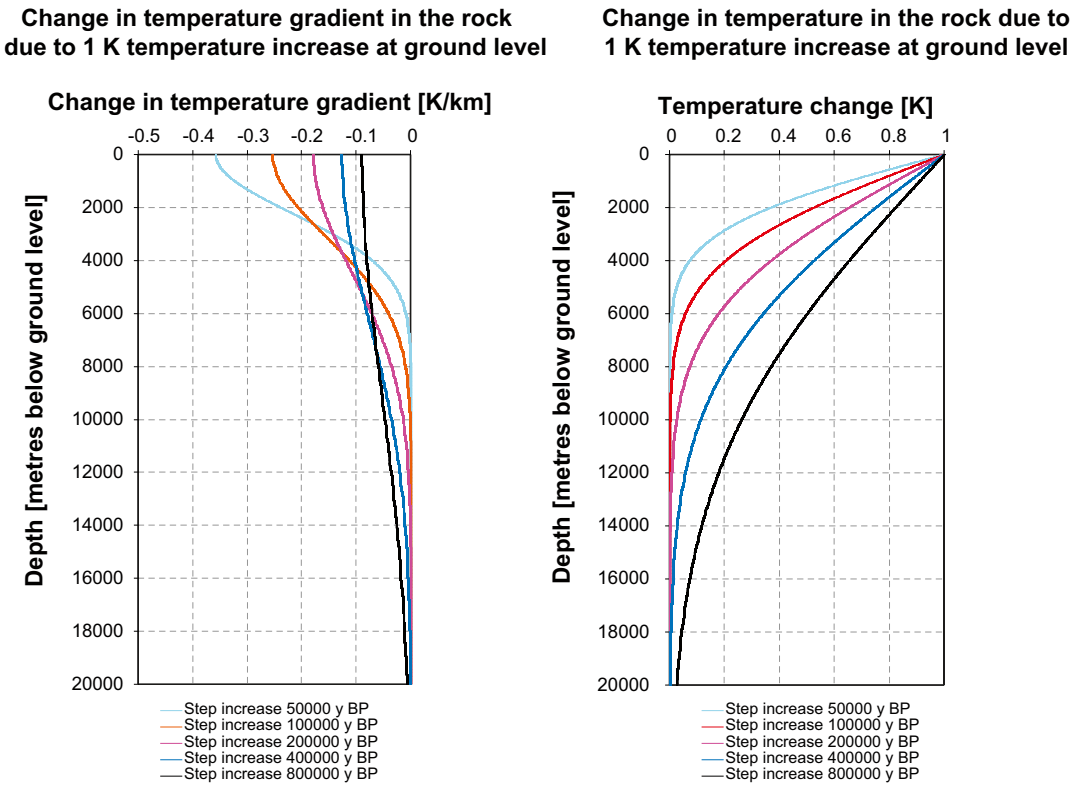

Figure 4-9. *The effect on temperature gradient (left) and temperature (right) in the rock at large depths (compare with Figure 4-8) when the ground surface temperature is increased 1K (step increase). Gradient in K/km. Thermal diffusivity=1.57·10⁻⁶ m²/s.*

4.3.4 Sensitivity to ground surface temperature in climate data

The ground surface temperature (Figure 4-6) is an important boundary condition for the model. Figure 4-10 and Figure 4-11 show the sensitivity to the present ground surface temperature and the ground surface temperature 120 kyrs before present, respectively. The black models are based on the temperature model in Figure 4-6. In Figure 4-10 the red and blue models illustrate alternative temperatures (7° and 6°C respectively, during the last 1,000 year BP). The present ground surface temperature has a substantial effect on the temperature gradient at low to middle depth. In Figure 4-11 the red and blue models illustrate alternative and reasonable temperatures (10° and 0°C respectively, for 120 kyrs BP). This factor gives a smaller but depth-consistent effect on the temperature gradient. The models consider both internal heat production and past climate variations according to Figure 4-6.

4.4 Sensitivity analysis conclusions

The results from this sensitivity analysis are useable in the coming geothermal calculations. Heat flow, thermal conductivity and current ground surface temperature are as expected the parameters that seem to have the greatest impact on the calculated temperature profiles. Another finding is that the geothermal profiles (temperature and temperature gradient) down to 1,000 m depth are affected by palaeoclimate more than 120 kyrs ago, and differ depending on the length of the climate model used.

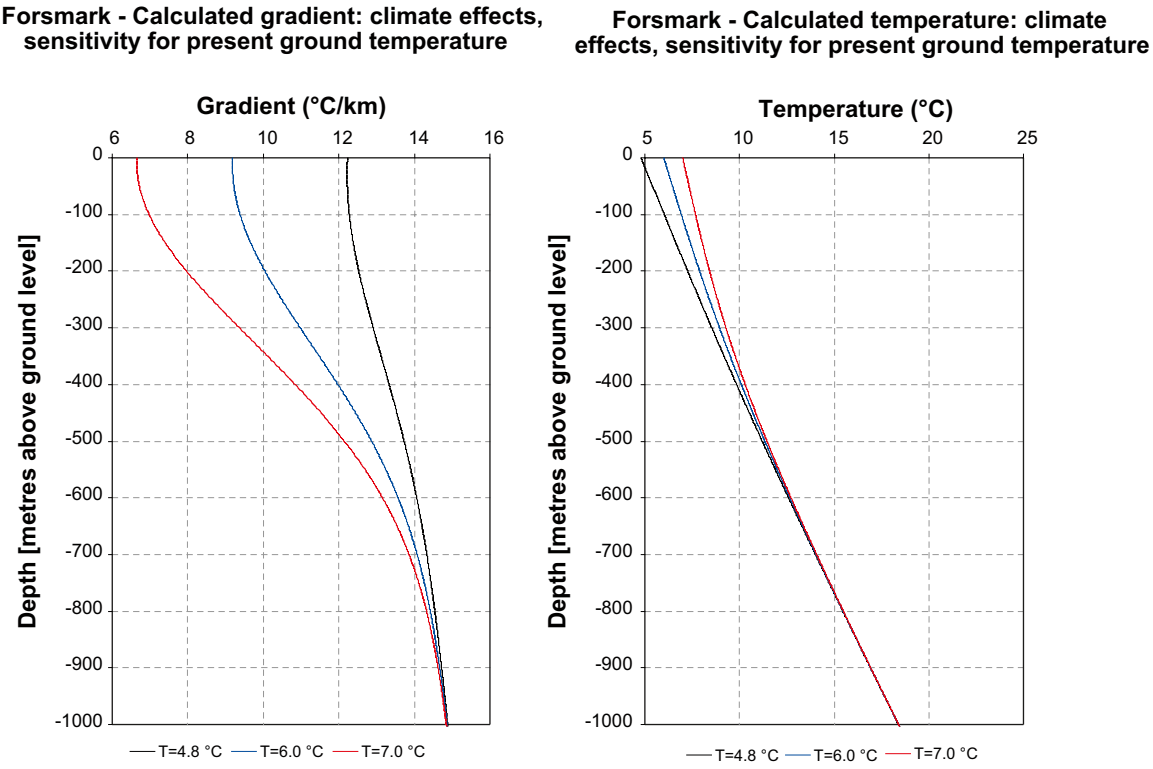

Figure 4-10. *Modelled temperature gradient (left) and temperature (right) at Forsmark, illustrating the sensitivity to present ground temperature in the model. The black models are based on the temperature model in Figure 4-6. The other models illustrate alternative temperatures.*

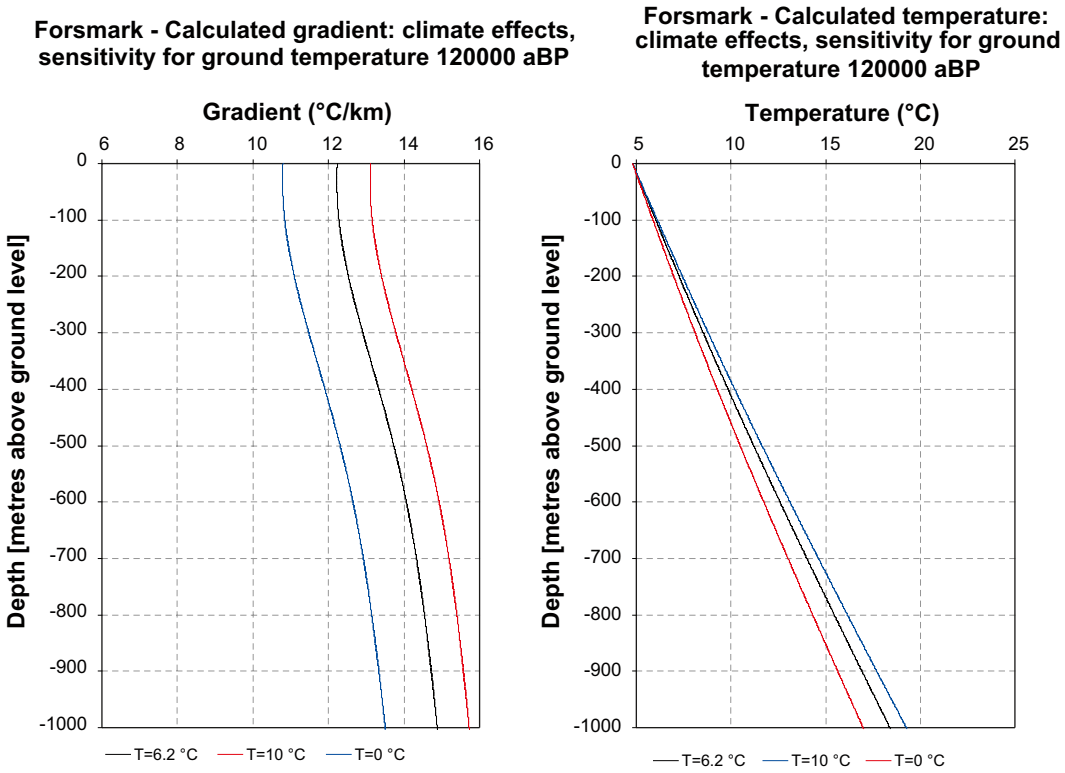

Figure 4-11. *Modelled temperature gradient (left) and temperature (right) at Forsmark, illustrating the sensitivity to the ground temperature at 120 kyrs BP in the model.*

5 Climate models

5.1 Climate models in SR-Can

Figure 5-1 and Figure 5-2 presents the original climate models for Forsmark and Laxemar spanning the past 120 kyrs used in SR-Can safety assessment /SKB 2006/. The temperature curve is based on the palaeotemperature curve from the GRIP ice core /Dansgaard et al. 1993/, modified by the numerical ice sheet model used in SR-Can, and in this process also extracted for each site /SKB 2006/. It is important to note that the uncertainty in these temperature reconstructions is considerable, estimated to up to around ±5 degrees for parts of the curve. The motivation for using these curves in the safety assessment lies in the chosen approach. The temperature curve is used for a reference evolution, which is subsequently complemented by other climate developments with potentially larger impact on repository safety, e.g. by doing dedicated sensitivity studies with the temperature curve, for instance by changing the temperature curve according to its estimated uncertainty and more /SKB 2006/. The uncertainty and applicability of the temperature curve for various studies will be further evaluated in the SR-Site climate report.

The temperature step models, used in this study, are simplified versions of these climate curves /SKB 2006/.

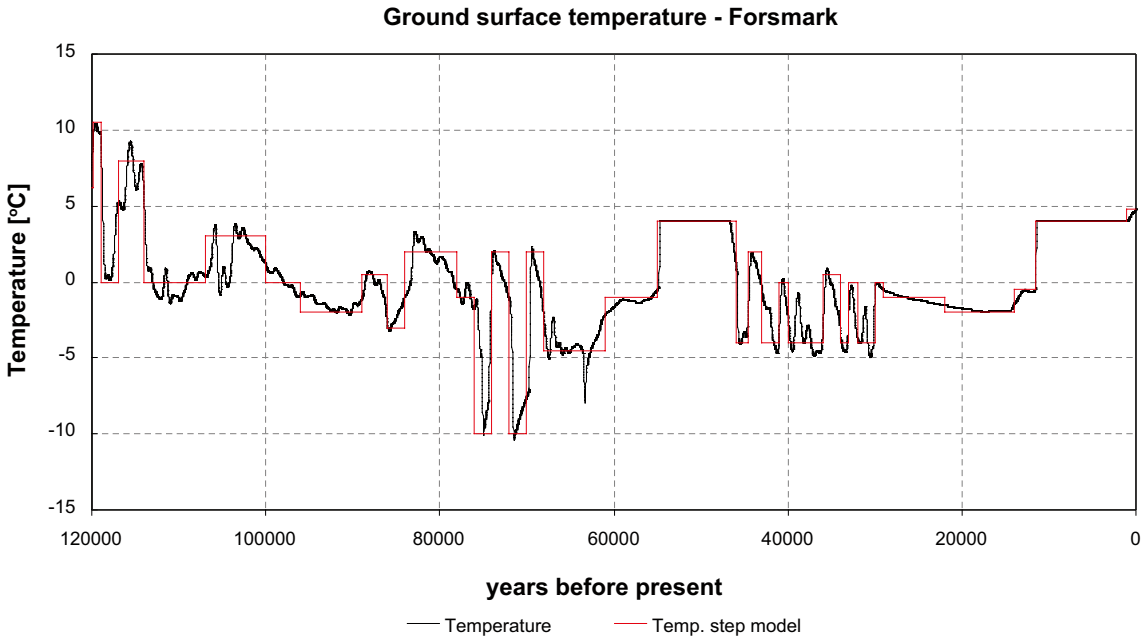

Figure 5-1. *Ground surface temperature model (red) for Forsmark spanning the past 120 kyrs. The temperature model is a simplified version of the estimated palaeotemperature model (black) for the last glacial cycle used in SR-Can safety assessment /SKB 2006/ (Figure 3-50).*

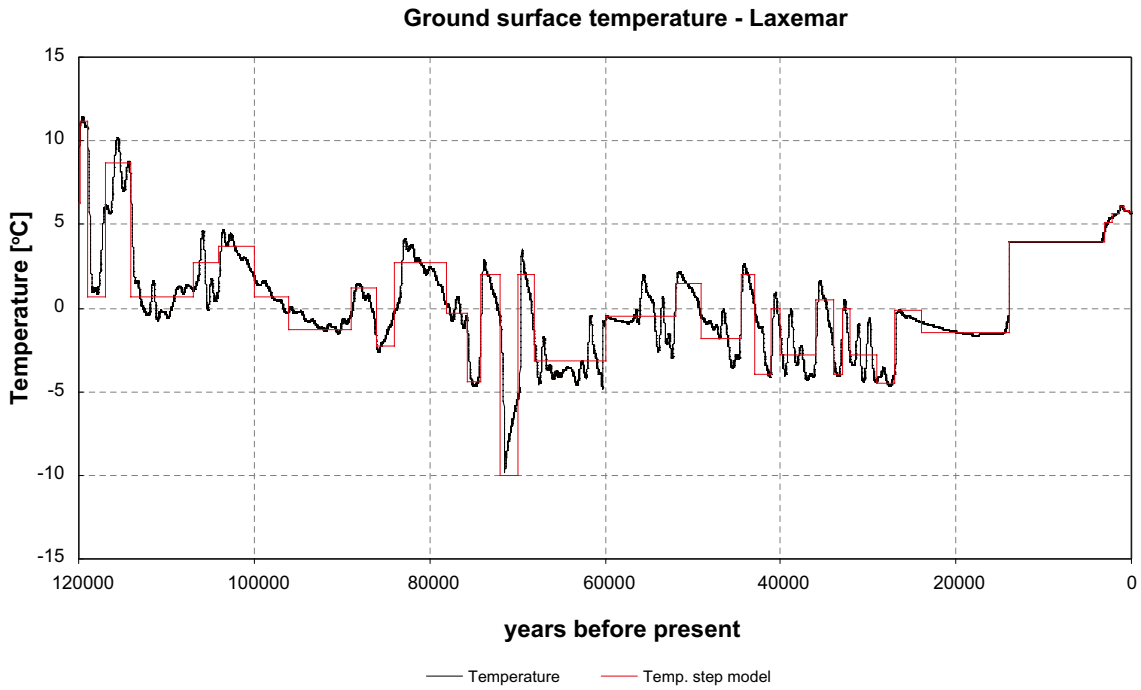

Figure 5-2. *Ground surface temperature model (red) for Laxemar spanning the past 120 kyrs. The temperature model is a simplified version of the estimated palaeotemperature model (black) for the last glacial cycle used in SR-Can safety assessment /SKB 2006/ (Figure 3-50).*

5.2 Modified climate models in present study

From the sensitivity analysis in Figure 4-9 it is obvious that the temperature gradient is influenced by long periods of climate change (longer than one glacial cycle), especially at larger depths. In the present study, the long term climate is assumed to be cyclical in nature. Therefore, the climate models have been extended to 228 kyrs BP, where the original climate model has been re-used for the period earlier than 126,500 aBP for Forsmark, and 129 kyrs BP for Laxemar. A coarse reconstruction of the timing and conditions during the Eemian interglacial period has been made using results from e.g. /Dansgaard et al. 1993/ and /Björck et al. 2000/, see Appendix 5. The timing of the reconstructed Eemian period is 129–114 kyrs BP for Laxemar and for 126.5–114 kyrs BP Forsmark. Figure 5-3 and Figure 5-4 present the resulting modified temperature curves for Forsmark and Laxemar.

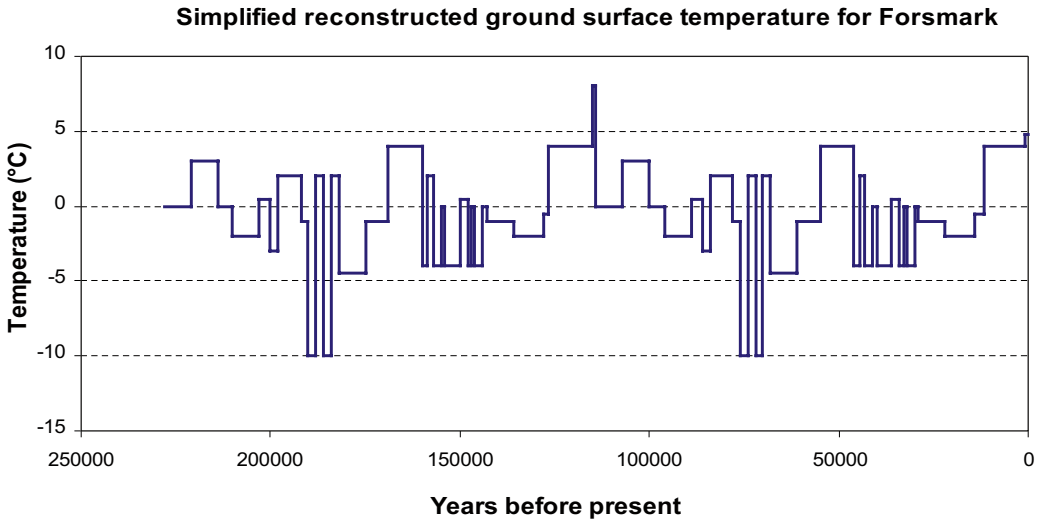

Figure 5-3. *Step model of ground surface temperature variations for Forsmark, modified from /SKB 2006/. Note that temperatures during the past 120 kyrs have an uncertainty of several degrees. Temperatures during the preceding period, during the Saalian glaciation, are highly tentative and should not be taken as representative of genuine conditions.*

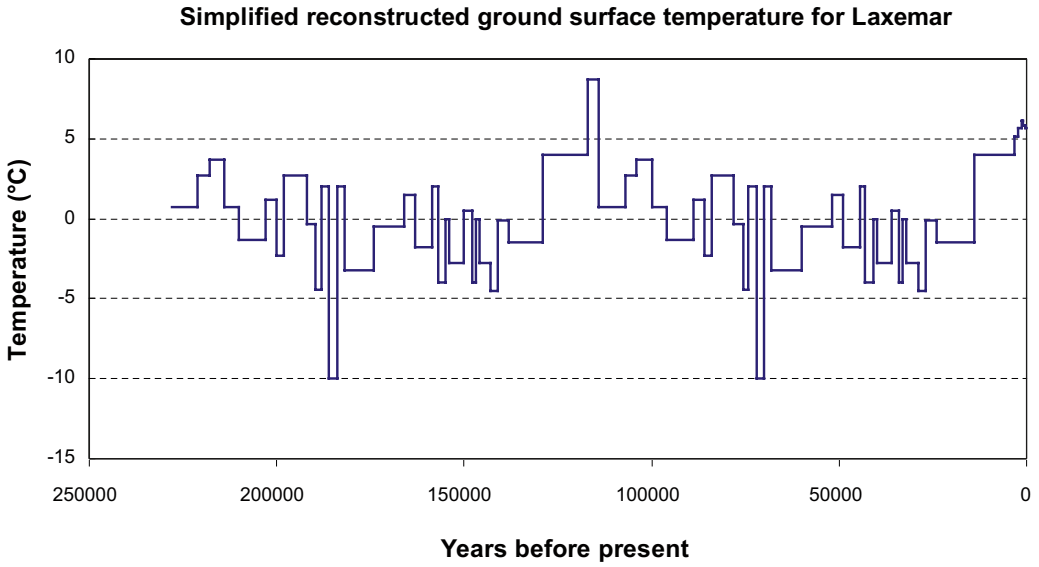

Figure 5-4. *Step model of ground surface temperature variations for Laxemar, modified from /SKB 2006/. Note that temperatures during the past 120 kyrs have an uncertainty of several degrees. Temperatures during the preceding period, during the Saalian glaciation, are highly tentative and should not be taken as representative of genuine conditions.*

6 Geothermal calculations – Forsmark

6.1 Thermal data

6.1.1 Geothermal gradient and temperature

During the site investigation programme in Forsmark, fluid temperature in deep boreholes has been logged and temperature gradient has been calculated. The temperature and gradient profiles have been investigated for eight boreholes ranging from KFM01A to KFM09B; see Figure 6-1. While data for additional boreholes exist, they were not considered reliable /Sundberg et al. 2008a/. The location for the different boreholes is showed in Appendix 4.

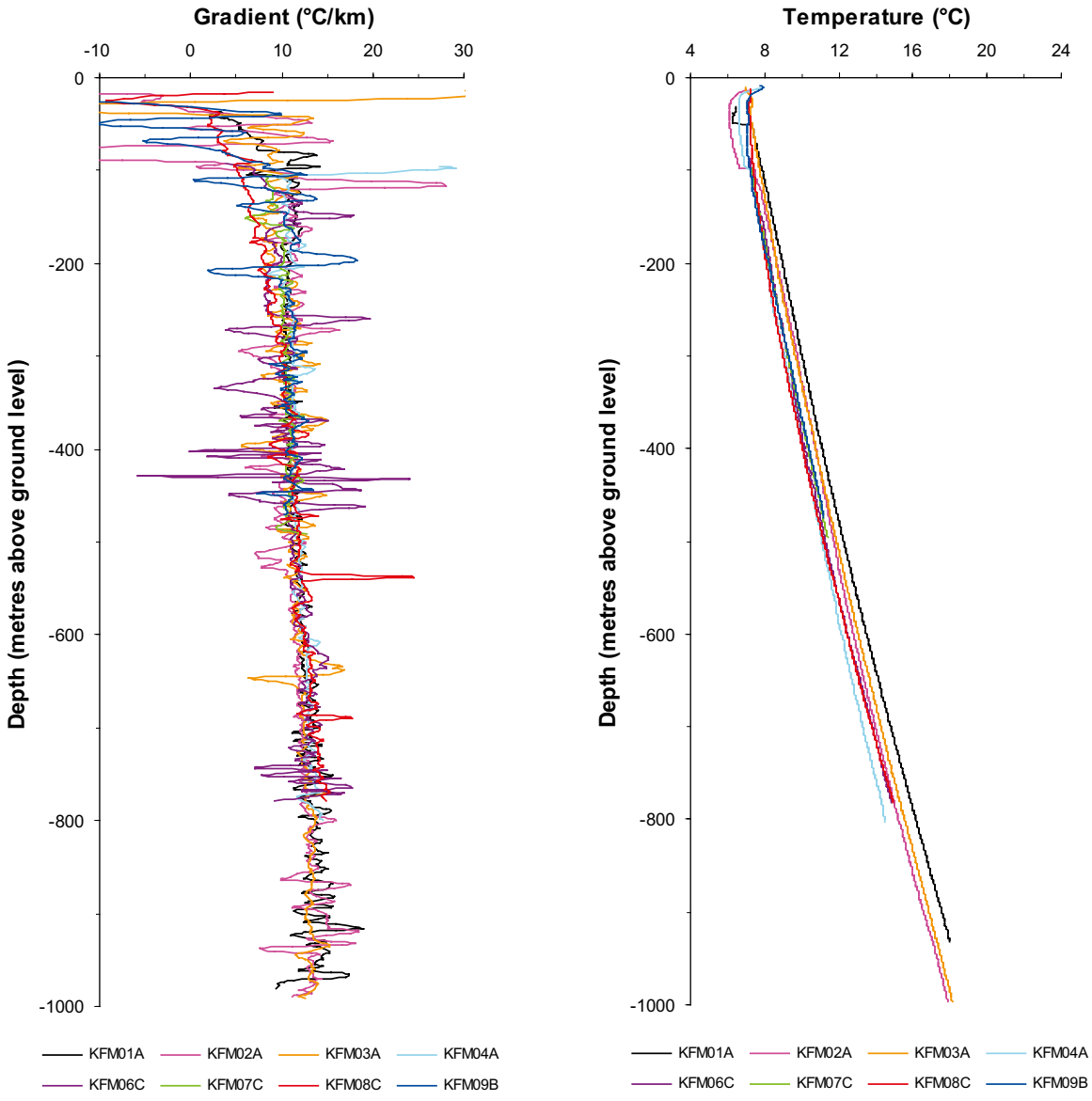

Figure 6-1. *Summary of temperature gradients (left) and temperatures (right) for the eight boreholes at Forsmark. The figure represents the raw data, before smoothing and exclusion. Results from fluid temperature loggings /Sundberg et al. 2008a/.*

The measured gradient profile for each borehole was smoothed with a 100 m moving average filter in order to reduce the significant "noise" in the original data. Certain data were also excluded; see Figure 6-2. For the mean temperature profile, only data between 100 m and 996 m was included in the fitting analysis. The corresponding span for the mean gradient profile was 100 m to 990 m. This data is used as basis for the mean profiles used as a reference in the modelling.

A mean profile for the different boreholes was then calculated for both the smoothed temperature and gradient profiles. In order to estimate the uncertainty of the measured mean profile, 95% confidence intervals were calculated; see Figure 6-3.

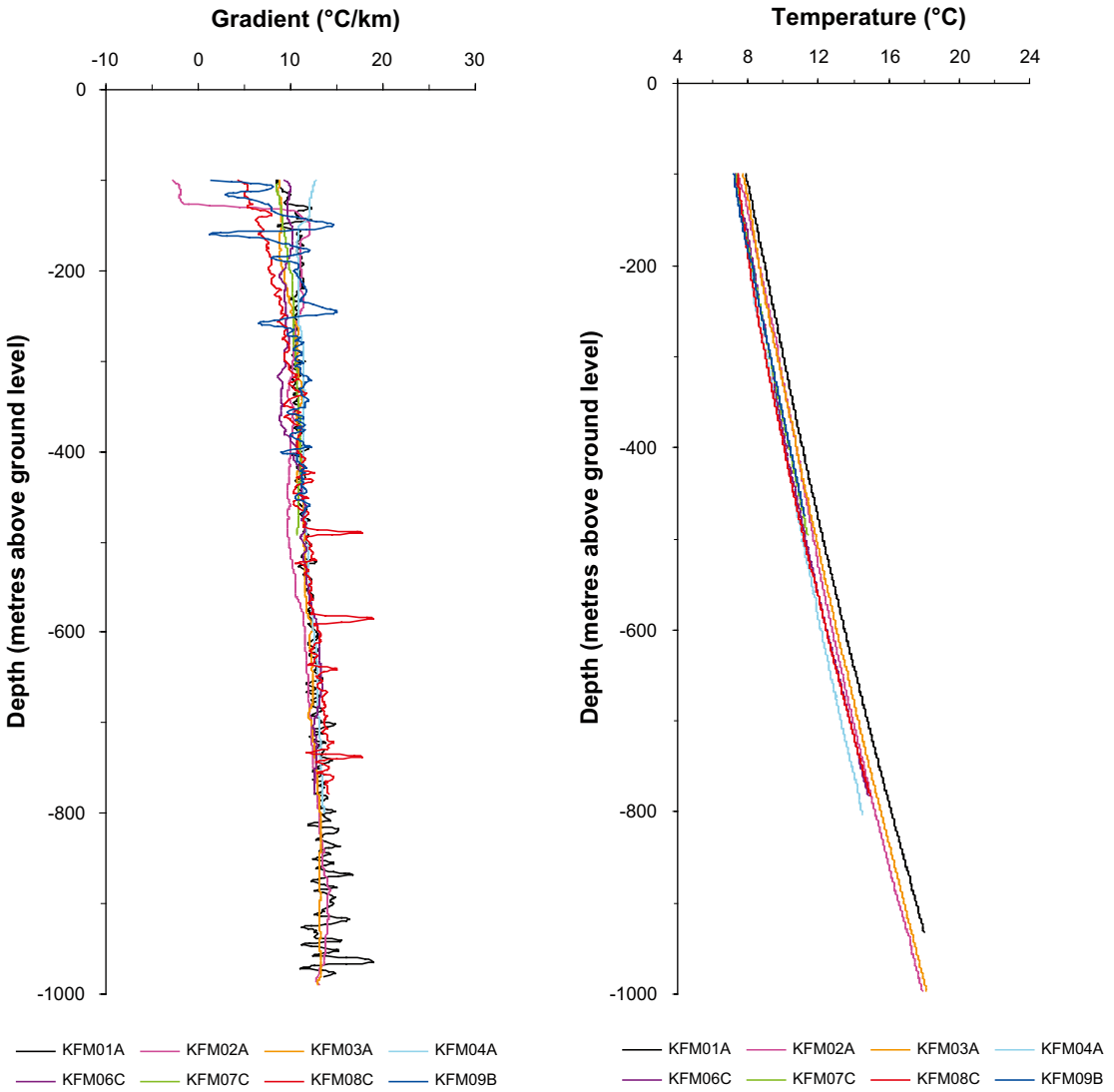

Figure 6-2. *Summary of temperature gradients (left) and temperatures (right) for the eight boreholes at Forsmark. Data above and below certain levels have been excluded, and the gradients have been smoothed out with a 100 m moving average. The displayed data is the basis for the mean profiles used as reference in the modelling, see Figure 6-3.*

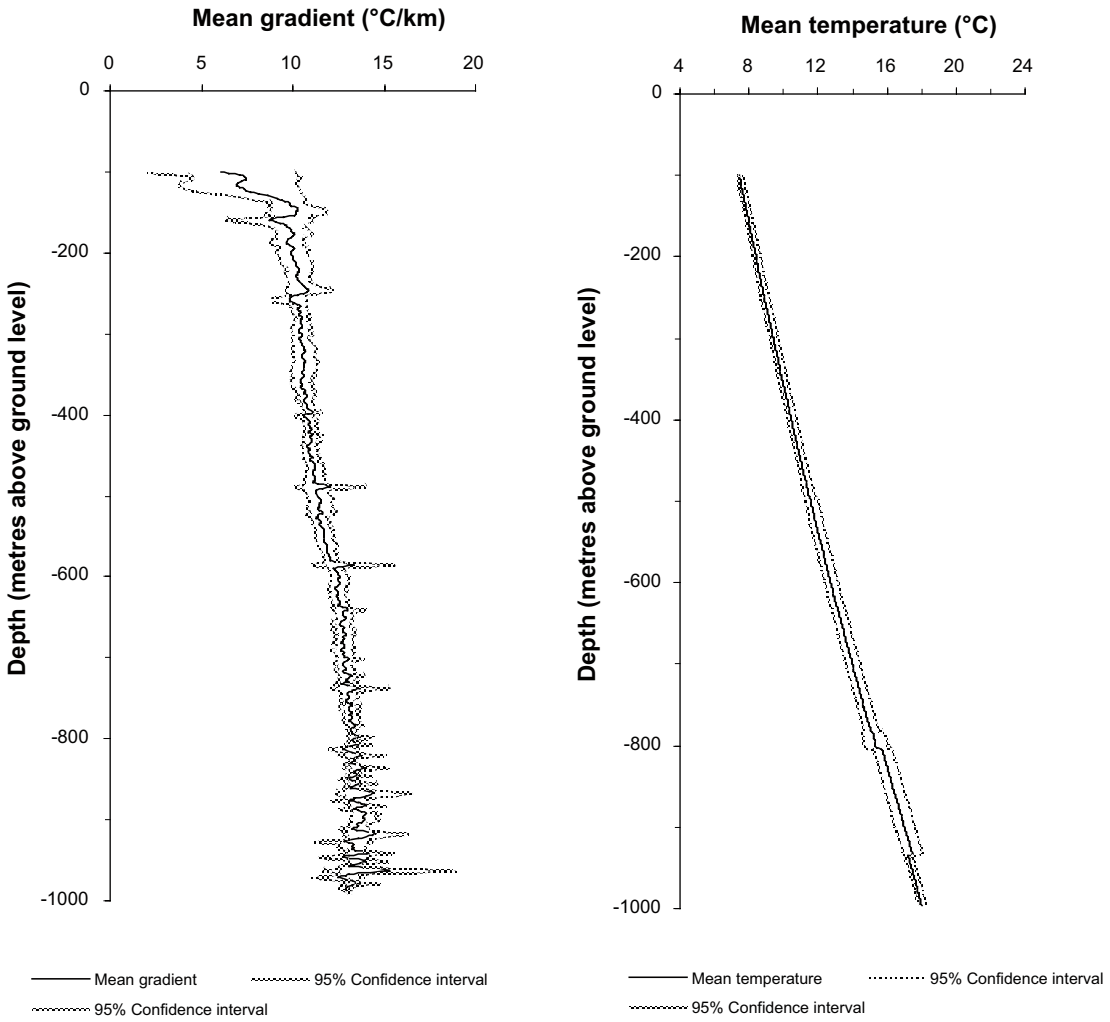

Figure 6-3. *Mean gradient (left) and mean temperature (right), used as reference in the modelling. Calculated 95% confidence intervals are also displayed.*

6.1.2 Ground surface temperature

The current ground surface temperature at Forsmark is 4.8°C according to /SKB 2006/. The logged borehole temperature data indicated a higher surface temperature. The current ground surface temperature was extrapolated from temperature data at larger depths using a linear model. A sensitivity analysis using different extrapolation ranges (the range of data that is used for the extrapolation) was then made (Table 6-1), and the current ground surface temperature was set to 6.5°C (200–100 m range).

Mean annual air temperatures recorded at meteorological stations close to the Forsmark area are between 5°C and 5.5°C /Johansson 2008/.

Table 6-1. Current ground surface temperature extrapolated from data at larger depths – sensitivity to extrapolation range.

	Extrapolated ground surface temperature, °C		
	200–100 m	250–100 m	300–100 m
KFM01A	6.78	6.79	6.79
KFM02A	6.24	6.28	6.30
KFM03A	6.82	6.79	6.77
KFM04A	6.28	6.39	6.28
KFM06C	6.30	6.35	6.32
KFM07C	6.38	6.35	6.33
KFM08C	6.72	6.67	6.61
KFM09B	6.17	6.20	6.16
Mean	6.46	6.48	6.45
Min	6.17	6.20	6.16
Max	6.82	6.79	6.79
Std. dev.	0.27	0.24	0.24
95% Confidence interval	6.28–6.65	6.31–6.64	6.28–6.61

6.1.3 Thermal conductivity, diffusivity and internal heat generation

Thermal conductivity and diffusivity for the different rock domains have been evaluated in the site descriptive model /Back et al. 2007, Sundberg et al. 2008a/. The mean thermal conductivity is approximately 3.5–3.6 W/(m·K) (see Figure 6-4) and the thermal diffusivity, calculated from domain mean on thermal conductivity and heat capacity, is approximately $1.7 \cdot 10^{-6}$ m^2/s in the dominating rock domains (RFM029: $1.73 \cdot 10^{-6}$ m^2/s; RFM045: $1.68 \cdot 10^{-6}$ m^2/s). However, there is large scale variability in the rock thermal conductivity within the rock domains affecting the thermal conductivity in individual boreholes. There is a thermal anisotropy at Forsmark. The thermal anisotropy factor is estimated to 15% in the dominant granite /Back et al. 2007/ (determined at one site at the margin of the lens where foliation dominates). It is reasonable to believe that the orientation of the thermal anisotropy coincides with the orientation of the foliation/lineation in the rock. Lineation dominates inside the tectonic lens and a subvertical foliation dominates the margins of the lens /SKB 2008/. The vertical component of the thermal conductivity due to anisotropy is judged to be in the interval 0–15% higher compared to the horizontal component.

The thermal conductivity and heat capacity is influenced by the temperature. The thermal conductivity for the dominating rocks in Forsmark decreases by 10% when the temperature increases by 100°C, and the heat capacity increases by approximately 30% for the same temperature increase. Temperature dependence aspects are not possible to consider due to limitations in the used model. However, the temperature effect on the thermal conductivity is judged to be relatively small. The temperature differs less than 12°C between 0 and 1,000 m depth, i.e. a thermal conductivity difference of less than (–) 1.2%. The temperature effect on the thermal diffusivity is larger at approximately (+) 4–5%.

Heat generation for different rock types has been calculated for borehole KFM02A from Equation 2-4 based on measurements of thorium, uranium and potassium for all investigated samples in Forsmark; see Table 6-2. In Figure 6-5 the rock types and the calculated heat generation for KFM02A are shown. The mean heat generation is 2.72 μW/m^3, calculated by weighting the occurrence of different rock types in the borehole. KFM02A was originally chosen due better quality in the temperature logging. Later more boreholes have been approved, see /Sundberg et al. 2008a/. The heat generation based on mean proportions of different rock types in the rock domains /Stephens et al. 2007/ and the content of U, Th and K /Petersson et al. 2004, Mattson et al. 2005/ is calculated to 3.16 and 3.11 μW/m^3 for domain RFM029 and RFM045 respectively. The reason for the slightly higher values for domain level is the significantly higher proportions of pegmatite (101061). However, for this and several others rock types only a few measurements are available, which makes the results less reliable. In the modelling below the heat generation for KFM02A has been used.

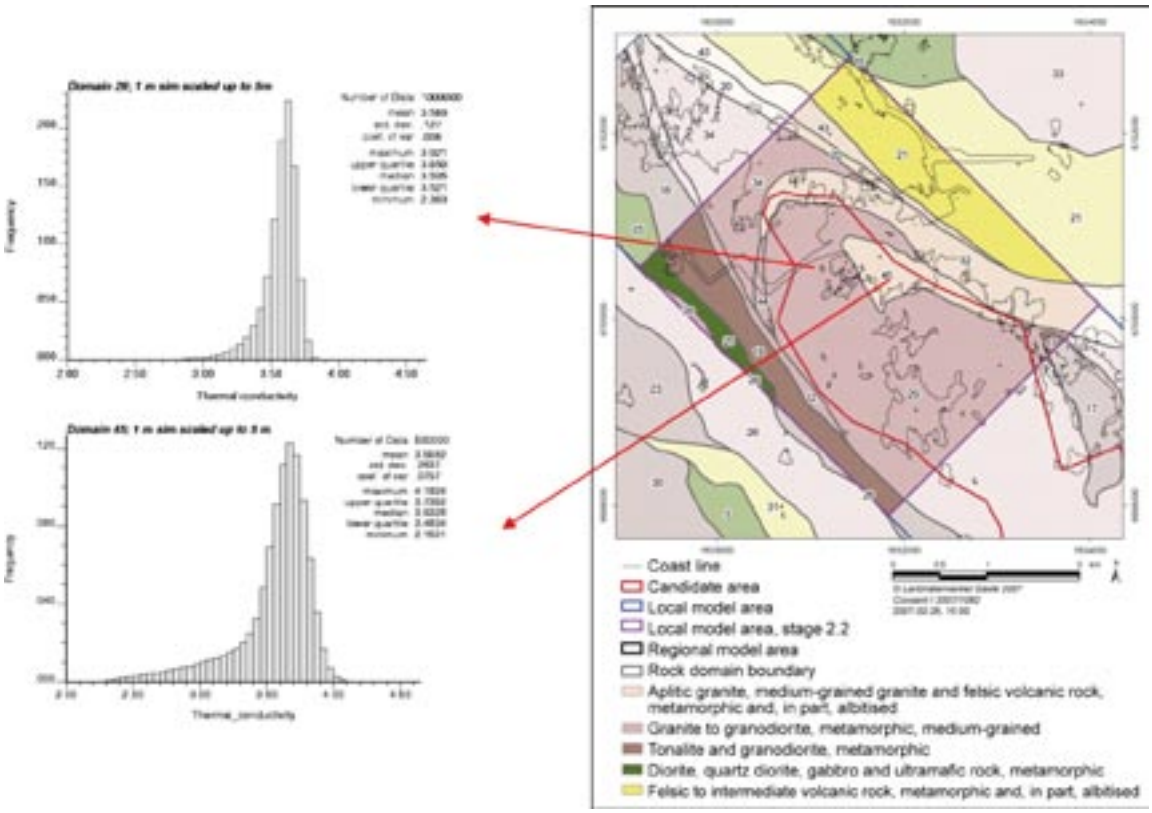

Figure 6-4. Overview of the thermal conductivity models at 5 m scale in rock domain RFM029 and RFM045 in Forsmark /SKB 2008/.

Table 6-2. Heat generation for some rock types in Forsmark based on the occurrence in KFM02A /Petersson et al. 2004/.

Rock type	Occurrence in KFM02A (%)	Heat production (μW/m³)	Standard deviation (μW/m³)	Number of measurements
101057, granite to granodiorite	79.5	2.80	0.843	28
102017, amphibolite	4.1	0.798	0.387	5
111058, granite	1.2	4.00	–	1
101061, pegmatite, pegmatitic granite	0.9	6.13	–	1
101051, granite, granodiorite and tonalite	14.3	2.51	1.54	7
Weighted mean		2.72		

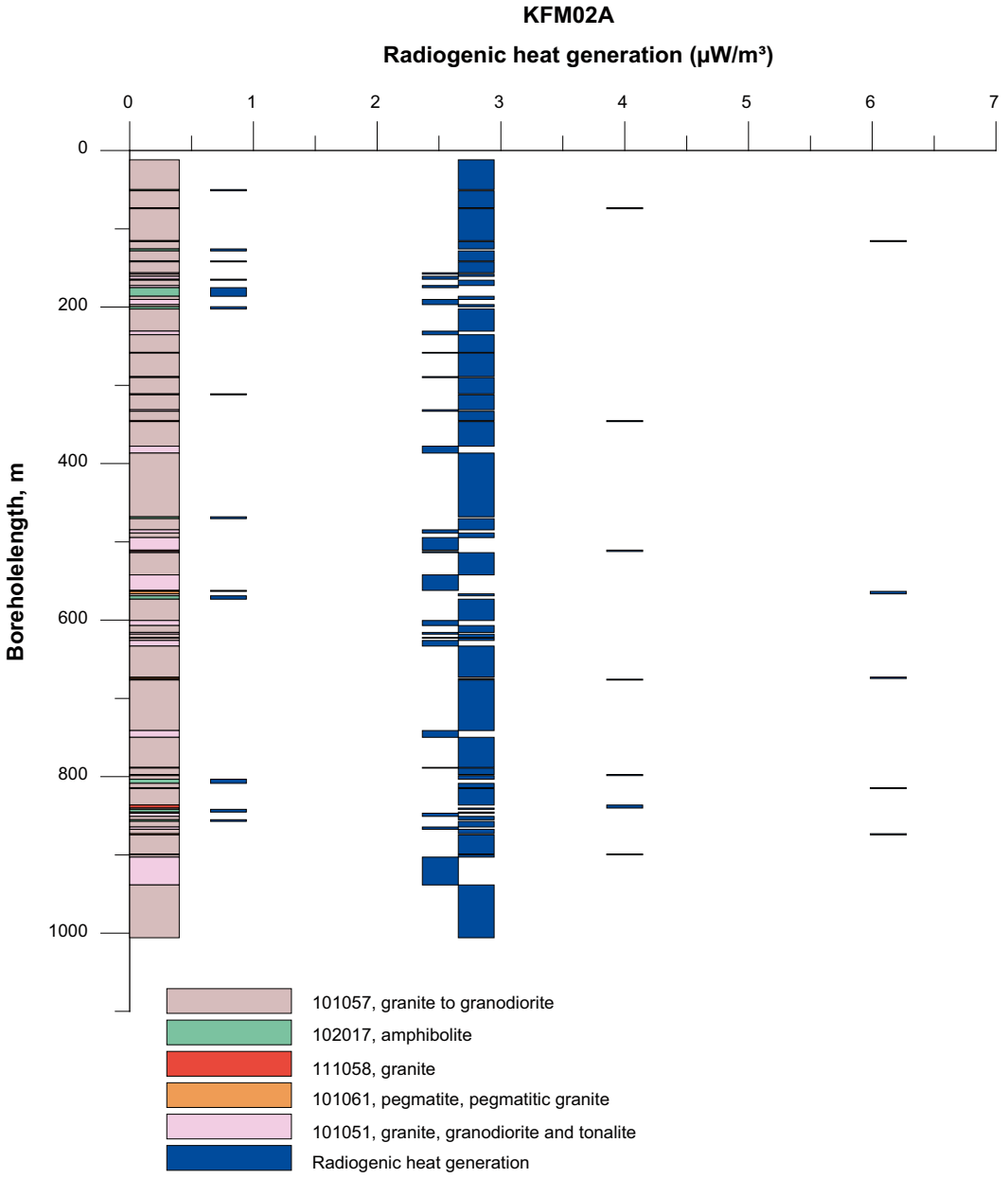

Figure 6-5. *Rock types and calculated radiogenic heat generation for borehole KFM02A.*

6.2 Model calculations

6.2.1 Introduction

The data used for the model calculations are partly based on the reference values in /SKB 2006/. The purposes of the model calculations were to study the effects of closer specifications concerning data from site models, and effects from changes in climate. Two sets of models were calculated. The "General models" study parameter changes that are closely bound to scientific data, while the "Additional models" give optimised fitting results to measured data, but with parameter changes that are less bound to scientific data. For example it is relatively easy to motivate a positive or negative bias of the temperature in the whole model or changes in the period earlier than approximately 120 kyrs BP, from a scientific point of view due to uncertainties. It is harder to motivate the different temperature changes for different time periods made in the "Addition models". For a description of the calculation procedure, see Appendix 1.

6.2.2 General models

Five general models are presented in Table 6-3 below. The modelled time periods with different ground temperatures at Forsmark are illustrated in Figure 6-6. No influence of anisotropy is assumed in the thermal parameters in the models, but is discussed in Section 8.1.

Model A represents the reference values as presented in /SKB 2006/ (the report compiles information on climate related issues relevant for the long-term safety of a repository and supports the safety assessment SR-Can), i.e. the objective is to present a model that represents the SR-Can data without adjustments. Results can be seen in Figure 6-7.

Model B represents site-specific data for thermal diffusivity, thermal conductivity and radiogenic heat production /Back et al. 2007, Sundberg et al. 2008a/. Results are presented in Figure 6-8. Only small adjustments are made compared to model A.

In Model C, the present ground temperature T_2 is increased from 4.8°C to 6.5°C, a value that was determined by extrapolation of the temperature profiles. Results can be seen in Figure 6-9.

Table 6-3. Parameters for the general models at Forsmark. κ = thermal diffusivity, λ = thermal conductivity, Q_0 = heat flow at ground level, A = radiogenic heat production, T_0 = ground temperature 228 kyrs BP, T_1 = ground temperature 11.4–1 kyrs BP, T_2 = ground temperature 1,000–0 yrs BP, ΔT_1 = ground temperature change 228–114 kyrs BP, ΔT_2 = ground temperature change 114–44.5 kyrs BP, ΔT_3 = ground temperature change 44.5–1 kyrs BP.

Model	κ [mm²/s]	λ [W/(m·K]	Q_0 [mW/m²]	A [μW/m³]	T_0 [°C]	T_1 [°C]	T_2 [°C]	ΔT_1 [°C]	ΔT_2 [°C]	ΔT_3 [°C]
A	1.57	3.6	59	2.5	0	4	4.8	0	0	0
B	1.7	3.5	59	2.7	0	4	4.8	0	0	0
C	1.7	3.5	59	2.7	0	4	6.5	0	0	0
D	1.7	3.5	60	2.7	0	4	6.5	0	0	0
E1	1.7	3.5	55	2.7	1.7	5.7	6.5	1.7	1.7	1.7
E2	1.7	3.5	61	2.7	–1	4	6.5	–1	0	0

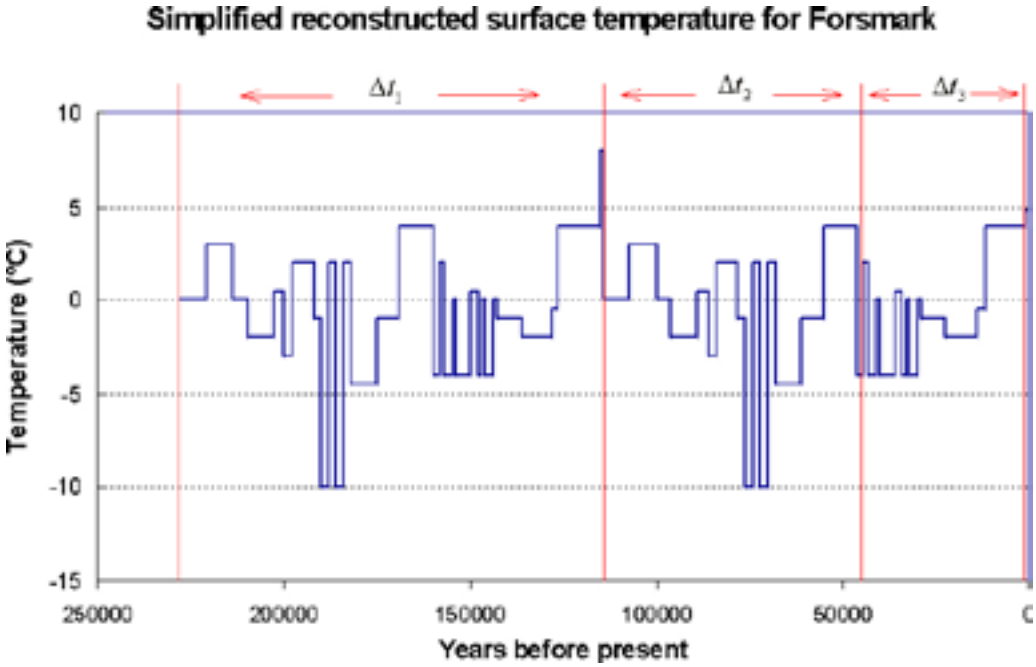

Figure 6-6. *Clarification of the time periods Δt_1, Δt_2 and Δt_3, corresponding to ΔT_1, ΔT_2, and ΔT_3.*

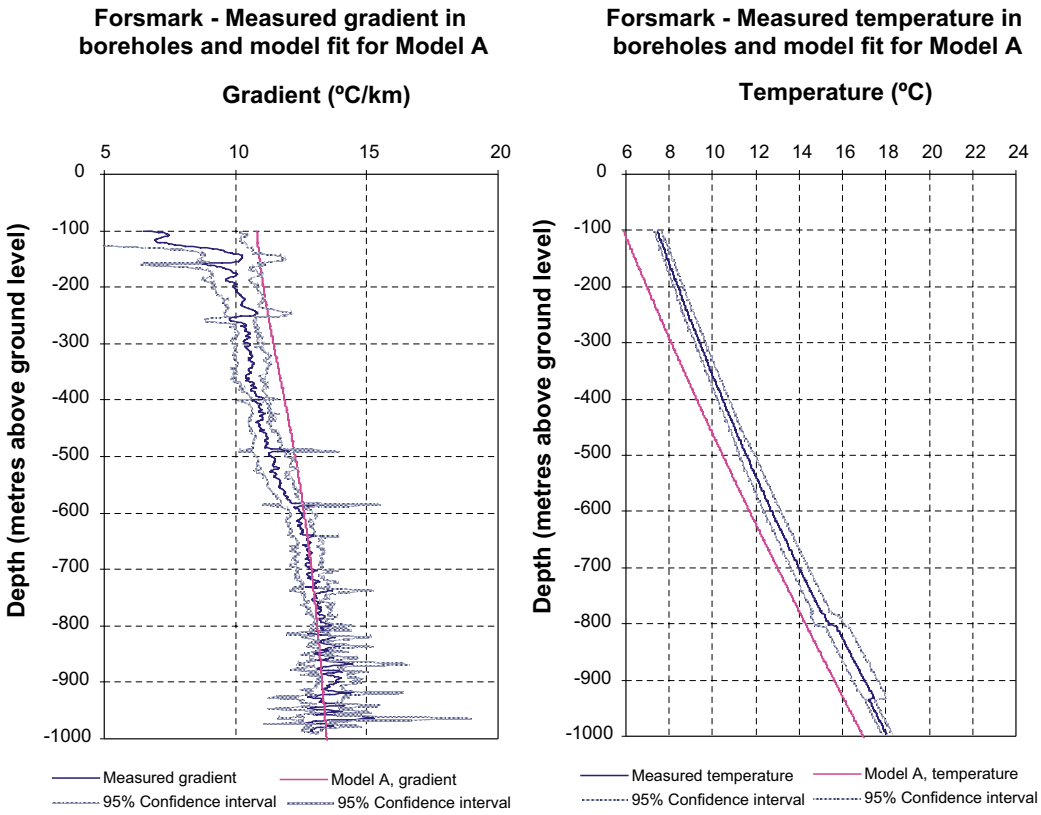

Figure 6-7. *Comparison between Model A and mean value from measurements: temperature gradient (left) and temperature (right).*

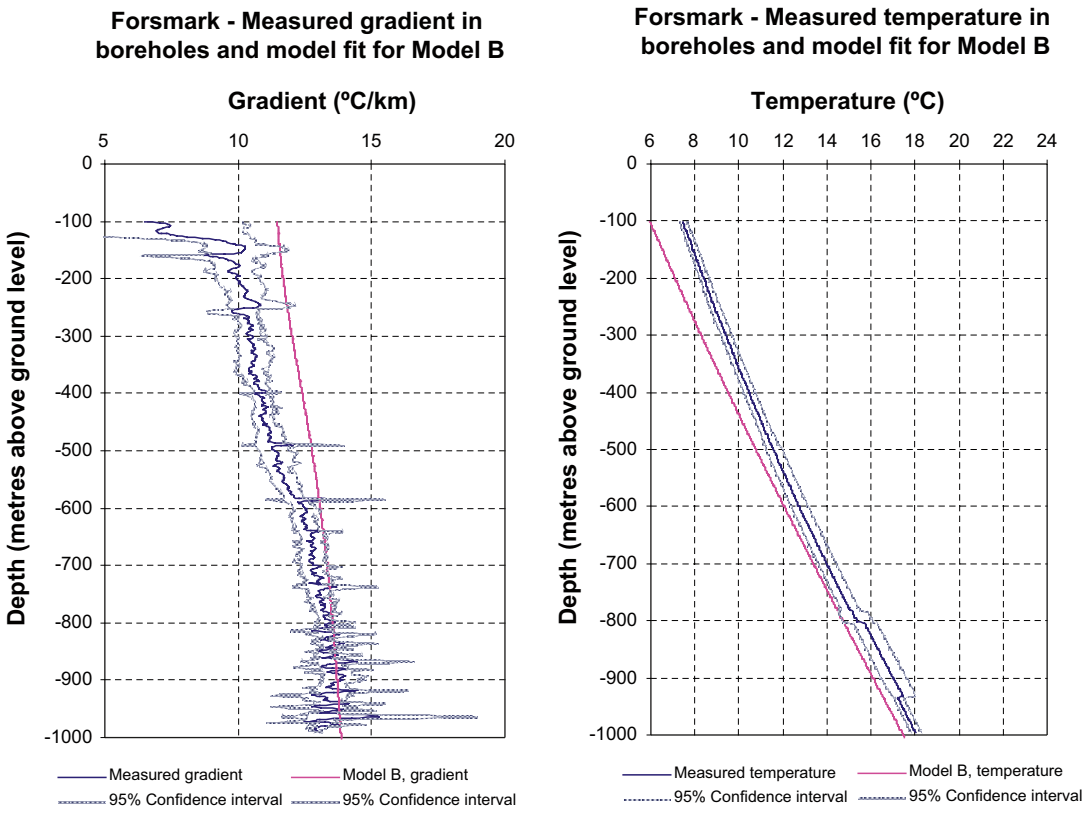

Figure 6-8. *Comparison between Model B and mean value from measurements: temperature gradient (left) and temperature (right).*

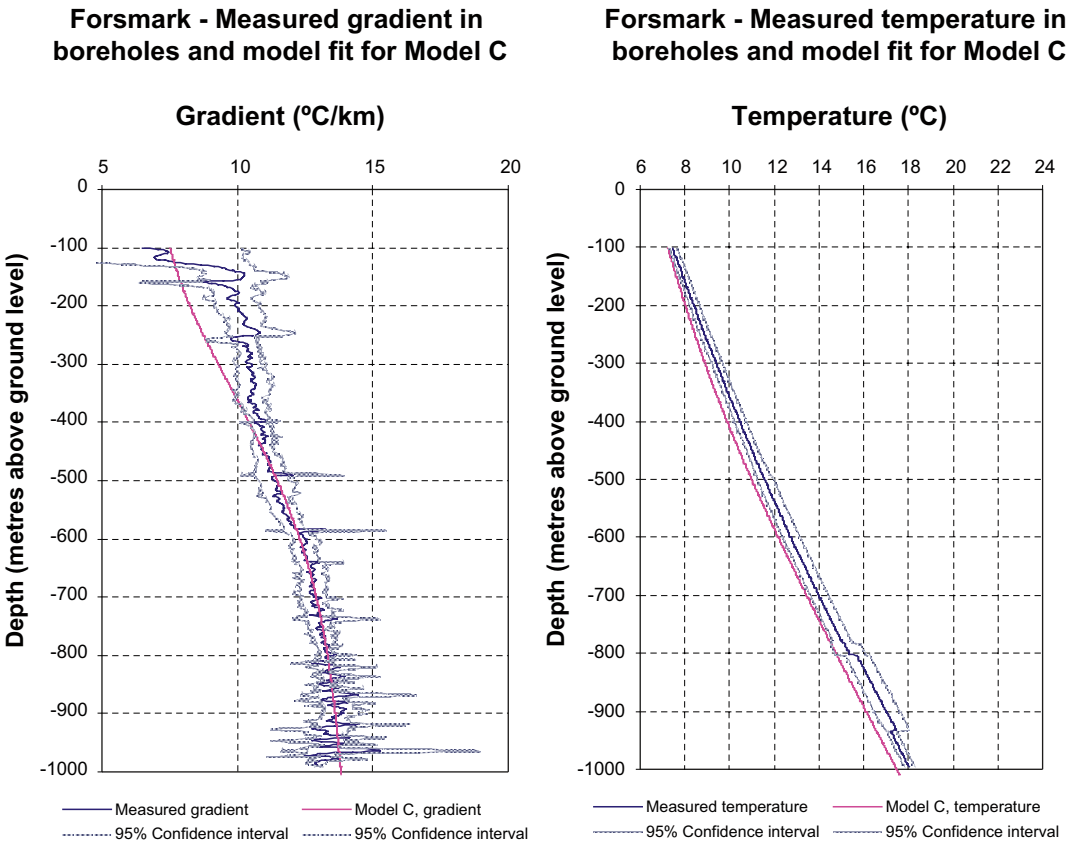

Figure 6-9. *Comparison between Model C and mean value from measurements: temperature gradient (left) and temperature (right).*

Model D is equal to Model C in all aspects except the heat flow, which is increased from 59 to 60 mW/m^2. The resulting profiles for Model D can be seen in Figure 6-10. Figure 6-13 displays the sensitivity of fitting results for different heat flow values.

In Model E1, the temperature of the whole climate model (except T_2) is increased by the same amount as T_2 was raised in Model C, i.e. 1.7°C. The heat flow is also optimized for these parameters. The resulting profiles for Model E1 can be seen in Figure 6-11. Figure 6-14 displays the sensitivity of fitting results for different heat flow values.

In Model E2, the temperature of the whole first glacial cycle (228–114 kyrs BP) is lowered when setting ΔT_1 to –1°C. The resulting profiles for Model E2 can be seen in Figure 6-12. The heat flow is also optimized for these parameters. Figure 6-15 displays the sensitivity of fitting results for different heat flow values.

Table 6-4 presents curve fitting statistics for the General models. Two numerical measures were calculated: the coefficient of determination (r^2) /Körner and Wahlgren 2000/ and the Root Mean Square Deviation (RMSD) /Schunn and Wallach 2005/. A recommendation for fitting of models to data is to use a combination of these two measures. The r^2 is a measure of how well the model captures the trend in data and the RMSD is a measure of the deviation from exact data locations. A good model will have an r^2-value close to 1 and a low RMSD.

Adjusting thermal parameters as in Model B seem to give a better temperature fit, but the gradient fit is worsened. Both Model C and D results in reasonably good fits, even though the RMSD values of Model D are slightly better. Model E1 and E2 that include changes in the past climate do not result in any drastic improvements compared to Model C and D. A factor in common to Model D, E1 and E2 is that they all experiment with changes in heat flow. Figure 6-13 to Figure 6-15 below present how RMSD is affected by changes in heat flow for these models.

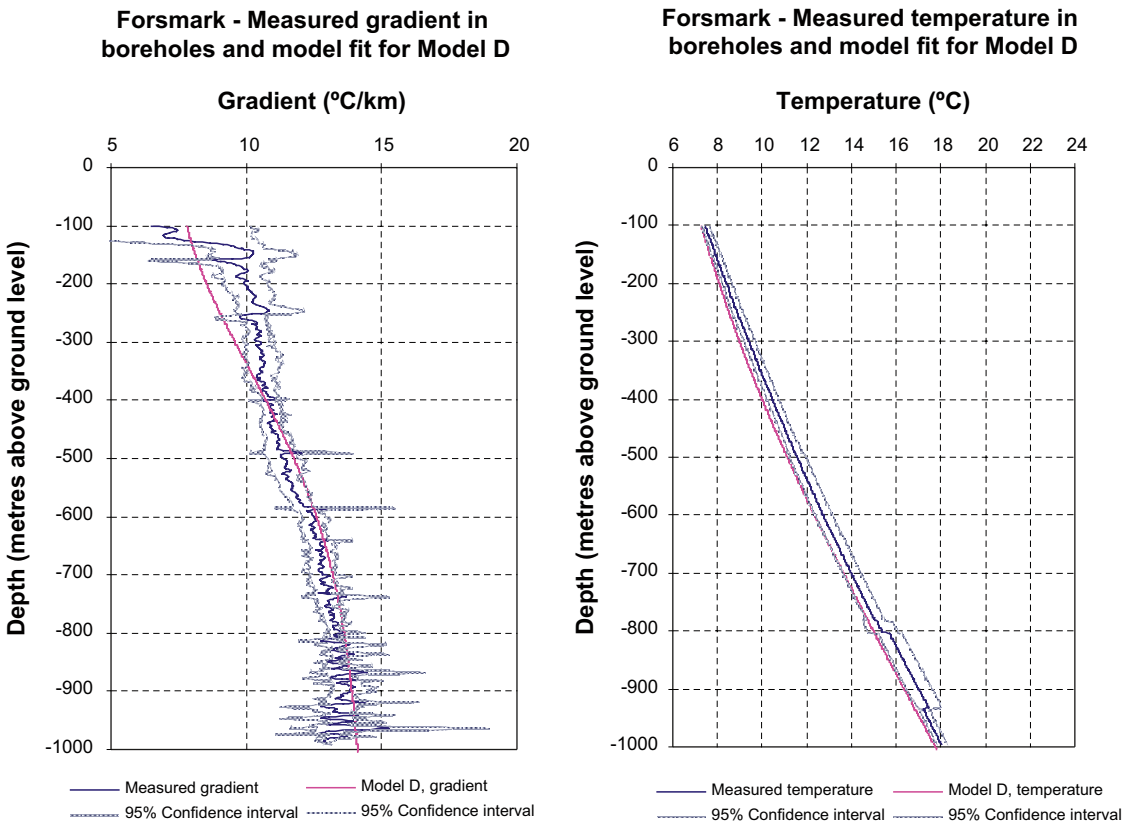

Figure 6-10. *Comparison between Model D and mean value from measurements: temperature gradient (left) and temperature (right).*

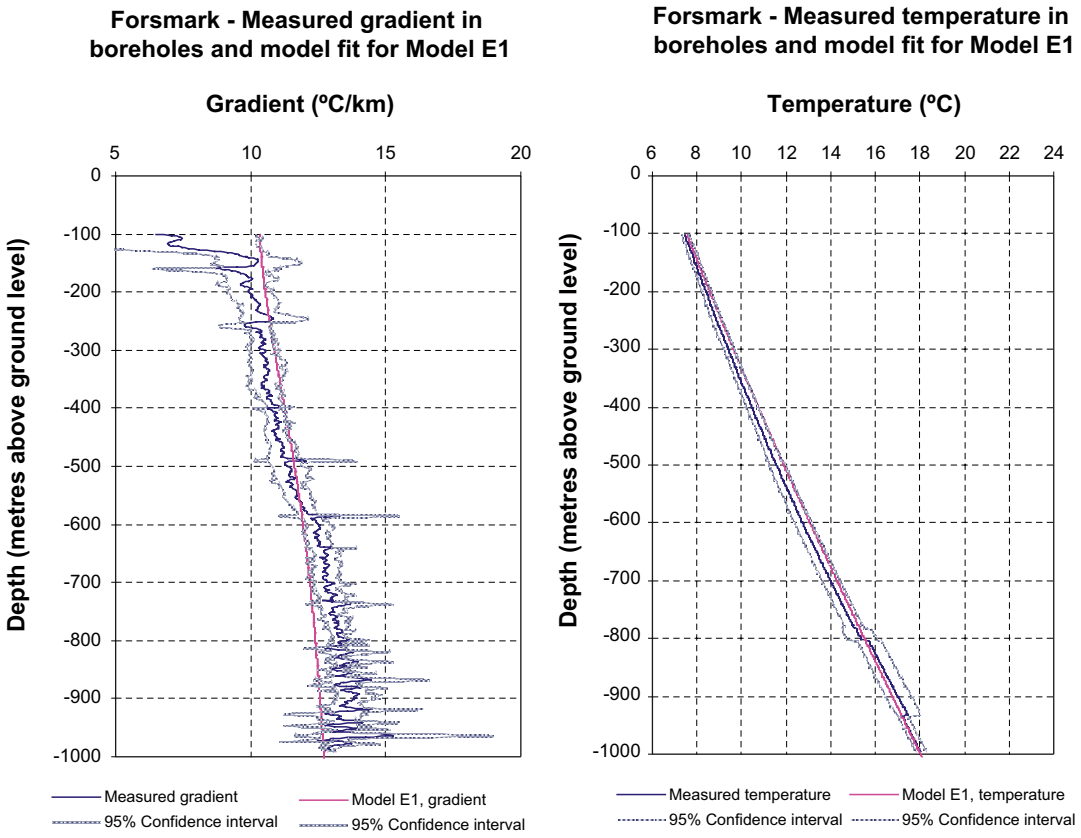

Figure 6-11. *Comparison between Model E1 and mean value from measurements: temperature gradient (left) and temperature (right).*

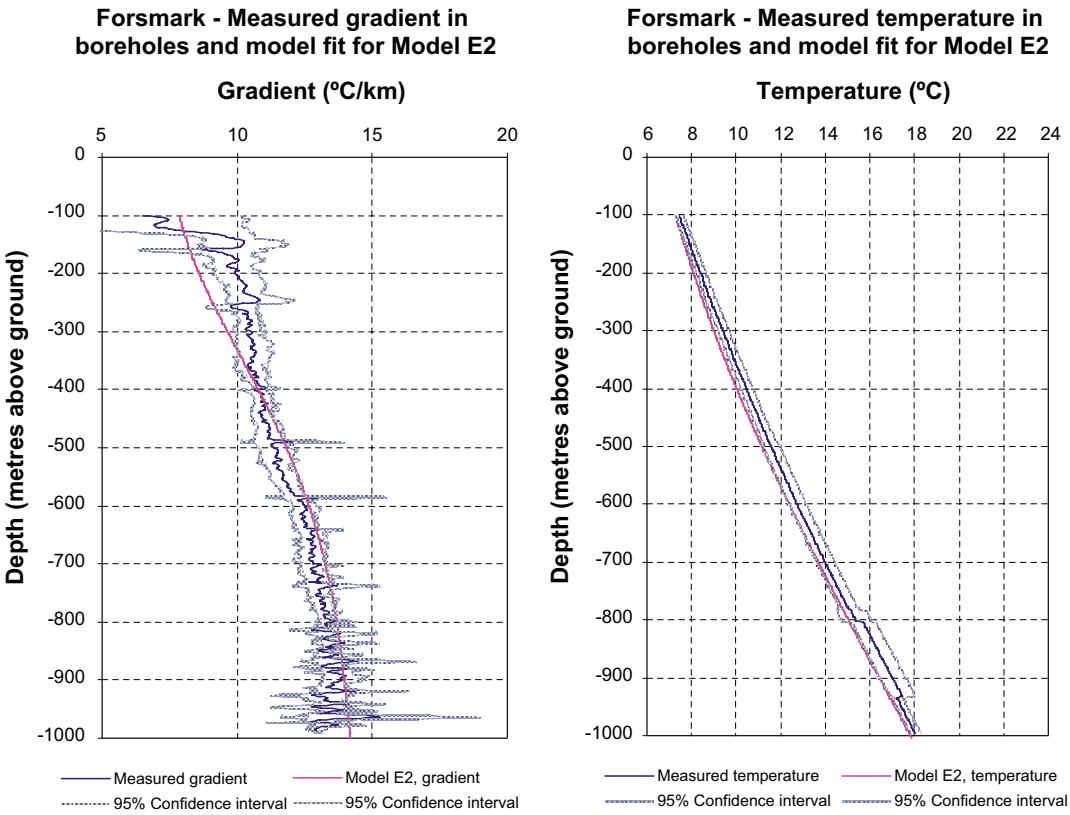

Figure 6-12. *Comparison between Model E2 and mean value from measurements: temperature gradient (left) and temperature (right).*

Table 6-4. Results for the general models at Forsmark. Model fit of gradient and temperature to measurements.

Model	Model fit of gradient		Model fit of temperature	
	r^2	RMSD [°C/km]	r^2	RMSD [°C/km]
A	0.89015	1.031	0.997482	1.227
B	0.889559	1.414	0.997166	0.939
C	0.887522	0.838	0.998905	0.593
D	0.887522	0.754	0.99894	0.429
E1	0.889559	0.926	0.997388	0.253
E2	0.88758	0.75	0.998945	0.396

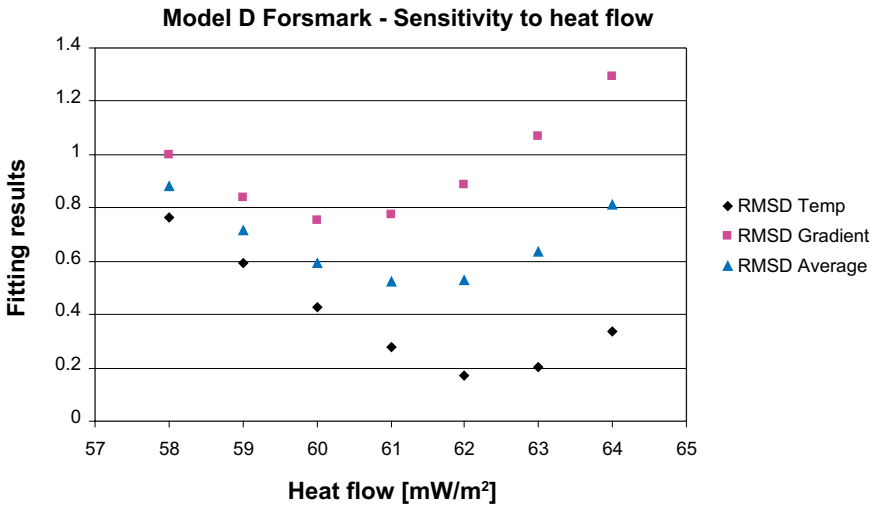

Figure 6-13. *Heat flow impact on RMSD for Model D. The RMSD average represents an average between the two other RMSD values.*

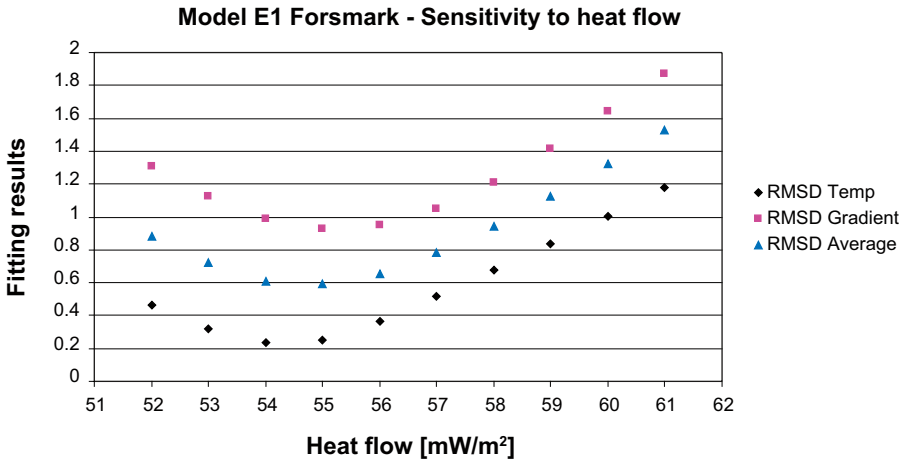

Figure 6-14. *Heat flow impact on RMSD for Model E1. The RMSD average represents an average between the two other RMSD values.*

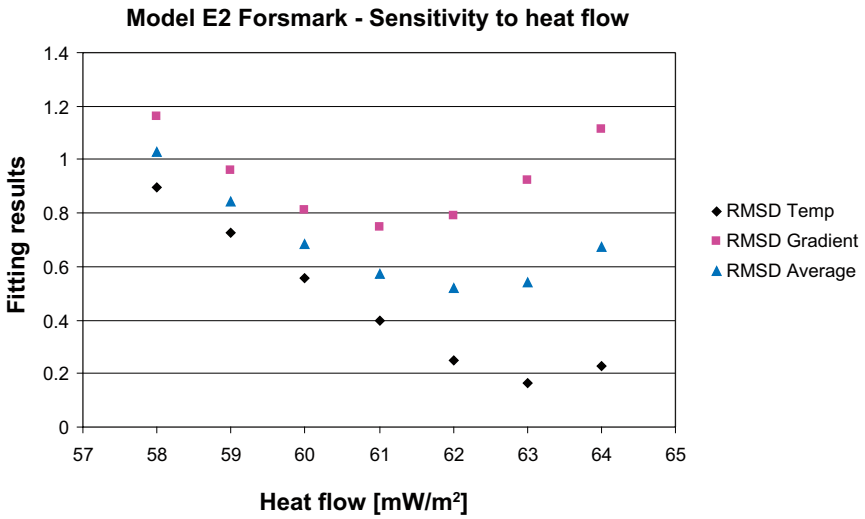

Figure 6-15. *Heat flow impact on RMSD for Model E1. The RMSD average represents an average between the two other RMSD values.*

The heat flow at which the temperature shows the best fit differs from the heat flow at which the gradient shows the optimal fit in all of the displayed models in Figure 6-13 to Figure 6-15. Larger weight should be put on the RMSD for the gradient profiles since the calculation method is based on the gradient, see Equation 2-7. The temperature profiles are calculated from the gradient model. The heat flow values in Table 6-3 for model D, E1 and E2 are the ones that result in the lowest gradient RMSD in Figure 6-13 to Figure 6-15.

The optimal heat flow varies between 55 to 61 mW/m^2 among the different models. However, except fitting results such as RMSD and r^2 it is important to look at the model profiles graphs to evaluate the visual fit. The data on larger depths is judged to be more reliable. Model C (see Figure 6-9) seem to have the best visual fit to data when putting larger weight on data at larger depth (better than the model with the slightly lower RMSD in Table 6-4, i.e. Model D). The heat flow of Model C is 59 mW/m^2.

6.2.3 Additional models

The parameters of the additional models are presented in Table 6-5 below. Additional models give optimised fitting results to measured data, but with parameter changes that are less bound to scientific data.

In Model F1 and F2, small adjustments are made to ΔT_3 and Q_0 compared to the general models in Section 6.2.2, in order to get a substantially better fit. Results are illustrated in Figure 6-16 and Figure 6-17.

Table 6-6 presents curve fitting statistics for the additional models.

There are no large differences between the fitting results for the two additional models. However, Model F2 has a significantly smaller portion outside the 95% confidence interval for the gradient profile. Both models remain within the 95% confidence interval for the temperature profile.

Table 6-5. Parameters of the additional models for Forsmark. κ = thermal diffusivity, λ = thermal conductivity, Q_0 = heat flow at ground level, A = radiogenic heat production, T_0 = ground temperature 228 kyrs BP, T_1 = ground temperature 11.4–1 kyrs BP, T_2 = ground temperature 1,000–0 yrs BP, ΔT_1 = ground temperature change 228–114 kyrs BP, ΔT_2 = ground temperature change 114–44.5 kyrs BP, ΔT_3 = ground temperature change 44.5–1 kyrs BP.

Model	K [mm^2/s]	λ [W/(m·K]	Q_0 [mW/m^2]	A [µW/m^3]	T_0 [°C]	T_1 [°C]	T_2 [°C]	ΔT_1 [°C]	ΔT_2 [°C]	ΔT_3 [°C]
F1	1.7	3.5	59	2.7	0	5	6.5	0	0	1
F2	1.7	3.5	58.5	2.7	0	5	6.5	0	0	1

Table 6-6. Results for the additional models in Forsmark. Model fit of gradient and temperature to measurements.

Model	Model fit of gradient		Model fit of temperature	
	r^2	RMSD [°C/km]	r^2	RMSD [°C/km]
F1	0.889772	0.588	0.998585	0.127
F2	0.889772	0.575	0.99861	0.14

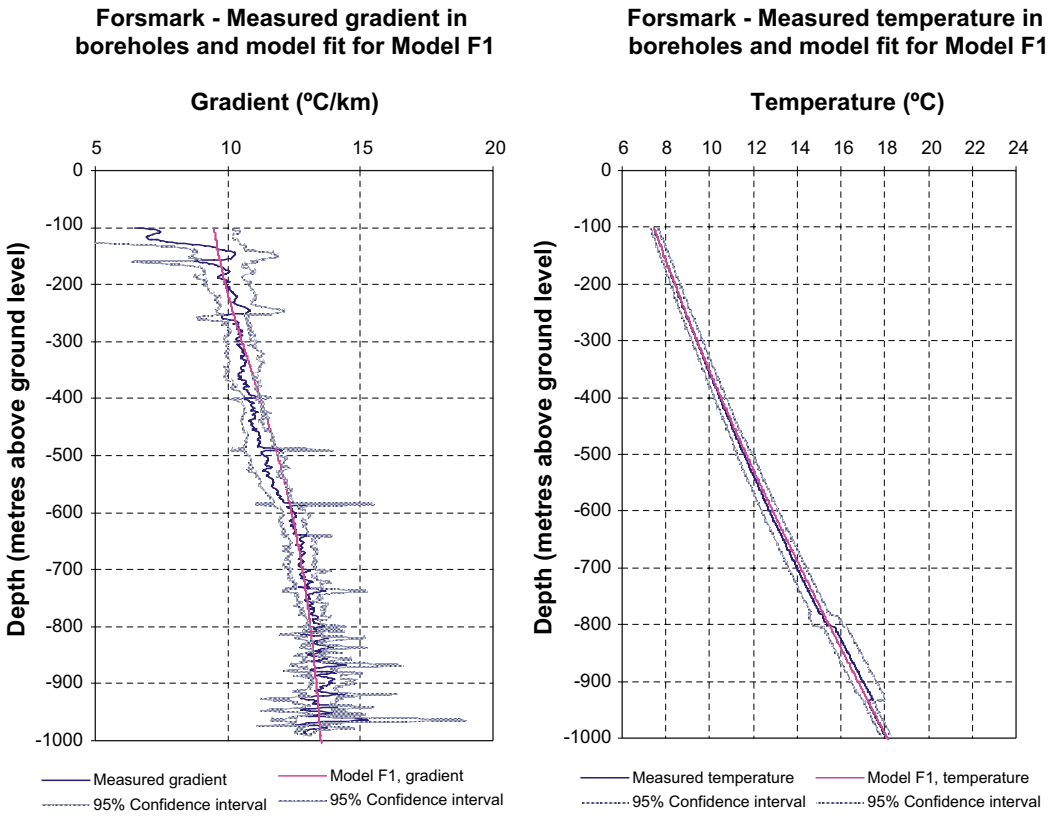

Figure 6-16. *Comparison between Model F1 and mean value from measurements: temperature gradient (left) and temperature (right).*

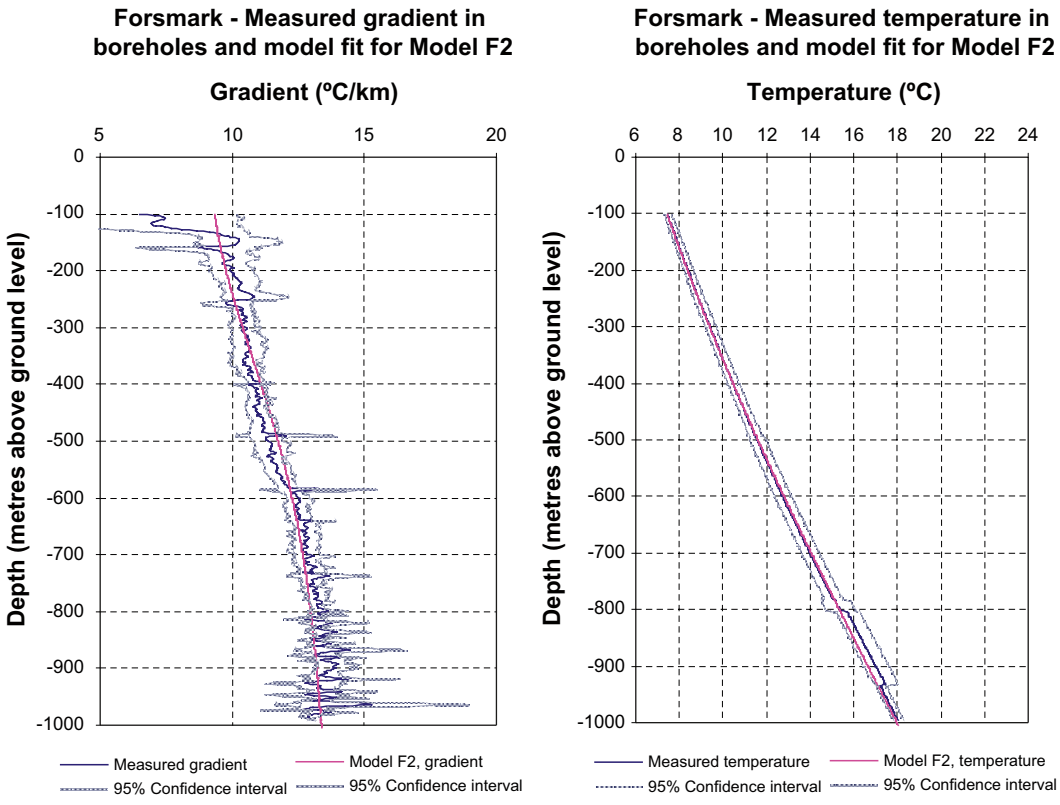

Figure 6-17. *Comparison between Model F2 and mean value from measurements: temperature gradient (left) and temperature (right).*

7 Geothermal calculations – Laxemar

7.1 Thermal data

7.1.1 Geothermal gradient and temperature

During the site investigation programme in Laxemar, fluid temperature in deep boreholes has been logged and temperature gradient has been calculated. The temperature and gradient profiles have been investigated for the "approved" boreholes KLX02, KLX05, KLX08, KLX18A and KLX20A, see Figure 7-1 /Sundberg et al. 2008b/. For location of boreholes, see Appendix 4.

As for Forsmark, the measured gradient profile for each borehole was smoothed with a moving average over about 100 m in order to reduce the significant "noise" in the original data. Certain data were also excluded, see Figure 7-2. Only data between 100 m and 892 m was included in the fitting analysis. The corresponding span for the mean gradient profile was 100 m to 864 m.

A mean profile between the different boreholes was then calculated for both the smoothed temperature and gradient profiles. In order to estimate the uncertainty of the measured mean profile, 95% confidence intervals were calculated, see Figure 7-3.

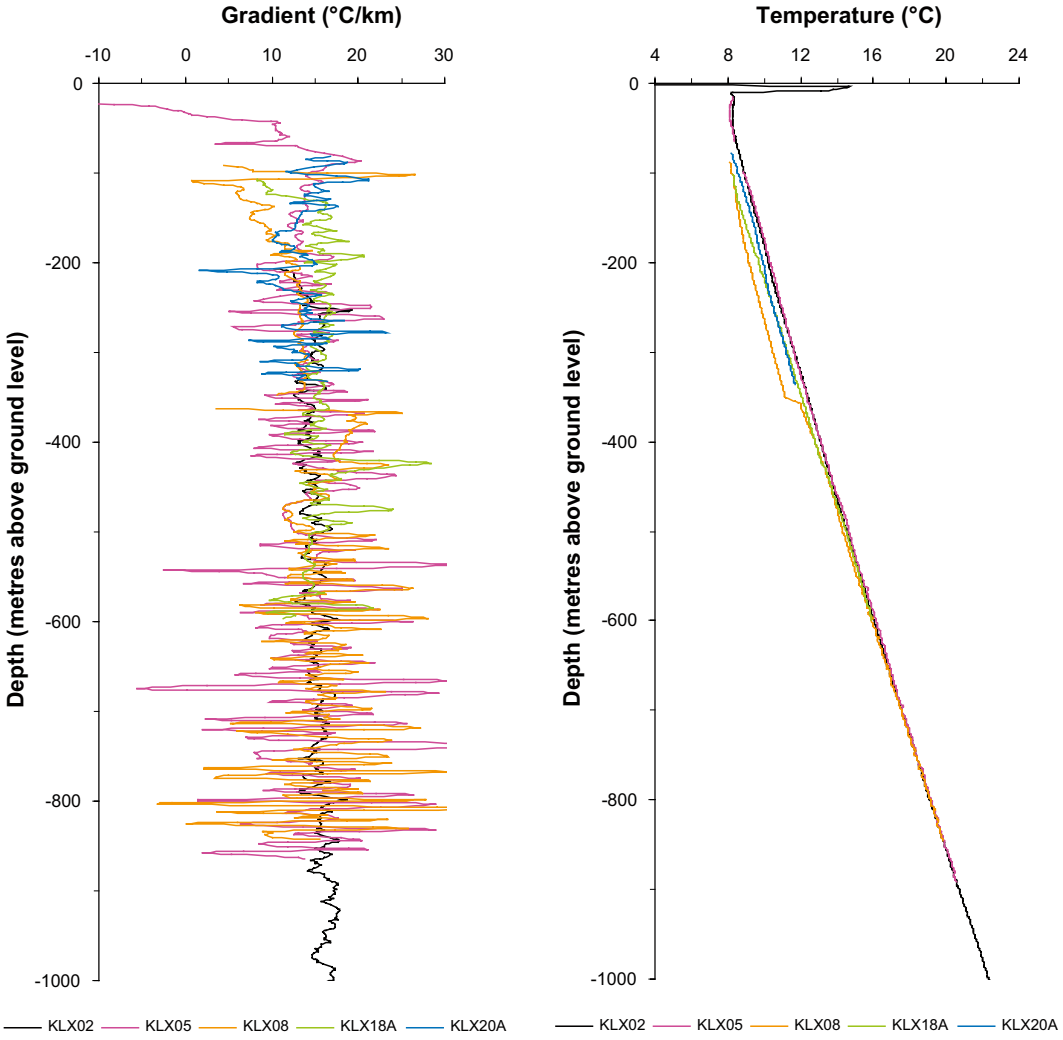

Figure 7-1. *Summary of temperature gradients (left) and temperatures (right) for the five reliable boreholes at Laxemar. The figure represents the raw data, before smoothing and exclusion. Results from fluid temperature loggings /Sundberg et al. 2008b/.*

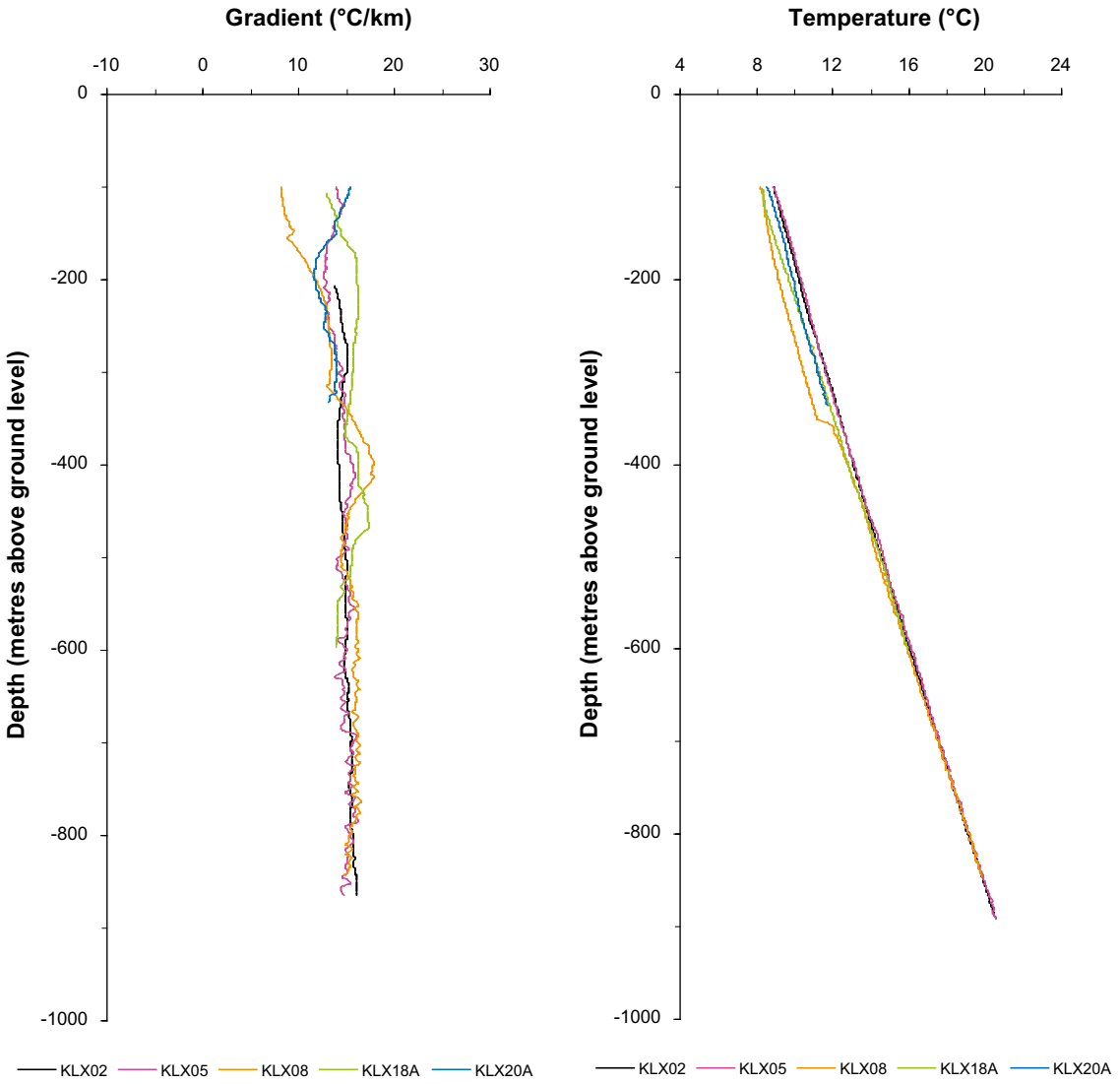

Figure 7-2. *Summary of temperature gradients (left) and temperatures (right) for the five boreholes at Laxemar. Data above and below certain levels have been excluded, and the gradients have been smoothed out with a 100 m moving average. The displayed data is the basis for the mean profiles used as reference in the modelling, see Figure 7-3.*

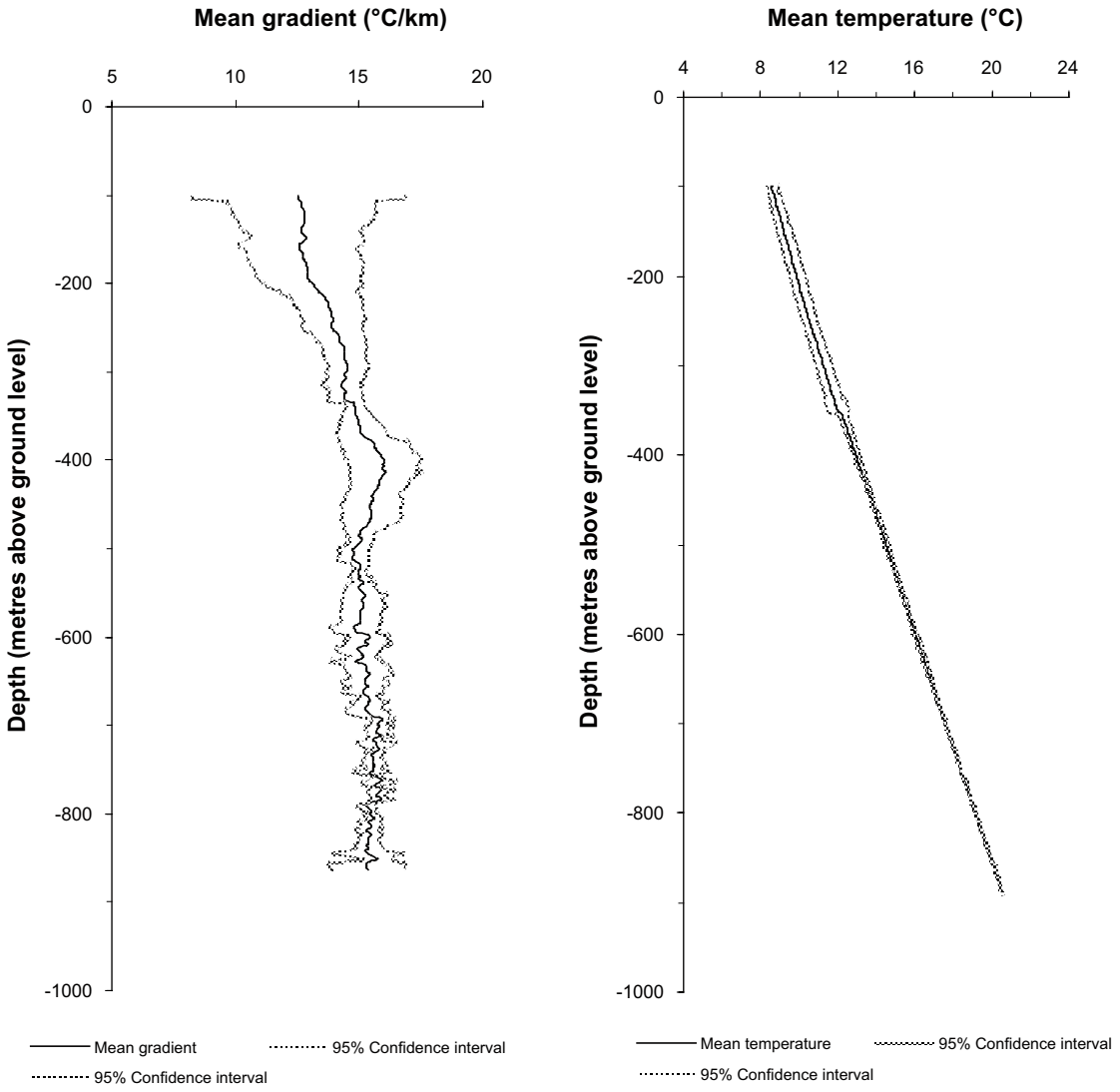

Figure 7-3. *The mean gradient (left) and mean temperature (right), used as reference in the modelling. 95% Confidence intervals are also displayed.*

7.1.2 Current surface temperature

The methodology for determining the current surface temperature is the same as for Forsmark. The current surface temperature according to /SKB 2006/ is 5.7°C. The logged borehole temperature data indicated a higher surface temperature. The current ground surface temperature was extrapolated from temperature data on larger depths using a linear model. A sensitivity analysis concerning different extrapolation ranges (the range of data that is used for the extrapolation) was then made (Table 7-1), and the current ground surface temperature was set to 7.27°C (202–102 m range).

The average annual air temperature recorded at Oskarshamn SMHI meteorological station, the "reference station" for air temperature in the Laxemar area, is 6.4°C /Werner et al. 2006/.

7.1.3 Thermal conductivity, diffusivity and internal heat generation

Thermal conductivity and diffusivity have been estimated in the site descriptive model /Sundberg et al. 2008b/. The mean thermal conductivity, heat capacity and thermal diffusivity at domain level is summarised in Table 7-2 for rock domains RSMA01, RSMM01 and RSMD01, respectively.

Domain RSMA01 has the highest mean thermal conductivity, RSMM01 the lowest. A thermal conductivity of 2.75 W/(m·K) has been used in the modelling for all rock domains. The main reason is that the area is rather complex. Each of the used boreholes penetrates up to three rock domains and it is only possible to use homogeneous rock properties due to model restrictions. There is also a large variability within each rock domain, see Figure 7-4. The mean value for the three domains is slightly higher than the chosen thermal conductivity. However, the Laxemar area is dominated by domain RSMM and RSMD which is the reason to put on more weight on the values for these domains. In a similar way the representative value of the thermal diffusivity has been chosen to $1.25 \cdot 10^{-6}$ m^2/s. A thermal anisotropy is also present at Laxemar. The mean thermal anisotropy factor is determined to be 15% in the Ävrö granite /Sundberg et al. 2008b/. It is reasonable to believe that the orientation of the thermal anisotropy coincides with the orientation of the foliation/lineation in the same way as earlier discussed for the Forsmark area. However, the orientation of the foliation varies in the Laxemar area. The vertical component of the thermal conductivity due to anisotropy is judged to be in the interval ±10% higher compared to the horizontal component.

Table 7-1. Extrapolated current ground surface temperature – sensitivity to extrapolation range.

	Extrapolated ground surface temperature, °C		
	202–102m	252–102m	302–102m
KLX02	7.58	7.60	7.54
KLX05	7.47	7.52	7.53
KLX08	7.27	7.16	7.09
KLX18A	6.85	6.79	6.77
KLX20A	7.19	7.28	7.25
Mean	7.27	7.27	7.24
Min	6.85	6.79	6.77
Max	7.58	7.60	7.54
Std. dev.	0.28	0.32	0.33
95% Confidence interval	7.02–7.52	6.99–7.55	6.95–7.52

Table 7-2. Mean thermal conductivity, heat capacity and thermal diffusivity of domain RSMA01, RSMM01 and RSMD01 /Sundberg et al. 2008b/. The thermal diffusivity is calculated from the thermal conductivity and the heat capacity.

Rock domain	Thermal conductivity W/(m·K)	Heat capacity MJ/(m^3·K)	Thermal diffusivity m^2/s
RSMA01	2.93	2.16	1.36E–6
RSMM01	2.65	2.21	1.20E–6
RSMD01	2.76	2.23	1.24E–6

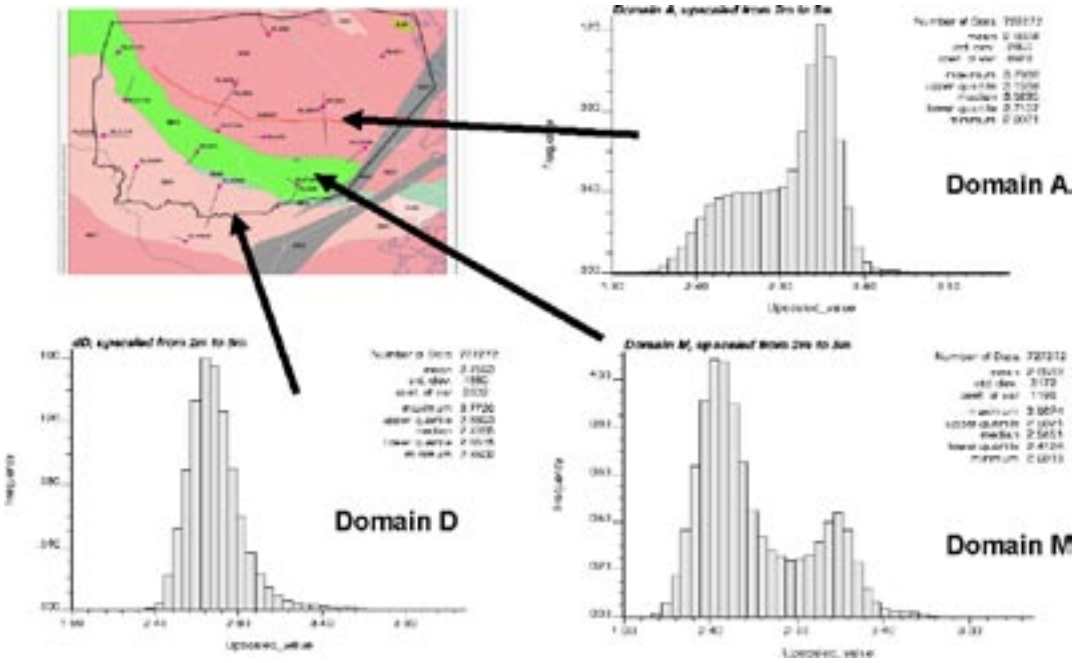

Figure 7-4. *Overview of the thermal conductivity in the different rock domains in Laxemar (modified from /Sundberg 2008b/).*

Both thermal conductivity and heat capacity are influenced by temperature. However, the thermal conductivity for the dominating rocks in Laxemar decreases by only a couple of percent when the temperature increases by 100°C. The heat capacity increases by approximately 25%. As mentioned above, temperature dependence aspects are not possible to consider due to limitations in the used model. However, the temperature effect on the thermal conductivity is judged to be insignificant. The temperature effect on the thermal diffusivity is larger approximately 4–5% in the actual temperature interval down to 1,000 m depth.

No spectrometry data for borehole samples was available in the Laxemar-Simpevarp area. Therefore no site-specific heat generation value was adopted. Instead a heat generation value from the data report to SR-Can /SKB 2006/ was used (3 μW/m³). However, surface spectrometer samples are available /Mattson et al. 2004/. In Table 7-3 internal radiogenic heat production is calculated from Equation 2-4 for the different rock types and domains. There is a large variability in data, especially for Ävrö granite and fine-grained granite. However, the variability is underestimated since for most samples there are no individual density determinations available, used to calculate the heat generation per volume. Instead a mean density has been used for most samples. The domain value for heat generation seems to be lower compared to the used value in the modelling below. The uncertainties in the used heat generation value are discussed in Chapter 8.

7.2 Model calculations

7.2.1 Introduction

The data used for the model calculations are partly based on the reference values in /SKB 2006/. As for Forsmark, the purposes of the model calculations were to study the effects of closer specifications concerning data from site models, and effects from changes in climate. Two sets of models were calculated. The General models (Table 7-4) study parameter changes that are closely bound to scientific data, while the Additional models (Table 7-6) give optimised fitting results to measured data, but with parameter changes that are less bound to scientific data. The reader is also referred to the reasoning given in Section 6.2.1 for Forsmark model calculations. For a description of the calculation procedure, see Appendix 1.

Table 7-3. Estimated internal heat generation for rock types and rock domains in Laxemar calculated from estimations of U, Th and K on surface samples /Petersson et al. 2004/ and for exception of a minor number of samples, mean densities for each rock type /Sundberg et al. 2008b/.

Rock type	Internal heat generation			Domain rock type proportion		
	Mean µW/m³	Std µW/m³	n	A %	M %	D %
Granite (501058)	2.13	0.68	6	1.0	2.0	0.4
Ävrö granite (501044)	2.07	0.61	62	88.0	75.0	1.1
Fine-grained granite (511058)	4.45	1.09	4	3.3	4.7	5.0
Pegmatite (501061)	2.76	–	1	0.3	0.5	1.4
Fine-grained dioritoid (501030)	2.17	0.27	3	2.7	0.4	0.3
Quartz monzodiorite (501036)	1.81	0.30	34	2.5	0.4	89.0
Fine-grained diorite-gabbro (505102)	0.89[1]	–	–	2.3	1.8	1.8
Diorite-gabbro (501033)	0.89	0.44	17	0.2	16.4	0.1
Dolerite (501027)	0.89[1]	–	–	–	–	2.1
Weighted mean internal heat generation				2.13	2.00	1.95

[1] Missing data, same value as for 501033 assumed

Table 7-4. Parameters for the general models at Laxemar. Data used for the model calculations at Laxemar. κ = thermal diffusivity, λ = thermal conductivity, Q_0 = heat flow at ground level, A = radiogenic heat production, T_0 = ground temperature 228 kyrs BP, T_1 = ground temperature 14–3.1 kyrs BP, T_2 = ground temperature 300–0 yrs BP, ΔT_1 = ground temperature change 228–114 kyrs BP, ΔT_2 = ground temperature change 114–44.5 kyrs BP, ΔT_3 = ground temperature change 44.5–3.1 kyrs BP, ΔT_4= ground temperature change 3,100–300 yrs BP.

Model	κ [mm²/s]	λ [W/(m·K)]	Q_0 [mW/m²]	A [µW/m³]	T_0 [°C]	T_1 [°C]	T_2 [°C]	ΔT_1 [°C]	ΔT_2 [°C]	ΔT_3 [°C]	ΔT_4 [°C]
A	1.25	2.75	63	3	0.7	4	5.7	0	0	0	0
C	1.25	2.75	63	3	0.7	4	7.27	0	0	0	0
D	1.25	2.75	58	3	0.7	4	7.27	0	0	0	0
E1	1.25	2.75	55	3	2.27	5.57	7.27	1.57	1.57	1.57	1.57
E2	1.25	2.75	59	3	–0.3	5.57	7.27	–1	0	0	0

7.2.2 General models

The general models are presented in Table 7-4 below. The modelled time periods with different ground temperatures at Laxemar are illustrated in Figure 7-5. No influence of anisotropy is assumed in the thermal parameters in the models but discussed in Section 8.1.

Model A (Figure 7-6) represents the reference values as presented in /SKB 2006/ (the report compiles information on climate related issues relevant for the long-term safety of a repository and supports the safety assessment SR-Can), i.e. the objective is to represent the SR-Can data without adjustments.

In Model C (Figure 7-7), the present ground temperature T_2 is raised to 7.27°C, a value that was found by extrapolation of the temperature profiles, see Table 7-1.

In Model D (Figure 7-8), Q is lowered from 63 to 58 mW/m². Figure 7-11 displays the sensitivity of fitting results for different RMSD values.

In Model E1 (Figure 7-9), the temperature of the whole climate data curve (except T_2) is raised with the same amount as T_2 was raised in Model C, i.e. 1.57°C. The heat flow is also changed to 55 mW/m². Figure 7-12 displays the sensitivity of fitting results for different RMSD values.

In Model E2 (Figure 7-10), the temperature of the whole first glacial cycle (228–114 kyrs BP) is lowered when setting ΔT_1 to –1°C. The heat flow is also changed to 59 mW/m². Figure 7-13 displays the sensitivity of fitting results for different RMSD values.

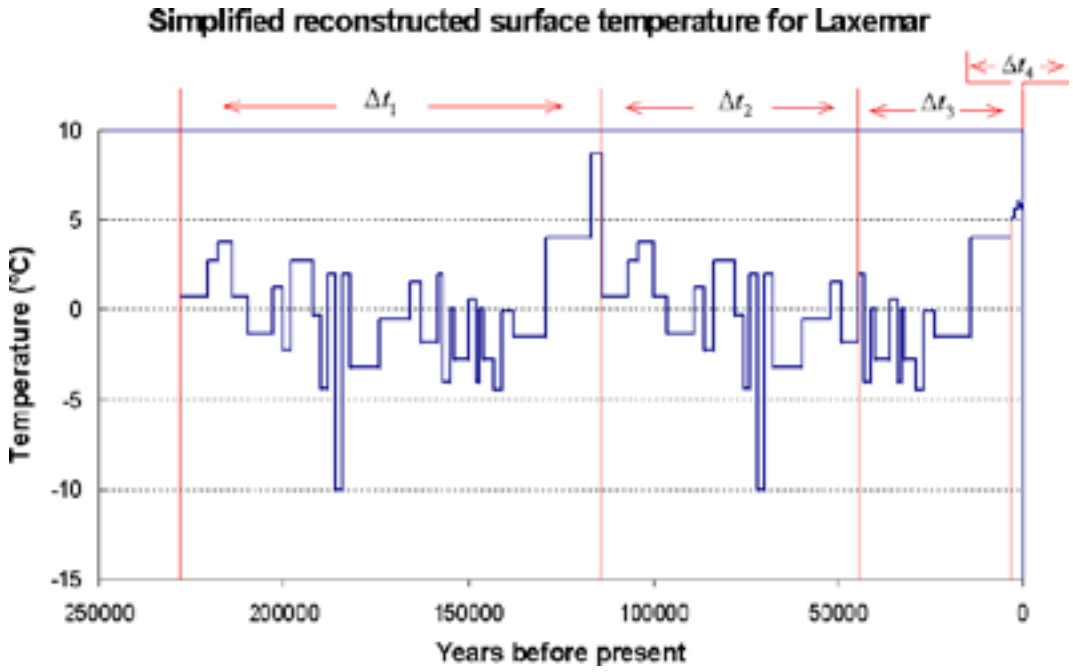

Figure 7-5. *Clarification of the time periods Δt_1, Δt_2, Δt_3, and Δt_4 corresponding to ΔT_1, ΔT_2, ΔT_3, and ΔT_4.*

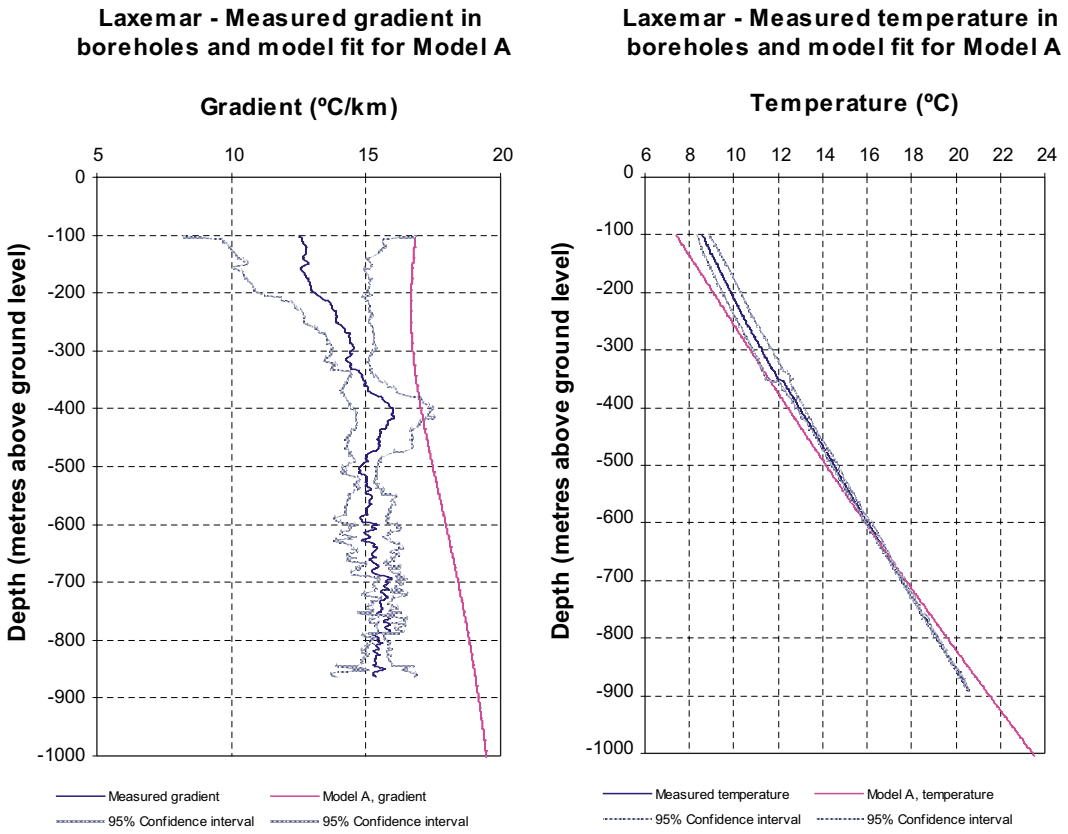

Figure 7-6. *Comparison between Model A and mean value from measurements: temperature gradient (left) and temperature (right).*

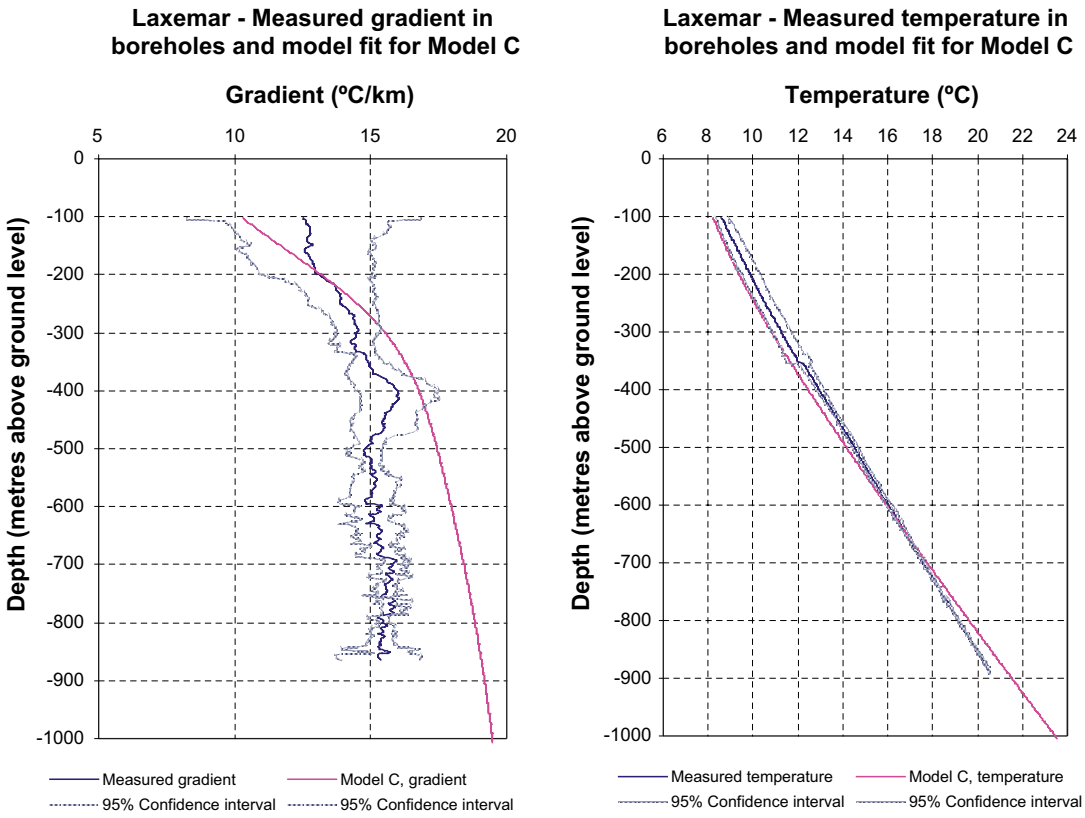

Figure 7-7. *Comparison between Model C and mean value from measurements: temperature gradient (left) and temperature (right).*

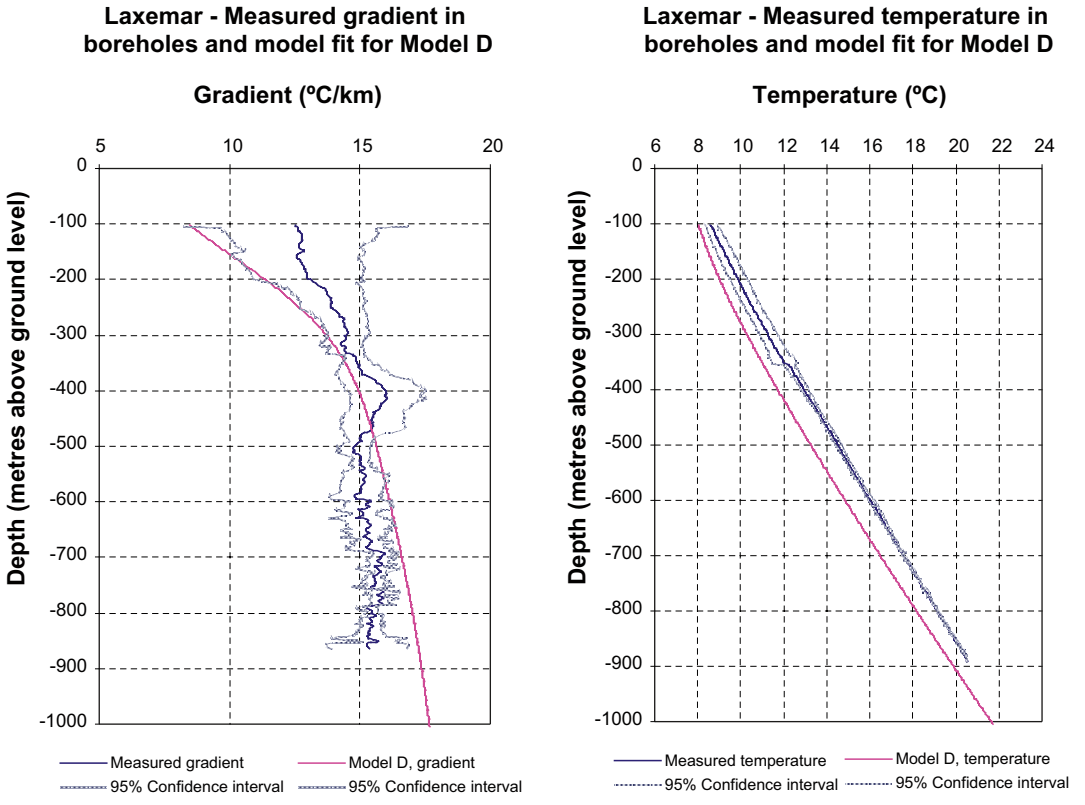

Figure 7-8. *Comparison between Model D and mean value from measurements: temperature gradient (left) and temperature (right).*

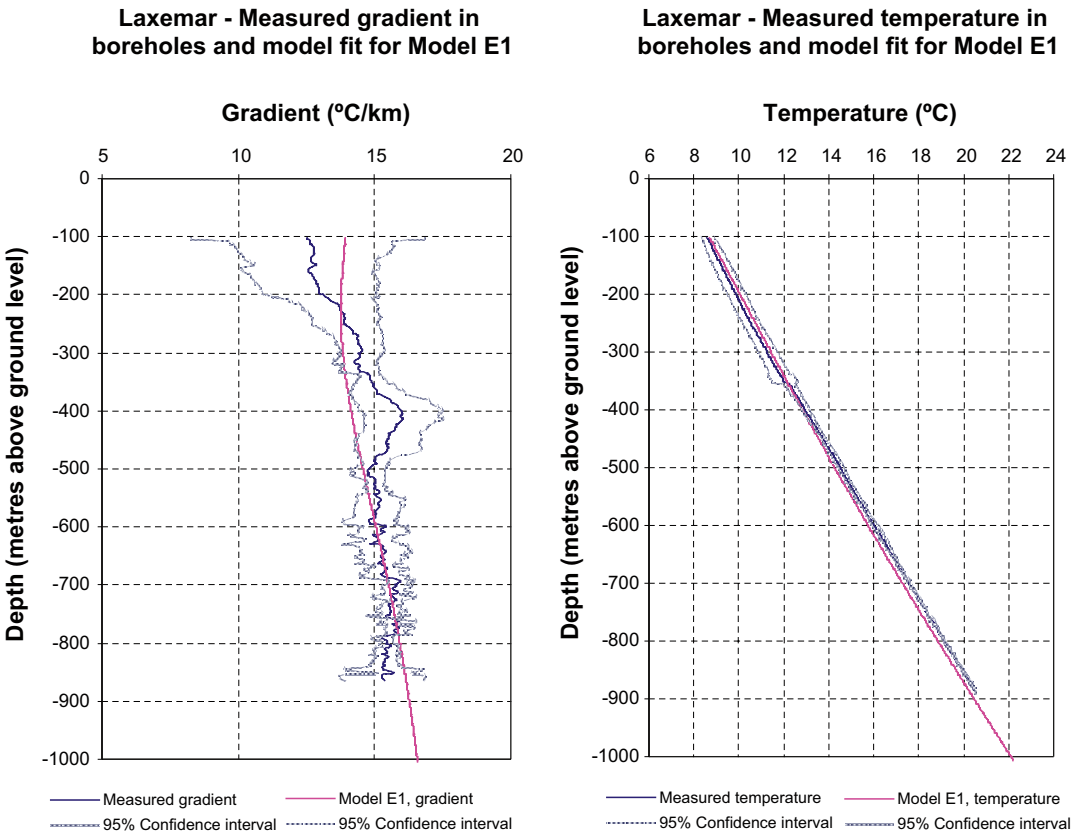

Figure 7-9. *Comparison between Model E1 and mean value from measurements: temperature gradient (left) and temperature (right).*

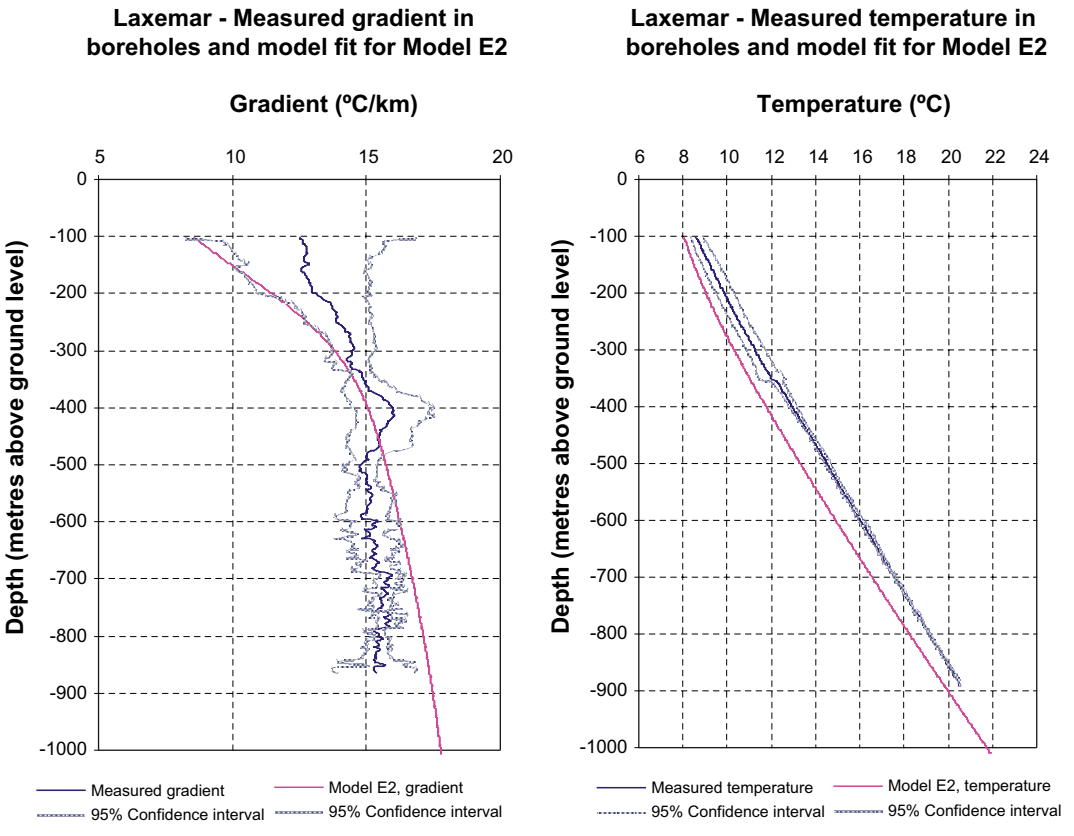

Figure 7-10. *Comparison between Model E2 and mean value from measurements: temperature gradient (left) and temperature (right).*

Model B was not calculated since no changes in thermal conductivity, thermal diffusivity and heat generation were needed compared to Model A.

Table 7-5 presents curve fitting statistics for the models concerning the sensitivity analysis. An explanation to r^2 and RMSD can be found in the corresponding section for Forsmark (6.2.2).

Model E1 seems to give the best fit among the general models concerning RMSD. The gradient r^2 (trend) value is however quite bad. Model D, E1 and E2 have the factor in common that they all experiment with changes of heat flow. Figure 7-11 to Figure 7-13 below present how RMSD is affected by changes in heat flow for these models.

The optimal heat flow regarding temperature differs from the optimal heat flow regarding gradient in all of the displayed models in Figure 7-11 to Figure 7-13. As for Forsmark, larger weight should be put on the RMSD for the gradient profiles since the calculation method is based on the gradient, see Equation 2-7. The temperature profiles are calculated from the gradient model. The heat flow values in Table 7-4 for model D, E1 and E2 are the ones that result in the lowest gradient RMSD in Figure 7-11 to Figure 7-13.

The optimal heat flow varies between 55 to 59 mW/m^2 among model D, E1 and E2. However, it is also important to study the results visually by looking at the profile graphs. When studying the profile graphs it is apparent that Model E1 (see Figure 7-9) generates a substantially lower gradient trend value compared to the other models, both on the upper and lower part of the profile. Regarding the trend fit on smaller depths it should be noted that the measured data is less reliable due to short term climate variations. On large depths the model profile have a lower slope than the measured profile. However, when looking at the deeper measured gradient profile used in Appendix 6 (KLX02 data was used in order to fit models to data on larger depths), that gradient profile also have lower slope on larger depths.

Model 3 in Appendix 6 is quite similar to Model E1 and it follows the measured gradient profile very well. Taking these facts into account, the low trend value of the E1 gradient can be seen as less important. This reasoning does also apply on Model D. A lower heat flow (than the current 58 mW/m^2 for Model D) would give a substantially better fit to the deeper part of the gradient profile. Figure 7-14 (left) displays a modified Model D in which the heat flow parameter has been lowered from 58 to 56 mW/m^2. The model is compared to the KLX02 measured gradient used in Appendix 6. A comparison to KLX02 data regarding Model E1 is also made, see Figure 7-14 (right).

It can be discussed whether Model D (with a lowered heat flow) or Model E1 give the best fit to gradient data at larger depths. However, both profiles argue for a heat flow around 56 mW/m^2.

Table 7-5. Results for the general models at Laxemar. Model fit of gradient and temperature to measurements.

Model	Model fit of gradient		Model fit of temperature	
	r^2	RMSD [°C/km]	r^2	RMSD [°C/km]
A	0.420958	2.878	0.999365	0.551
C	0.861559	2.269	0.998215	0.419
D	0.861559	1.477	0.997691	1.05
E1	0.420958	0.771	0.999214	0.227
E2	0.861344	1.477	0.997718	0.998

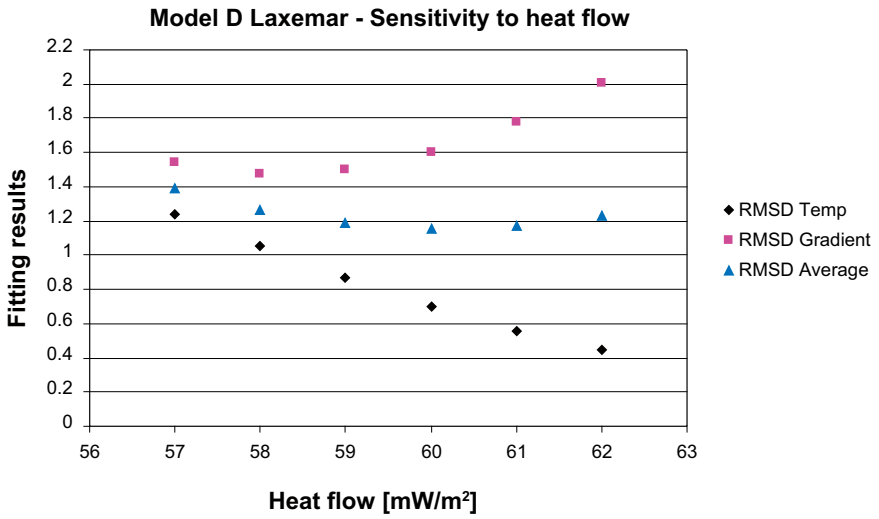

Figure 7-11. *Heat flow impact on RMSD for Model D. The RMSD average represents an average between the two other RMSD values.*

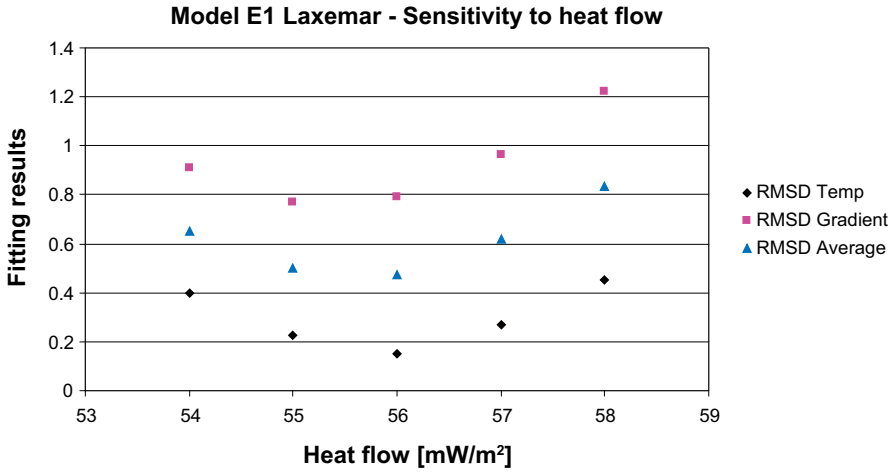

Figure 7-12. *Heat flow impact on RMSD for Model E1. The RMSD average represents an average between the two other RMSD values.*

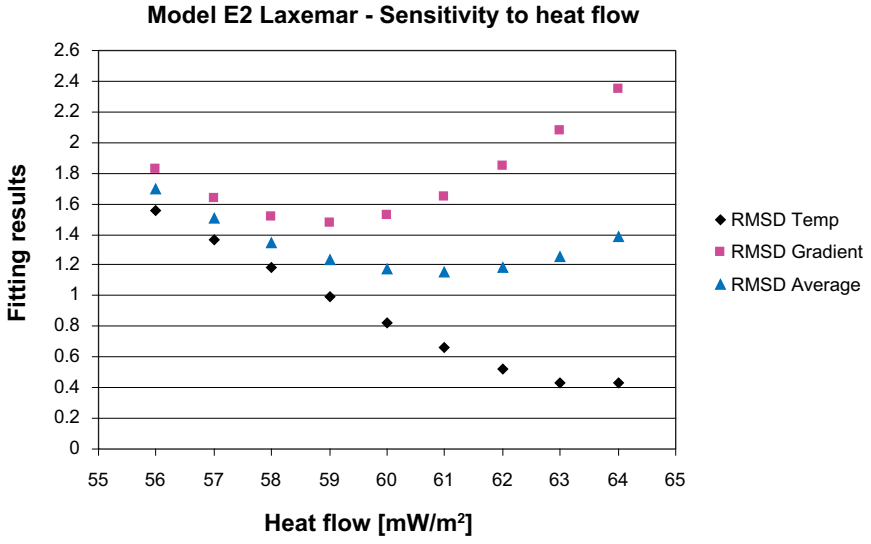

Figure 7-13. *Heat flow impact on RMSD for Model E2. The RMSD average represents an average between the two other RMSD values.*

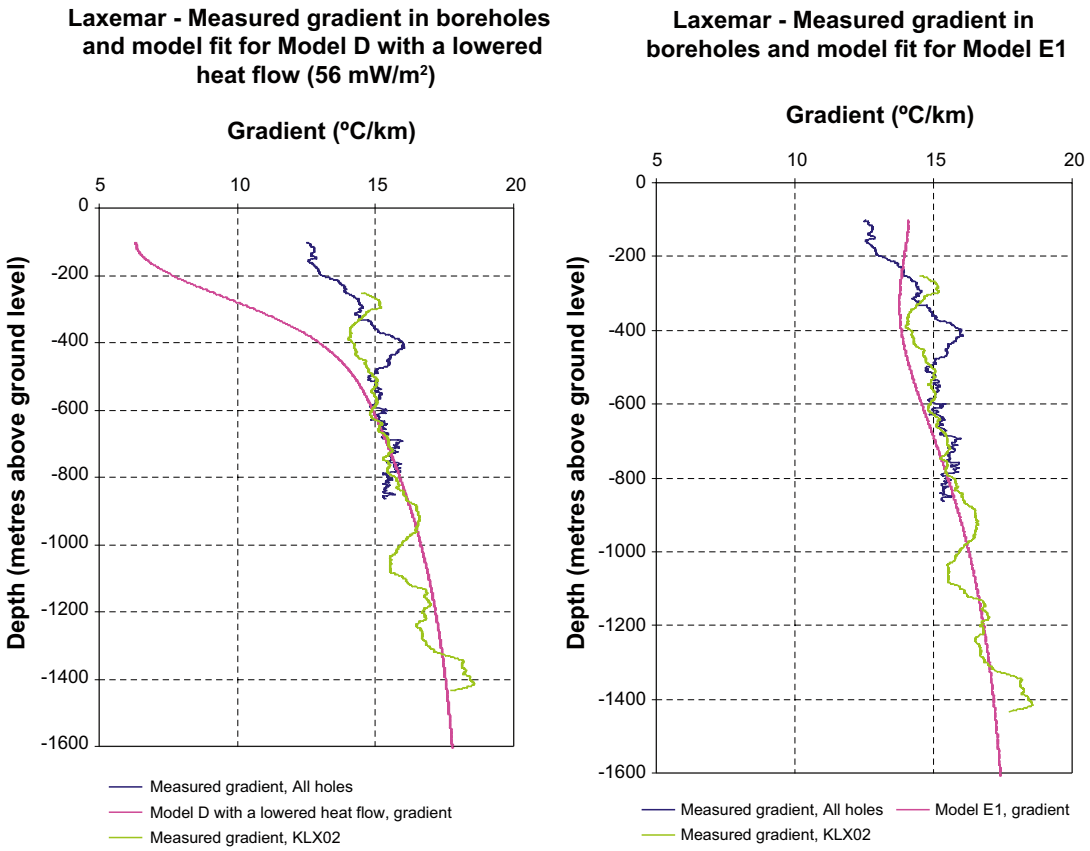

Figure 7-14. *Comparison to measured KLX02 gradient data. Modified Model D (left) and Model E1 (right). The modified Model D experiments with a lowered heat flow from 58 to 56 mW/m² in order to get a better fit on the deeper part of the gradient profile. Model E1 represents a heat flow of 55 mW/m².*

7.2.3 Additional models

The additional models are presented in Table 7-6 below. Additional models give optimised fitting results to measured data, but with parameter changes that are less bound to scientific data.

In Model F1 (Figure 7-15), F2 (Figure 7-16) and F3 (Figure 7-17), adjustments are made to Q_0 and climate parameters in order to get a substantially better fit.

Fitting results concerning the additional models are presented in Table 7-7 below.

The fact that Model F3 has the clearly best temperature fit and the next best gradient fit probably makes it the most accurate model. None of the models remains completely within the 95% confidence interval for gradient or temperature measurements, although both F2 and F3 are very close.

Table 7-6. Parameters for the additional models at Laxemar. Data used for the model calculations at Forsmark. κ = thermal diffusivity, λ = thermal conductivity, Q_0 = heat flow at ground level, A = radiogenic heat production, T_0 = ground temperature 228 kyrs BP, T_1 = ground temperature 14–3.1 kyrs BP, T_2 = ground temperature 300–0 yrs BP, ΔT_1 = ground temperature change 228–114 kyrs BP, ΔT_2 = ground temperature change 114–44.5 kyrs BP, ΔT_3 = ground temperature change 44.5–3.1 kyrs BP, ΔT_4= ground temperature change 3,100–300 yrs BP.

Model	K [mm²/s]	λ [W/(m·K)]	Q_0 [mW/m²]	A [µW/m³]	T_0 [°C]	T_1 [°C]	T_2 [°C]	ΔT_1 [°C]	ΔT_2 [°C]	ΔT_3 [°C]	ΔT_4 [°C]
F1	1.25	2.75	58	3	0.7	5	7.27	1	1	1	1
F2	1.25	2.75	55	3	0.7	7	7.27	0	1	1	1
F3	1.25	2.75	56	3	0.7	7	7.27	0	1	1	1

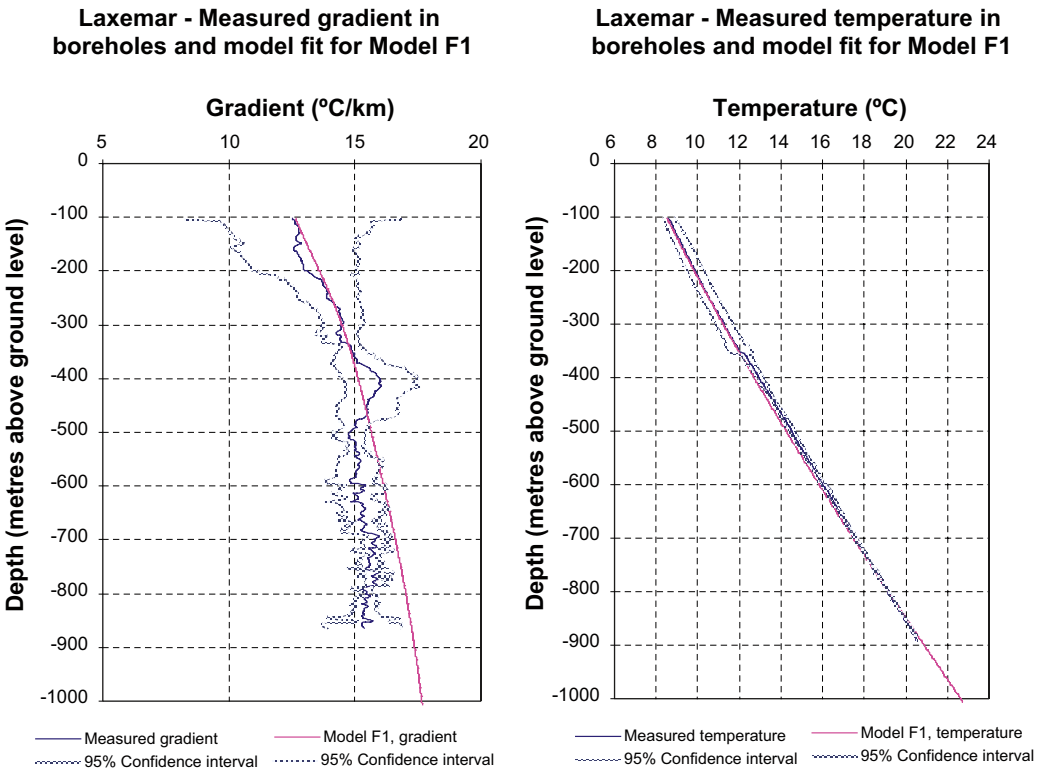

Figure 7-15. *Comparison between Model F1 and mean value from measurements: temperature gradient (left) and temperature (right).*

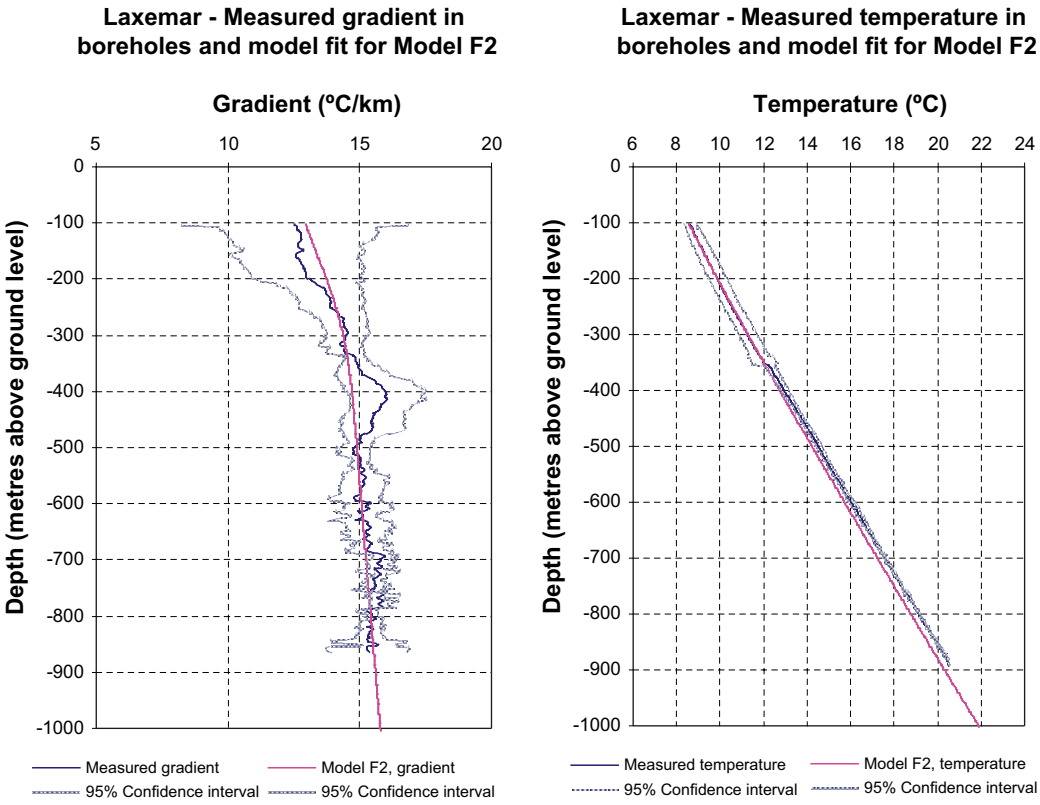

Figure 7-16. *Comparison between Model F2 and mean value from measurements: temperature gradient (left) and temperature (right).*

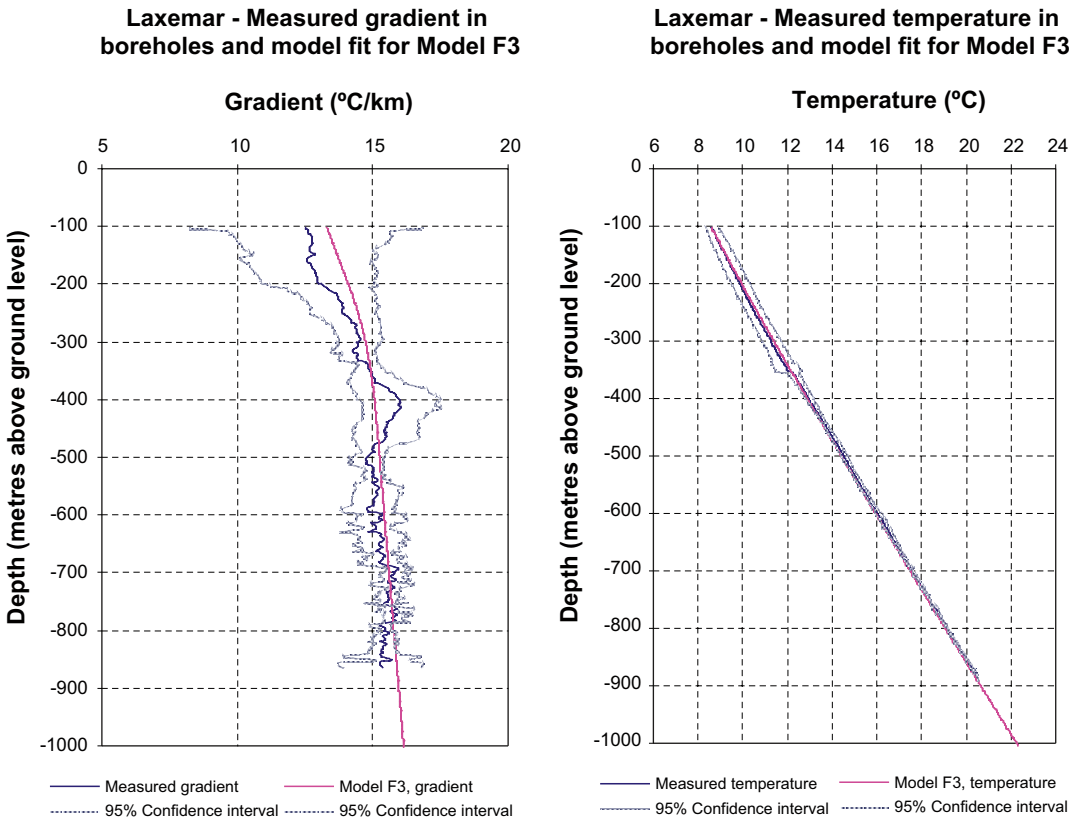

Figure 7-17. *Comparison between Model F3 and mean value from measurements: temperature gradient (left) and temperature (right).*

Table 7 7. Results for the additional models at Laxemar. Model fit of gradient and temperature to measurements.

Model	Model fit of gradient		Model fit of temperature	
	r^2	RMSD [°C/km]	r^2	RMSD [°C/km]
F1	0.7457	0.882	0.9990	0.151
F2	0.8381	0.465	0.9997	0.257
F3	0.8381	0.511	0.9997	0.089

8 Discussion

8.1 Discussion from a heat flow perspective

There is no independent way of determining the surface heat flow. The heat flow is normally calculated from the geothermal gradient and the rock thermal conductivity, and corrected for historical climate effects at the surface. According to Equation 2-7 there are also influences from internal heat generation in the rock and the rock thermal diffusivity. The latter has a significant effect on the penetration depth from a change in surface temperature. In addition, the data quality of these thermal parameters has a significant influence on the determined heat flow values.

The palaeoclimatically corrected surface mean heat flow at Forsmark and Laxemar has been calculated to 59 and 56 mW/m^2 respectively (see Section 6.2.2 and 7.2.2 respectively). In Laxemar, the gradient data from the deep borehole KLX02 (Appendix 6) has been one important reason for the calculated value instead of a slightly higher value. In the evaluation "best estimates" of thermal conductivity and other parameters have been used. However, there is a potential bias related to the thermal anisotropy at the sites. The estimated thermal anisotropy factor is of the same order of magnitude for the two sites. However, in Forsmark the vertical component of the thermal conductivity due to anisotropy is judged to be in the interval 0–15% higher than the horizontal component, see Section 6.1.3. The mean vertical component of the thermal conductivity for the different borehole sites is therefore judged to be 4% higher than the mean value of the thermal conductivity for each site. This means that the vertical component of the thermal conductivity may be 4% higher compared to the mean value used in the calculations in Section 6.2. The influence on the heat flow is of the same order of magnitude which implies that the heat flow in Forsmark may be underestimated by approximately 2 mW/m^2 (61 instead of 59 mW/m^2). In Laxemar the dip of foliation plane varies in the area (see Section 7.1.3) implying that the influence is judged to be small on the mean vertical component of the thermal conductivity.

The resulting palaeoclimatically corrected surface mean heat flow at Forsmark and Laxemar is estimated to 61 and 56 mW/m^2 respectively. The difference in heat flow between the two sites is small. The Laxemar area is rather close to the young Götemar granite with its significantly higher heat flow, which is mainly due to higher internal heat production. However, this situation seems not to affect the heat flow in Laxemar.

The heat flows uncorrected for palaeoclimatic effects are considerably lower than palaeoclimatically corrected surface heat flows. According to Equation 2-1 the uncorrected heat flow can be calculated from the geothermal gradient and the thermal rock conductivity. At the Forsmark site the uncorrected heat flow is 37 mW/m^2 using the gradient at 200 m depth (see Figure 6-3) and 50 mW/m^2 at approximately 900 m depth. At Laxemar the uncorrected heat flow is 36 mW/m^2 using the gradient at 200 m depth (see Figure 7-3) and 43 mW/m^2 at approximately 700–800 m depth. At both sites the heat production from the surface to the specific depth above should be added to calculate the uncorrected surface heat flows, approximately 0.5 and 2 mW/m^2 (0–200 m and 0–800 m). The correction for climate effects has a large influence on the surface heat flow evaluations in the Laxemar and Forsmark areas.

The above evaluated heat flows can be compared to other heat flow determinations from the Baltic shield. Palaeoclimatically corrected heat flows determined from 18 boreholes in the middle and south of Finland have been evaluated by /Kukkonen 1987/. The mean heat flow (mean of all depths and sites) increased from 32 mW/m^2 to 38.4 mW/m^2 after application of climatic corrections. A heat flow map over Sweden, corrected for palaeoclimatic effects, was published by /Balling 1995/, based on data from e.g. /Malmqvist et al. 1983, Landström et al. 1980/. The climate corrected heat flow value for the Forsmark area according to /Balling 1995/ is approximately 60 mW/m^2 and approximately the same in Laxemar. The above references are based on a limited number of data points which influences the resolution in the heat flow maps. In /Näslund et al. 2005/ a more detailed spatially distributed heat flow map of Finland and Sweden is presented. The map is based on measured γ-emission. The heat flow in the Forsmark area is estimated to 50–55 mW/m^2 based on the map. The corresponding value for the Laxemar area is estimated to 55–65 mW/m^2.

The evaluated site-specific surface heat flow for the two sites is of the same order of magnitude as for values given by other references /Balling 1995, Näslund et al. 2005/. However, the palaeoclimatical correction seems to be slightly larger in Forsmark and Laxemar compared to other references. The mean values of effect of palaeoclimatical compensation reported by /Kukkonen 1987/ and /Balling 1981/ are in the interval 6–8 mW/m^2 (central Finland and Denmark respectively) compared to 9 and 13 mW/m^2 in Forsmark and Laxemar respectively. It is reasonable to have different corrections for these locations due to differences in palaeoclimate. This implies the importance to use site-specific palaeoclimatic corrections if possible, as made in Forsmark and Laxemar.

The determined heat flow is associated with a number of uncertainties in (1) geothermal gradient, (2) palaeoclimatic correction, (3) radiogenic heat generation, (4) thermal conductivity and (5) thermal diffusivity.

The geothermal gradient, and indirectly the heat flow, can be disturbed by water movements /e.g. Drury and Jessop 1982, Kukkonen 1988/. The gradient is in general disturbed by water movements along parts of the borehole and by water bearing zones. However, this is judged to have only a minor influence on the large-scale gradient for the two investigation sites. Larger influences are also normally characterised by gradient anomalies and can be identified. However, if a major water-bearing zone, transporting a significant amount of thermal energy, occurs below a borehole, it is theoretically possible to have a biased gradient that can not be evaluated. However, there are no indications of such zones at the investigation sites in Forsmark and Laxemar.

The palaeoclimatic correction on the heat flow made in the present study is based on the climate curves described in Section 5.1–5.2. Because of the inherent uncertainty of these temperature curves, estimated to up to ±5 degrees in parts of the curve spanning the past 120 kyrs, a corresponding uncertainty is transferred to the palaeoclimatic correction. However, the comparison of the resulting climate correction made here, and the one made for geothermal heat flow in Finland and Denmark, shows that the correction made is in the same order of magnitude. The higher correction discussed above can be justified. The resulting uncertainty of the palaeoclimatic correction on the heat flow is estimated to be ±30% (i.e. ±3–4 mW/m^2). However, the uncertainty in earlier periods (before 120 kyrs BP) may be larger compared to ±5 degrees, resulting in a larger correction.

In the general models (A–E) the shape of the climate curve for each site is unchanged, except for the ground surface temperature, i.e. the curve is only shifted upwards or downwards in the different models. However, in the optimised models different parts of the climate curve is changed in order to create a better fit. The implications of this have not been further penetrated in this report.

According to the sensitivity studies, the temperature gradient decreases by approximately 3% when the climate model length is doubled to 240 kyrs. For a climate model length of 360 kyrs the gradient decreases approximately 5% in comparison to the 120 kyrs case. This means that the gradient in the modelling may be slightly overestimated, since a period of about 228 kyrs has been used. Consequently, the heat flow could be slightly overestimated in the modelling.

The radiogenic heat production has rather large uncertainties due to sparse data and uncertainties in data. This is further discussed in Section 8.2. However it is integrated in the surface heat flow value. In the modelling above, the heat generation influences the fit to the thermal gradient (see Figure 4-3). The influence is rather small when the heat generation is low, as at the investigated depths in both Forsmark and Laxemar. Therefore, any error in the heat generation is judged to provide only a minor contribution to the total uncertainty of the heat flow. A small influence on the thermal gradient fit should however be expected.

The thermal conductivity is approximately proportional to the heat flow. Uncertainties in the thermal conductivity are therefore directly transformed to uncertainties in the heat flow determination. There is variability in the large scale thermal conductivity, especially in Laxemar. This variability causes an uncertainty in the determined surface heat flow. However, this uncertainty is judged to be rather low since mean values have been used for both thermal conductivity and geothermal gradients. The uncertainty may however be larger in Laxemar than Forsmark since the different rock domains in Laxemar have larger differences in means compared to Forsmark. If we assume that the differences in mean thermal conductivity between the different domains correspond to the uncertainty in the heat flow, than the heat flow uncertainty can be approximated to ±5% in Laxemar and even lower

in Forsmark. The uncertainty related to anisotropy and the vertical component of the thermal conductivity should also be added.

In an ideal case, the temperature gradient reflects the large scale spatial distribution in thermal conductivity. Disturbances of the temperature loggings from water movements have made it difficult to evaluate this influence. However, part of the differences between the gradient in different boreholes are probably a result of different thermal conductivity. The large scale thermal conductivity is verified.

The temperature dependence on thermal conductivity would have a similar influence on the gradient as the internal heat generation. For the same reason as for inhomogeneous properties, this influence cannot be considered in the model. The temperature dependency is low in Laxemar but slightly larger in Forsmark. However, since the temperature change is small in the actual depth interval, temperature effects are judged to have a very small influence on evaluated heat flow (slight overestimation in Forsmark).

The thermal diffusivity controls the resulting temperature development in the ground due to changes in climate. In the evaluation, the ground temperature effect of variance in the diffusivity interferes with the variability in the lengths and change of different periods in the ground surface temperature curve. The effect of minor variations in the thermal diffusivity on the geothermal gradient is small at larger depths but such variations have a larger effect closer to the ground surface. Thus the effect of the temperature dependency for the thermal diffusivity is also small at here discussed depths.

It should be noted that there are uncertainties in the temperature logging data for the boreholes, and significant noise is apparent at both sites. The uncertainty is generally higher for Laxemar than for Forsmark since only five boreholes were considered reliable at Laxemar, in contrast to eight at Forsmark. Studying the confidence intervals in Figure 6-3 and Figure 7-3 it can be concluded that the Forsmark temperature data are more uncertain at greater depths than closer to the ground surface, while the opposite is true for Laxemar. Concerning temperature gradients, the Laxemar data is more uncertain than the data from Forsmark. The gradient for the deeper KLX02 (Appendix 6) has a different slope compared to other boreholes.

Studying the additional modelling at the two sites, it can be noted that a better fit is obtained when changing the shape of the climate curve and lowering the heat flow.

The mean heat flow may be slightly overestimated according to the discussion above. However, the evaluated palaeoclimatically corrected surface mean heat flows are suggested to be unchanged due to the overall uncertainties. If all uncertainties are considered, including data uncertainties, the total uncertainty in the heat flow determination is judged to be within +12 to –14% for both sites. However, if the climate in reality would be substantial different from the data used in this report, this may result in larger uncertainty interval for the heat flow.

8.2 Surface temperature and heat generation

Estimations of the current ground surface temperature have been made by extrapolations from measured temperature loggings (see Section 6.1.2 and 7.1.2). The mean extrapolated ground surface temperature in Forsmark and Laxemar is estimated to 6.5° and 7.3°C respectively. This is approximately 1.7°C higher for Forsmark, and 1.6°C higher for Laxemar compared to data in /SKB 2006/. The uncertainty in terms of 95% confidence interval is 6.3°–6.6°C in Forsmark and 7°–7.6°C in Laxemar.

Comparison with air temperature measurements shows that the extrapolated ground temperature is approximately 1–1.5°C higher for Forsmark (see Section 6.1.2), and 0.9°C higher for Laxemar (see Section 7.1.2). The difference between the air temperature and the extrapolated values is probably due to factors such as local climate conditions, heat contact resistance, and freezing processes near the ground surface. This deviates slightly from the calculations made in Figure 3-43 in /SKB 2006/. The Figure indicates no difference between the air temperature and the ground surface temperature at the actual mean annual air temperatures.

The calculated heat generation in Section 6.1.3 and 7.1.3 for the two sites have uncertainties. The mean heat generation in Forsmark and Laxemar is calculated to 3 $\mu W/m^3$ and 2 $\mu W/m^3$ respectively. The main reason for the higher value in Forsmark is the higher heat production in the dominant rock type, compared to Laxemar. The uncertainty is primarily related to subordinate rock type with significantly different (higher) heat production together with sparse data for these rock types. Especially pegmatite in Forsmark and fine-grained granite in Laxemar seems to have twice the heat production in dominant rock types. The uncertainty is related to very sparse data and lack of individual density determinations for these subordinate rock types. The uncertainty is judged to be within ±30% based on ±1 std for the dominant rock types.

9 Conclusions

9.1 Overall conclusions

A reasonably good fit was achieved between models and data for both Forsmark and Laxemar. However, none of the general models (A–E) achieved a fit within the 95% confidence interval of the measurements. This was in some cases achieved for the additional optimised models.

Several of the model parameters are uncertain. A good model fit does not automatically imply that "correct" values have been used for these parameters. Similar model fits can be expected with different sets of parameter values.

The palaeoclimatically corrected surface mean heat flow at Forsmark and Laxemar is suggested to be 61 and 56 mW/m^2 respectively, according to the discussion in the previous chapter. The gradient data from the deeper KLX02 in Laxemar (Appendix 6) has been one important reason for the calculated value.

The total uncertainty in the heat flow determination is judged to be within +12 to –14% for both sites, provided that the climate in reality was not substantial different from the data used in this report. The corrections for palaeoclimate are quite large and verify the need of site-specific climate descriptions.

The current ground surface temperature has been estimated by extrapolations from measured temperature loggings. The mean extrapolated ground temperatures in Forsmark and Laxemar are estimated to 6.5°C and 7.3°C respectively (7.6°C for KLX02 in Appendix 6). The extrapolated temperature values are higher compared to data in /SKB 2006/. Comparison with air temperature measurements shows that the extrapolated ground temperature is approximately 1–1.5°C higher. This deviates slightly from the calculations made in /SKB 2006/ which indicated no difference between the air temperature and the ground surface temperature for the actual mean annual air temperatures.

The parameters heat flow, thermal conductivity and current ground surface temperature have the greatest impact on the calculated temperature gradient and the temperature profiles. The calculated temperature gradient and the temperature profiles are also very sensitive to the modelling of the climate (surface ground temperature) during last 10 kyrs. Another conclusion is that the calculated temperature gradient profiles down to 1,000 m are affected by palaeoclimate occurring more than 240 kyrs ago even though the influence is rather small. The thermal conductivities estimated in the site descriptive models (SDM-Site) have been verified at large scale for each site.

The heat generation for the two sites have been calculated. The mean heat generation in Forsmark and Laxemar is estimated to 3 μW/m^3 and 2 μW/m^3 respectively. The uncertainty is judged to be within ±30%. The conducted study could be complemented with i) an improved evaluation of the effects of the spatial distribution, anisotropy and rock thermal conductivities and temperature dependence in thermal properties on the determination of heat flow, ii) an evaluation of the uncertainty in different parts of the palaeoclimate curve to achieve a better understanding of the effects on the geothermal gradient, and iii) an investigation of geothermal gradient and temperature profile in other deeper boreholes with site specific data.

9.2 Specific model conclusions for Forsmark

- Calculated gradient and temperature based on original data (reference values in /SKB 2006/) did not match corresponding measured data (Model A).
- While the updated site-specific parameters (Model B) produced a better fit to measured temperature data compared to Model A, the gradient fit was actually worse.
- By extrapolation of measured temperature data in boreholes it is indicated that the present ground temperature should be increased from 4.8°C to approximately 6.5°C. This was performed in Model C, with a substantially better fit as a result.
- Increasing the heat flow from 59 to 60 mW/m^2 (Model D) results in slightly better fitting values than Model C. However, when excluding the shallow depth interval because of data uncertainty, Model C gives a better fit.
- Shifting the whole climate curve upwards (except T_2) by the same amount as T_2 was increased in Model C (1.7°C) and lowering the heat flow to 55 mW/m^2 did not give a better fit (Model E1). On the contrary, a worse fit was achieved.
- In Model E2 the temperature of the whole first glacial cycle (228–114 kyrs BP) was lowered by 1°C and the heat flow was increased to 61 mW/m^2. The resulting fitting values were slightly better than to those of Model E1.
- In the additional Model F1, the temperature during 44.5–1 kyrs BP was increased by 1°C, resulting in the best-fit model according to the fitting statistics. The lowering of geothermal heat flow in model F2 resulted in not quite as good fitting measures for the temperature but slightly better gradient fit. The model remained within the 95% confidence interval for the temperature gradient data to a larger extent than model F1.

9.3 Specific model conclusions for Laxemar

- Calculated gradient and temperature based on original data (reference values) did not match corresponding measured data (Model A).
- By extrapolation of measured temperature data in boreholes it is indicated that the present ground temperature should be increased from 5.7°C to 7.3°C. This was performed in Model C, and while a better-than-earlier fit was achieved, the impact on this change was not as profound as in Forsmark.
- In model D the geothermal heat flow was lowered from 63 to 58 W/m^2. This resulted in an improved gradient fit, with the drawback of a worse temperature fit.
- In Model E1 the whole climate curve (except T_2) was shifted upward by the same amount as T_2 was increased in Model C (1.57°C). The heat flow was also decreased to 55 mW/m^2. While this resulted in a considerably better RMSD fit, the r^2 (trend) fit got worse. The trend fit to deeper KLX02 data was however judged to be good, and thus E1 was considered to achieve the best fit
- In model E2 the temperature of the whole first glacial cycle (228–114 kyrs BP) was lowered by 1°C and the heat flow was adjusted to 61 mW/m^2, resulting in a fit that is very similar to Model D.
- As regards the additional models, it should be noted that while Model F2 has the best gradient fit, it also has the worst temperature fit. Model F3 has a slightly worse gradient fit, but a considerably better temperature fit. Model F1 has clearly the worst gradient fit, but a reasonably good temperature fit. However, the considerably higher increase of T_1 in Model F2 and F3 might be questionable. None of the models remained completely within the 95% confidence interval of the measurements, even though Model F2 and F3 are very close.

9.4 Conclusions for KLX02 in Laxemar

In Appendix 6, specific model calculations on data from the deep borehole KLX02 have been made and evaluated. The following conclusion can be made:

- The best fit to measured data was obtained with a heat flow of 54 mW/m^2. This differs from the heat flow of 56 mW/m^2 that was obtained in the Laxemar simulations in Chapter 7.
- The dip of the foliation plane (the thermal anisotropy is assumed to coincide with the orientation of foliation) is based on very few measurements and is therefore uncertain. Also the local anisotropy factor is uncertain. These uncertainties are transferred to the calculation of the thermal conductivity in the vertical direction, which in turn is strongly related to the calculation of the heat flow.
- The current ground surface temperature extrapolated from KLX02 temperature loggings is 7.6°C, i.e. 0.3°C higher than in the overall Laxemar simulations, and nothing in the modelling suggests another value.
- Model 3 in Appendix 6 modifies the climate data by increasing the whole climate history curve except the current temperature by 1.88°C. This is equal to the difference between the current ground surface temperature for Laxemar in /SKB 2006/ and the extrapolated current ground surface temperature. The heat flow was also adjusted to 54 mW/m^2. These modifications result in a good fit for the gradient and especially for the temperature.

Acknowledgements

The report has been much improved by comments and suggestions from the appointed reviewers: Prof. Lars O Ericsson (Chalmers University of Technology, Göteborg) and PhD Thomas Wallroth (Bergab).

References

Back P-E, Wrafter J, Rosén L, Sundberg J, 2007. Thermal properties – Site descriptive modelling Forsmark – stage 2.2. SKB R-07-47, Svensk Kärnbränslehantering AB.

Balling N, Kristiansen J I, Breiner N, Poulsen K D, Rasmussen R, Saxov S, 1981. Geothermal Measurements and Subsurface Temperature Modelling in Denmark, Department of Geology, Aarhus University.

Balling N, 1995. Heat flow and thermal structure of the lithosphere across the Baltic shield and northern Tornquist zone. Tectonophysics, 244: 13–50.

Beardsmore G R, Cull J P, 2001. Crustal Heat Flow, A Guide to Measurement and Modelling, Cambridge University Press.

Björck S, Noe-Nygaard N, Wollin J, Houmark-Nielsen M, Hansen H J, Snowball I, 2000. Eemian lake development, hydrology and climate – a multi-stratigraphic study of the Hollerup site in Denmark. Quaternary Science Reviews, 19: 509–536.

Dansgaard W, Johnsen S J, Clausen H B, Dahl-Jensen D, Gundestrup N S, Hammer C U, Hvidberg C S, Steffensen J P, Sveinbjörnsdottir A E, Jouzel J, Bond G, 1993. Evidence for general instability of past climate from a 250-kyr ice-core record. Nature 364: 218–220.

Drury MJ, Jessop AM, 1982. The effect of a fluid filled fracture on the temperature profile in a borehole. Geothermics, vol. 11, pp 145–152.

Jaeger JC, 1965. Application of the theory of heat conduction to geothermal measurements. In: Lee WHK (ed), Terrestrial Heat Flow. Geophys. monograph Ser. 8, 7–23. Am. Geophys. Un., Washington DC8.

Johansson P-O, 2008. Description of surface hydrology and near-surface hydrogeology at Forsmark Site descriptive modelling SDM-Site Forsmark. SKB R-05-06, Svensk Kärnbränslehantering AB.

Kappelmeyer O, Haenel R, 1974. Geothermics with special reference to application. Geoexpl. Monogr. ser. 1, 4, 238 pp.

Kukkonen I, 1987. Vertical variation of apparent and palaeoclimatically corrected heat flow densities in the central Baltic shield. J. of Geodynamics 8: 33–53.

Kukkonen I, 1988. Terrestrial heat flow and ground water circulation in the bedrock in the central Baltic shield. Tectonophysics, 156: 59–74.

Körner S, Wahlgren L, 2000. Statistisk dataanalys. Studentlitteratur.

Landström O, Larson S-Å, Lind G, Malmqvist D, 1979. Värmeflöde i berg. Geologiska institutionen. B137. Chalmers University of Technology.

Landström O, Larson S, Lind G, Malmqvist D, 1980. Geothermal investigations in the Bohus granite area in the southwestern Sweden. Tectonophysics, 64: 131–162.

Malmqvist D, Larson S, Landström O, Lind G, 1983. Heat flow and heat production from the Malingsbo granite, central Sweden. Bull. Geol. Inst. Univ. Uppsala, 9: 137–152.

Mattsson H, Thunehed H, Isaksson H, 2005. Forsmark site investigation, Interpretation of petrophysical data from the cored boreholes KFM04A, KFM05A and KFM06A. SKB P-05-204, Svensk Kärnbränslehantering AB.

Mattsson H, Thunehed H, Triumf C-A, 2004. Oskarshamn site investigation, Compilation of petrophysical data from rock samples and in situ gamma-ray spectrometry measurements, Stage 2 – 2004 (including 2002). SKB P-04-294, Svensk Kärnbränslehantering AB.

Näslund JO, Jansson P, Fastook JL, Johnson J, Andersson L, 2005. Detailed spatially distributed heat-flow data for modeling of basal temperatures and meltwater production beneath the Fennoscandian ice sheet, Annals of Glaciology, 40:95–101.

Petersson J, Berglund J, Danielsson P, Wängnerud A, Tullborg E-L, Mattsson H, Thunehed H, Isaksson H, Lindroos H, 2004. Forsmark site investigation, Petrography, geochemistry, petrophysics and fracture mineralogy of boreholes KFM01A, KFM02A and KFM03A+B. SKB P-04-103, Svensk Kärnbränslehantering AB.

Schunn C D, Wallach D, 2005. Evaluating goodness-of-fit in comparison of models to data. In W. Tack (Ed.)., Psychologie der Kognition: Reden and Vorträge anlässlich der Emeritierung von Werner Tack (pp. 115–154). Saarbrueken, Germany: University of Saarland Press.

Sibbit W L, Dodson J G , Tester J W, 1979. Thermal conductivity of crystalline rocks associated with energy extraction from hot dry rock geothermal systems. J. Geophys. Res., 71, p 12.

SKB, 2006. Climate and climate-related issues for the safety assessment SR-Can. SKB TR-06-23, Svensk Kärnbränslehantering AB.

SKB, 2008. Site description of Forsmark at completion of the site investigation phase (SDM-Site Forsmark) SKB TR-08-05, Svensk Kärnbränslehantering AB.

SKB, 2009. Site description of Laxemar at completion of the site investigation phase (SDM-Site Laxemar) SKB TR-09-01, Svensk Kärnbränslehantering AB.

Stephens M, Fox A, La Pointe P, Simeonov,A, Isaksson H, Hermanson, J, Öhman J, 2007. Geology Forsmark. Site descriptive modelling Forsmark stage 2.2. SKB R-07-45, Svensk Kärnbränslehantering AB.

Sundberg J, 1993. Influence on temperature distribution in boreholes from rock type and water movements. Theoretical study and evaluation of field data. SKB AR 44-93-016, Svensk Kärnbränslehantering AB.

Sundberg J, Wrafter J, Ländell M, Back P E, Rosén L, 2008a. Thermal properties Forsmark. Modelling stage 2.3: Complementary analysis and verification of the thermal bedrock model. SKB R-08-65, Svensk Kärnbränslehantering AB.

Sundberg J, Wrafter J, Back P E, Rosén L, 2008b. Thermal properties Laxemar. Site description modelling. SDM-Site Laxemar. SKB R-08-61, Svensk Kärnbränslehantering AB.

Walsh J B, Decker E R, 1966. Effect of pressure and saturating fluid on the thermal conductivity of compact rock, J. Geophys. Res., 71, 12.

Werner K, Bosson E, Berglund S, 2006. Description of climate, surface hydrology, and near-surface hydrogeology. Preliminary site description Laxemar subarea – version 1.2. SKB R-05-61, Svensk Kärnbränslehantering AB.

Appendix 1

Calculation model

In order to generate the temperature and temperature gradient for the depth profile, a Mathcad model was constructed based on Equation 2-7. The model calculates the impacts of different factors and then combines them. A gradient vector for each factor is created and each vector element represents a value at a certain depth below ground.

The gradient vectors from each effect (geothermal heat flow, radioactive heat generation and climate changes) are added to form a new aggregated gradient vector. This gradient vector is then used together with the current ground surface temperature (T_2) to form a temperature vector (Equation 2-8). The current ground surface temperature is used as start value for the temperature vector (i.e. the temperature at ground level).

Regarding the gradient effect from climate changes; the ground surface temperature data is discretised and translated into two vectors; one concerning the absolute temperature in step format and one concerning the time for each temperature step change (see Figure 5-3 and Figure 5-4). Another vector (ΔT) is then produced concerning the size of the temperature step changes, i.e. the relative difference from one discrete temperature level to another (for example, absolute temperature vector 4, 10, 3, 6 becomes 6, –7, 3 in relative form). Equation 2-5 (a part of Equation 2-7) is used to calculate the temperature gradient effect from climate changes. More exactly, the gradient effect from a *single* temperature step change (at a specified number of years back in time) is calculated. The gradient is thus calculated in several steps, one for each climate temperature step change (Figure A1-1), and then superimposed to form an aggregated gradient vector for all the climate temperature steps combined.

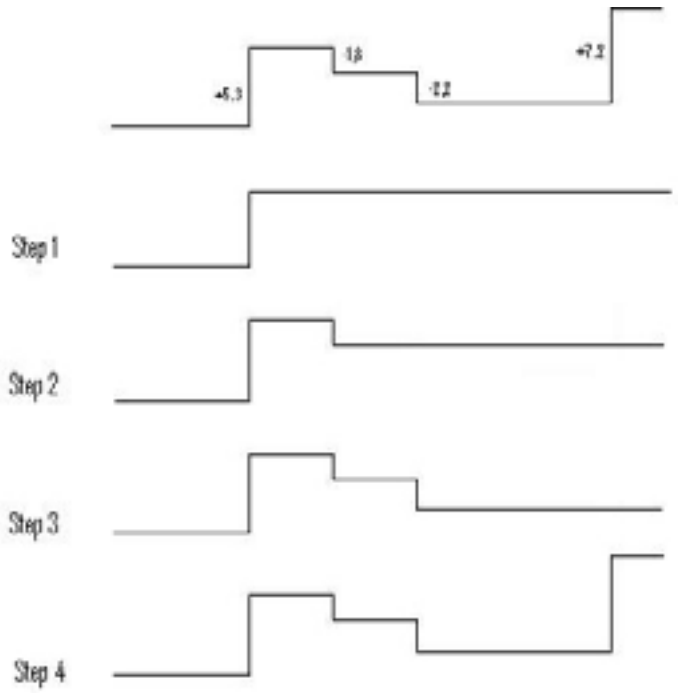

Figure A1-1. *The different steps used when calculating the temperature gradient profile.*

It is important to point out that the only relevant climate input data for the temperature gradient are the *relative* climate temperature changes and how long time that has passed since they occurred, i.e. not the absolute temperatures.

In other words, raising or lowering the whole climate history curve will not result in a different gradient vector as long as the present ground surface temperature also is changed by the same amount. It will however affect the temperature vector since it uses the present ground surface temperature as start value. In the above calculations, a constant value of the current ground surface temperature has been used, with the exception of early adjustments.

When the final gradient and temperature vectors (geothermal heat flow, radioactive heat generation and climate effects) have been calculated they are compared to measured temperature and gradient data. Statistical measures (goodness-of-fit statistics) of how well the model fits the measured data are then produced (r^2 and RMSD).

As input, the model needs parameters of thermal diffusivity (κ), thermal conductivity (λ), heat flow at ground level (Q), heat production in rock due to radioactivity (A), and discretised climate temperature history data.

Appendix 2

Extended depth graphs – Forsmark

Here, the fitting graphs for Forsmark are presented, with the maximum depth of 4,000 meters below ground, instead of 1,000 meters as shown earlier. Please note that no confidence intervals are displayed in this section.

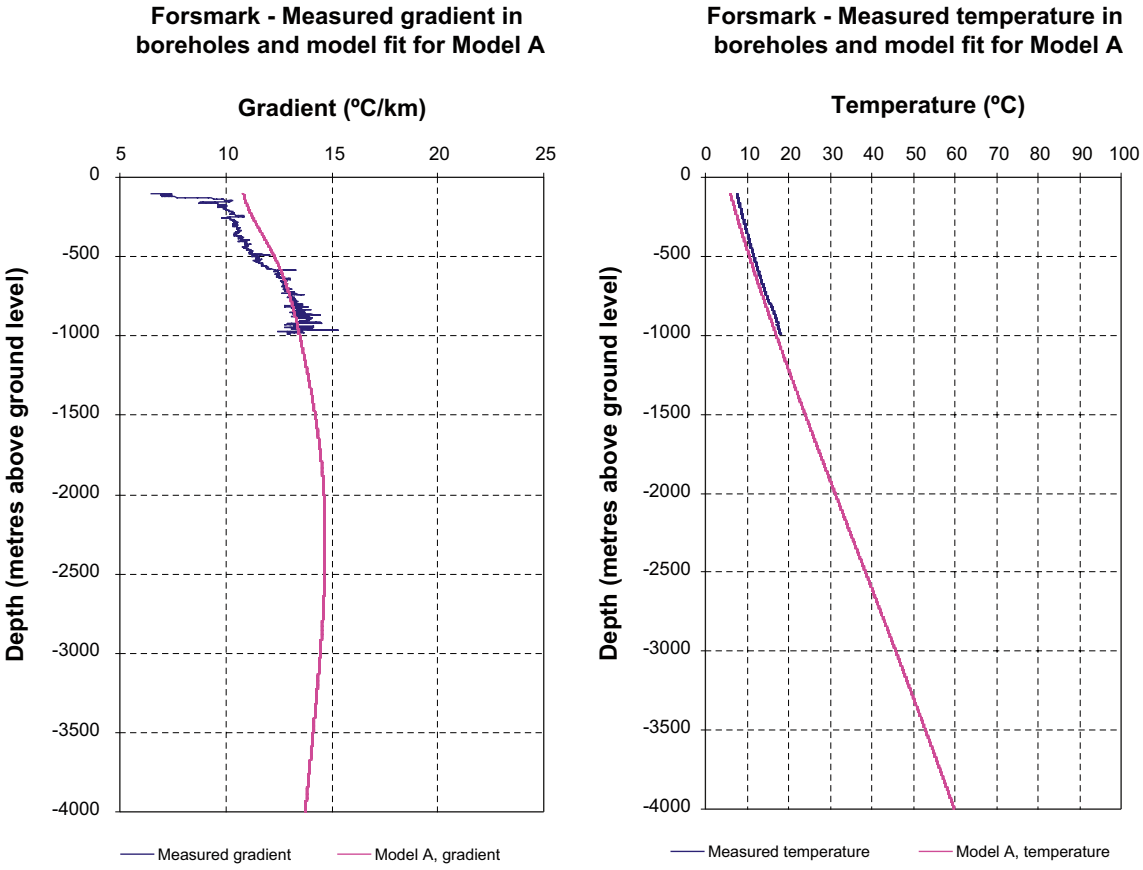

Figure A2-1. *Model A, 4,000 meters downwards instead of 1,000 m.*

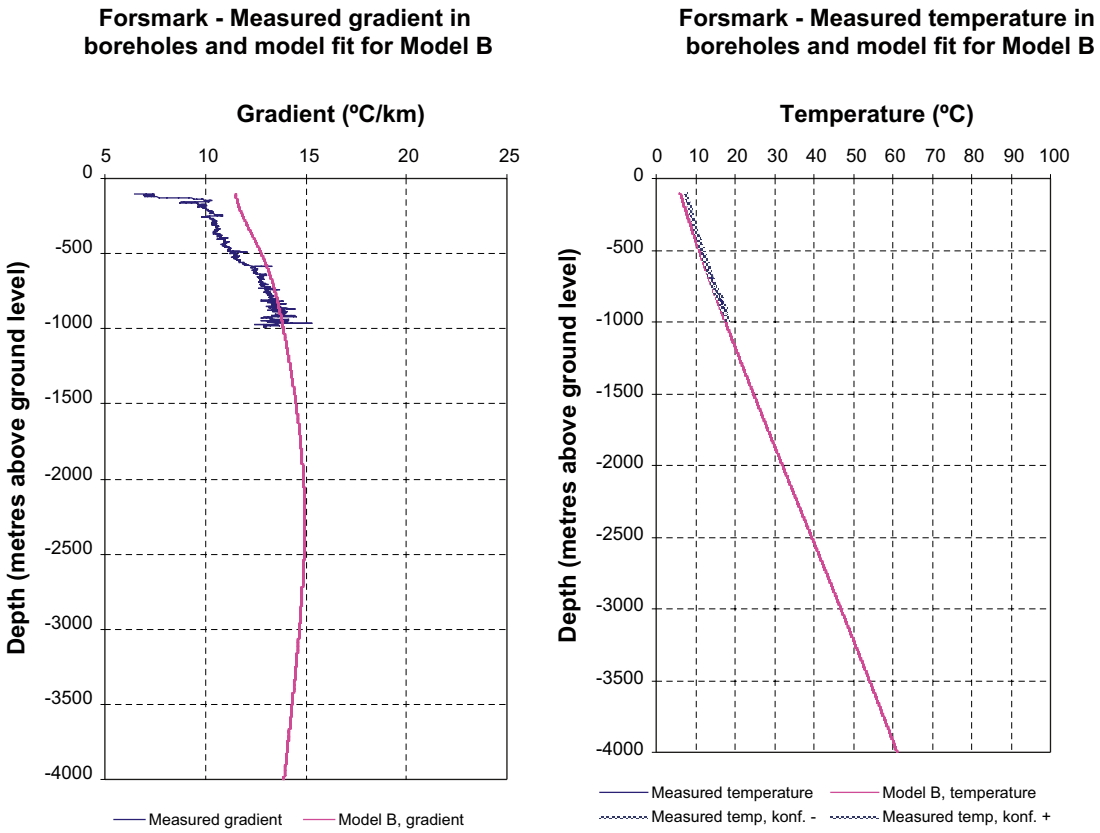

Figure A2-2. *Model B, 4,000 meters downwards instead of 1,000 m.*

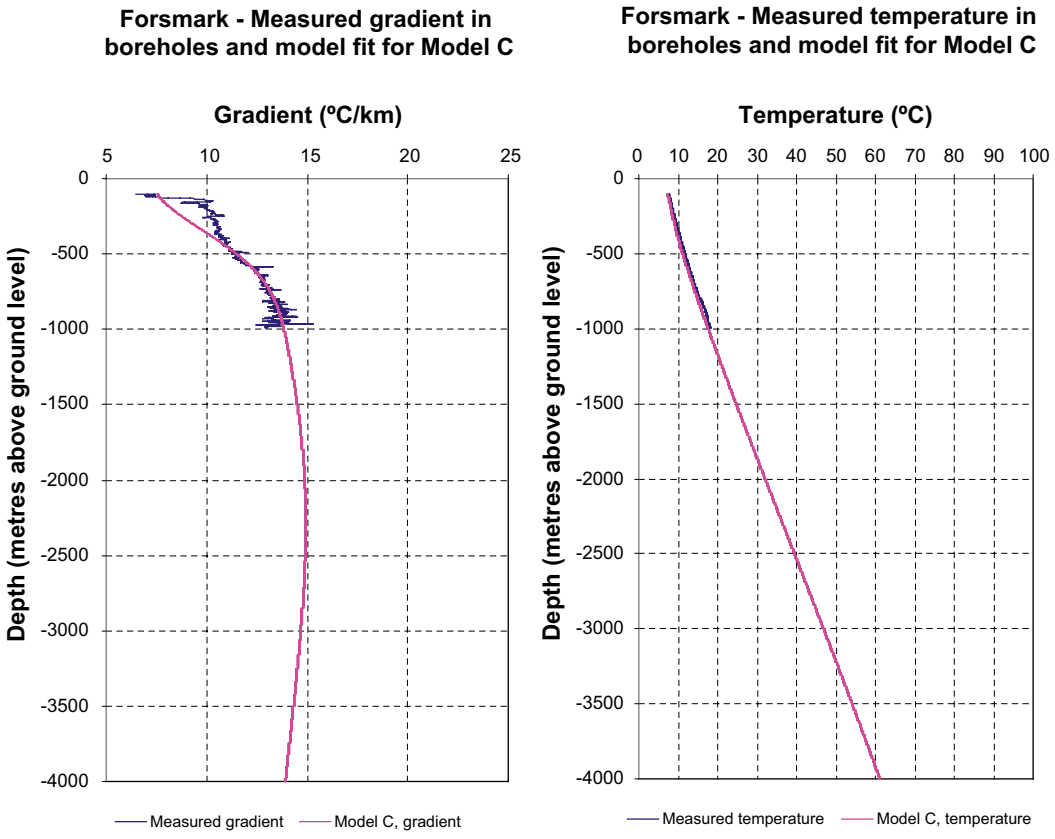

Figure A2-3. *Model C, 4,000 meters downwards instead of 1,000 m.*

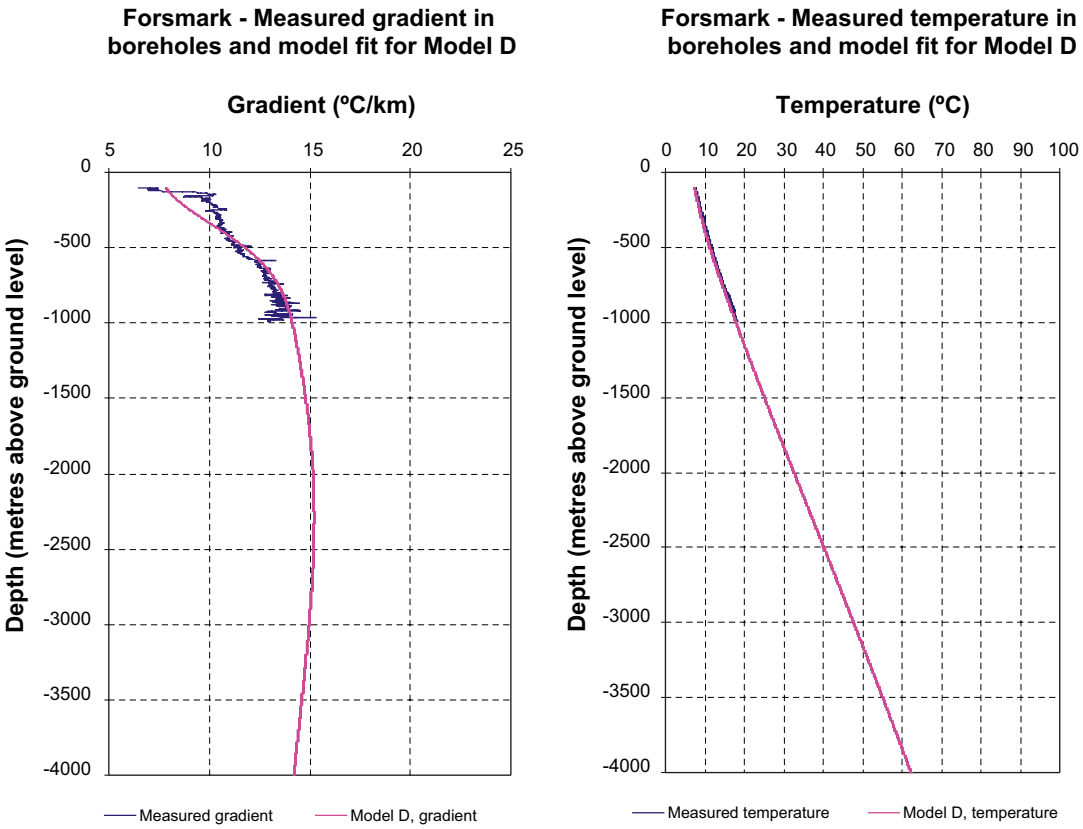

Figure A2-4. *Model D, 4,000 meters downwards instead of 1,000 m.*

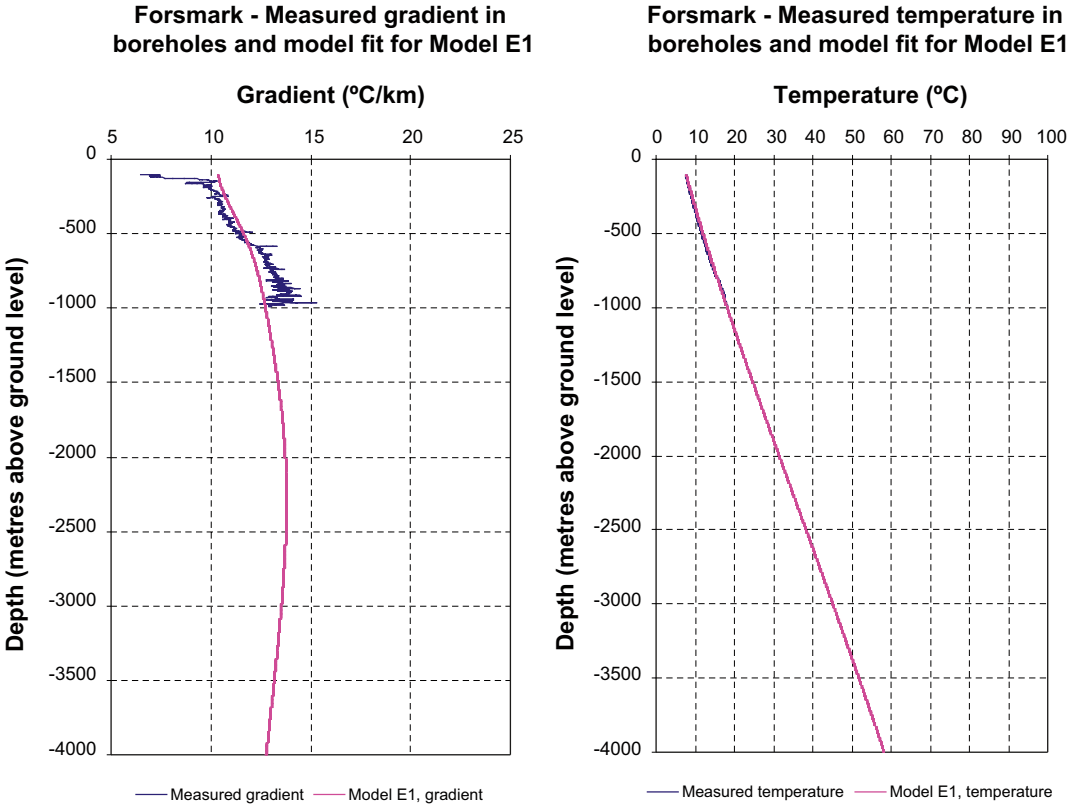

Figure A2-5. *Model E1, 4,000 meters downwards instead of 1,000 m.*

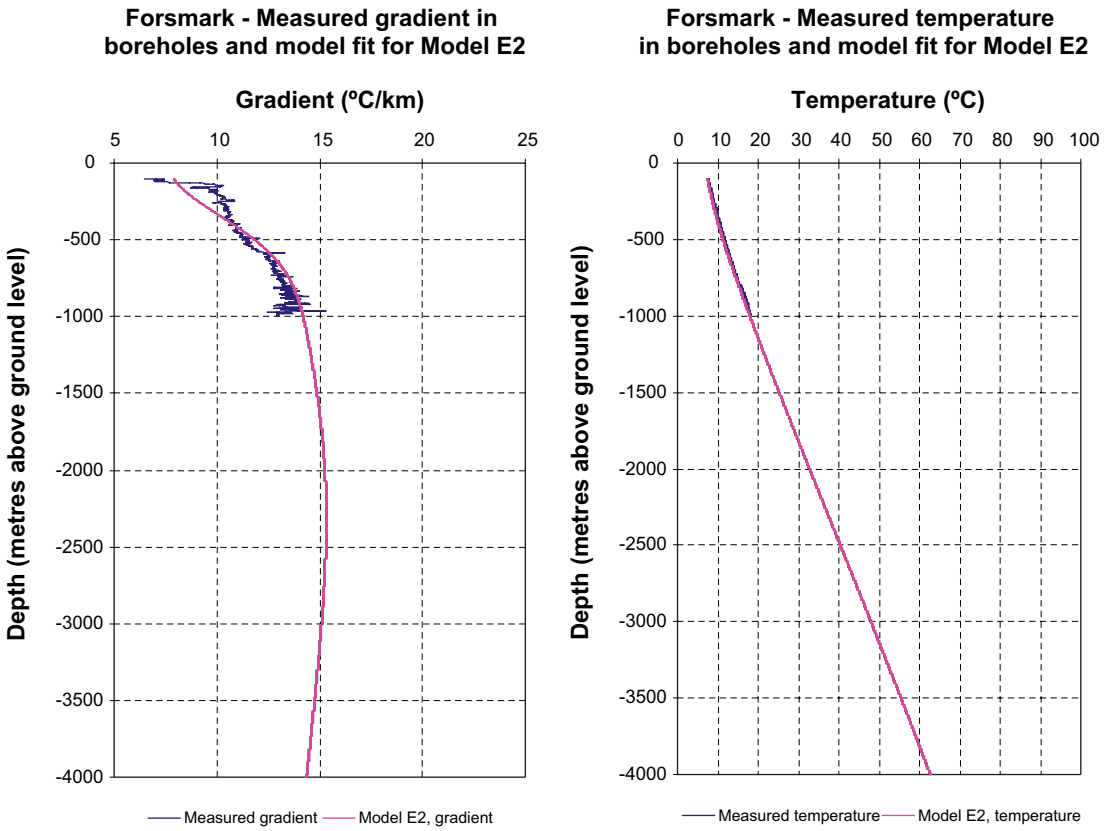

Figure A2-6. *Model E2, 4,000 meters downwards instead of 1,000 m.*

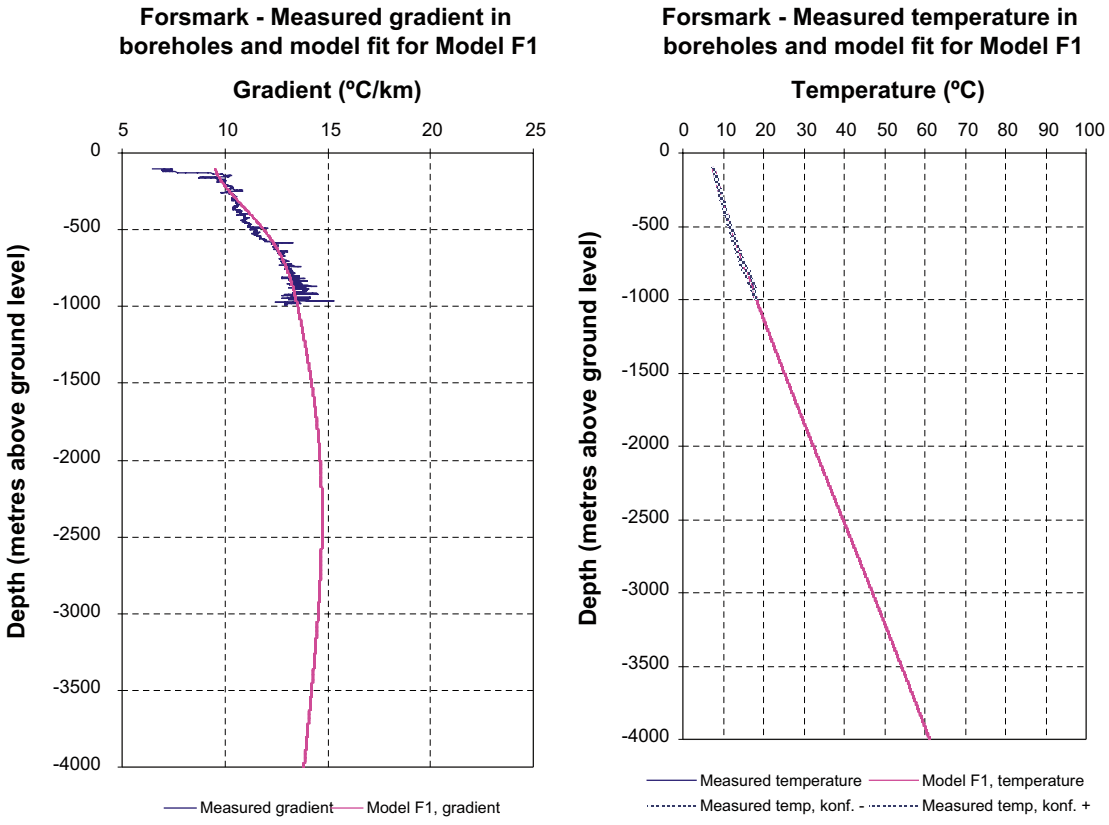

Figure A2-7. *Model F1, 4,000 meters downwards instead of 1,000 m.*

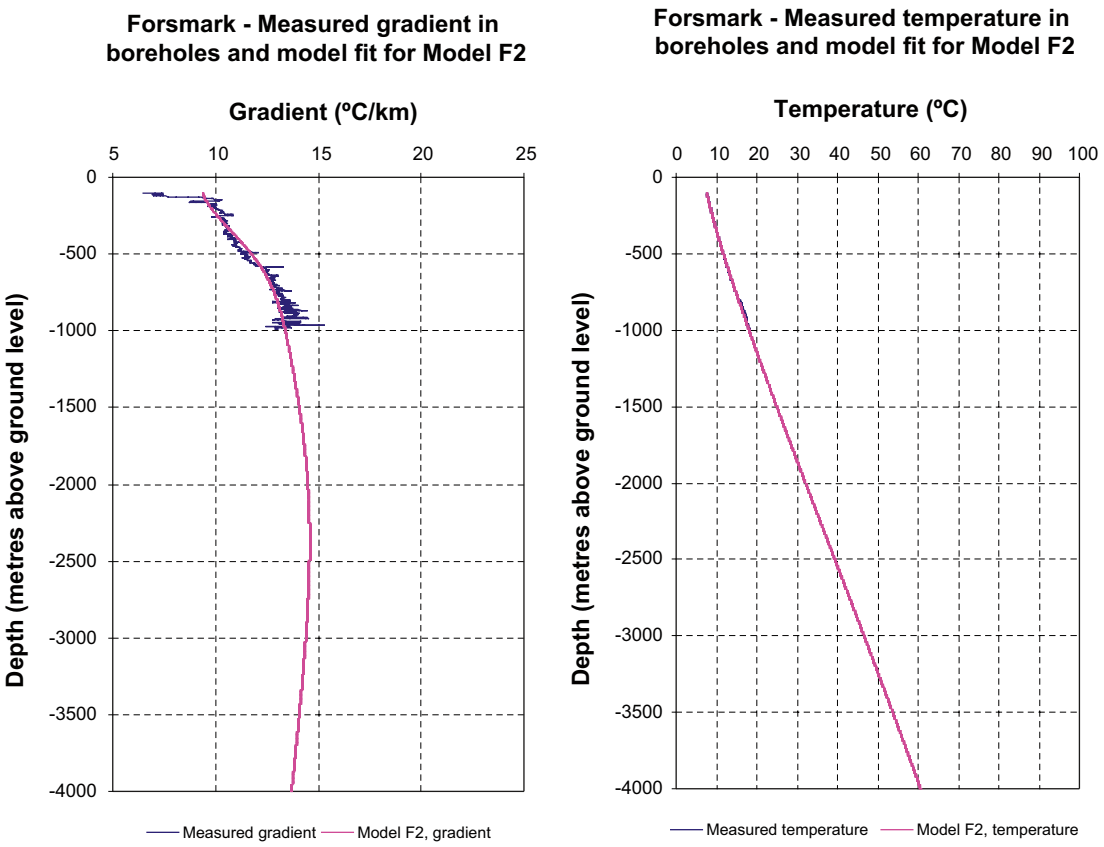

Figure A2-8. *Model F2, 4,000 meters downwards instead of 1,000 m.*

Appendix 3

Extended depth graphs – Laxemar

Here, the fitting graphs for Laxemar are presented, with the maximum depth of 4,000 meters below ground, instead of 1,000 meters as shown earlier. Please note that no confidence intervals are displayed in this section.

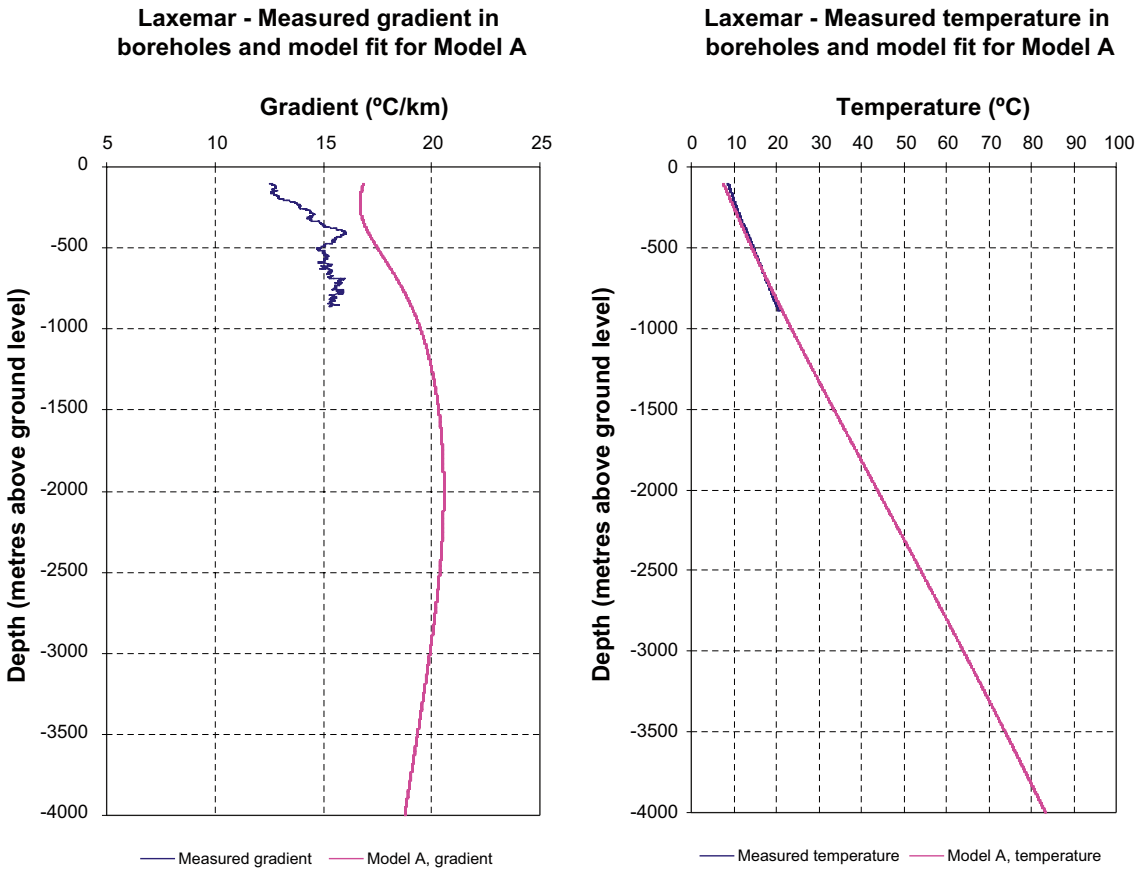

Figure A3-1. *Model A, 4,000 meters downwards instead of 1,000 m.*

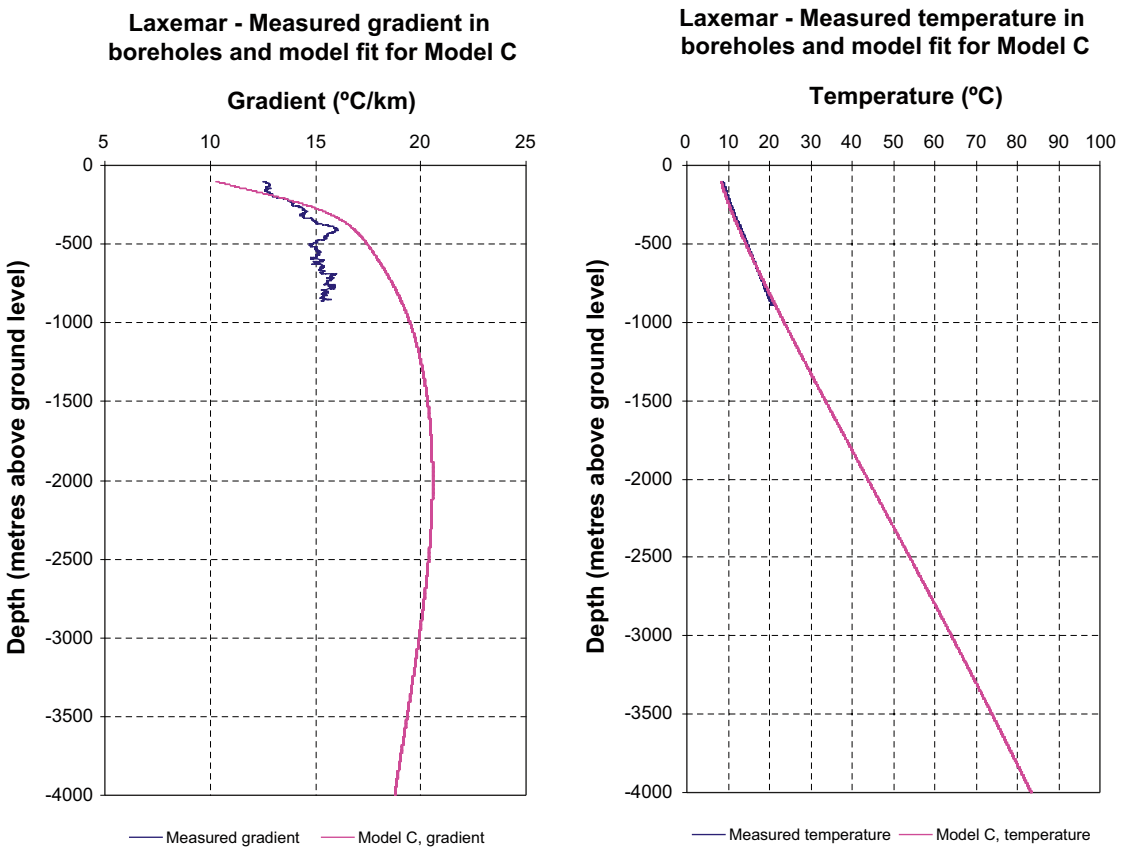

Figure A3-2. *Model C, 4,000 meters downwards instead of 1,000 m.*

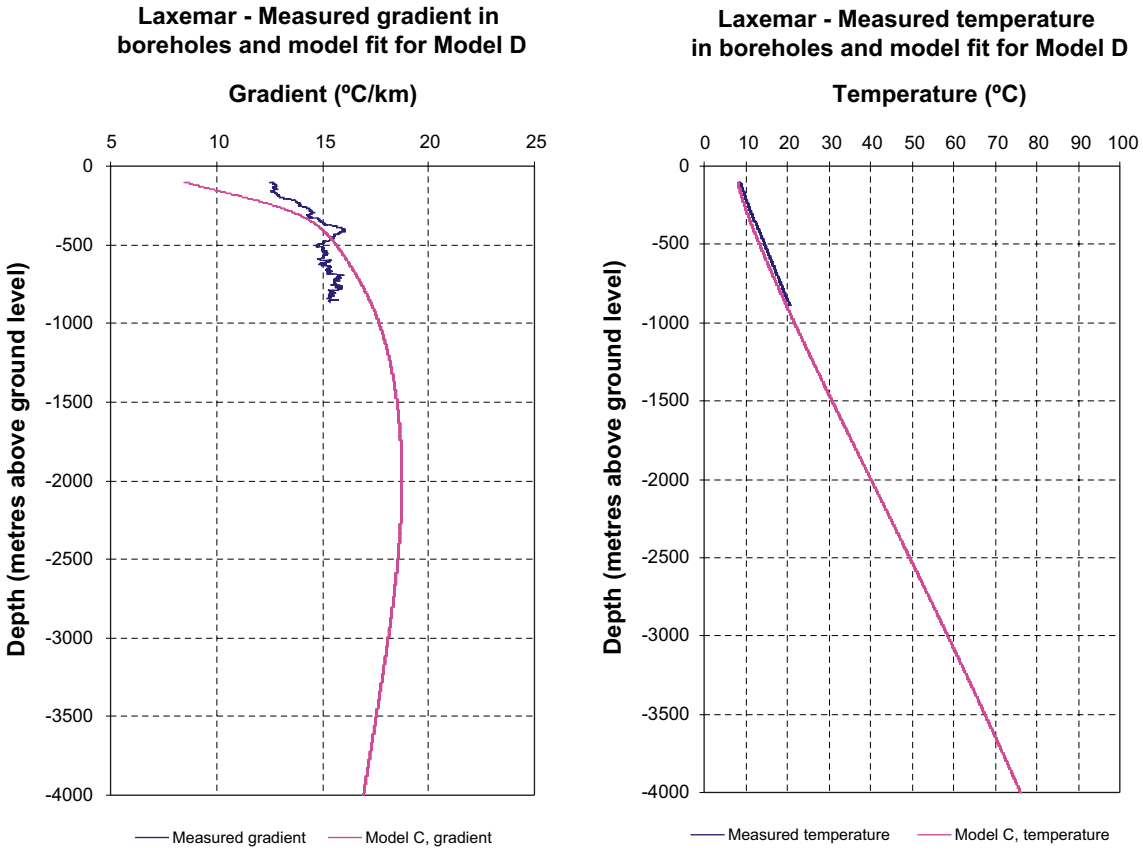

Figure A3-3. *Model D, 4,000 meters downwards instead of 1,000 m.*

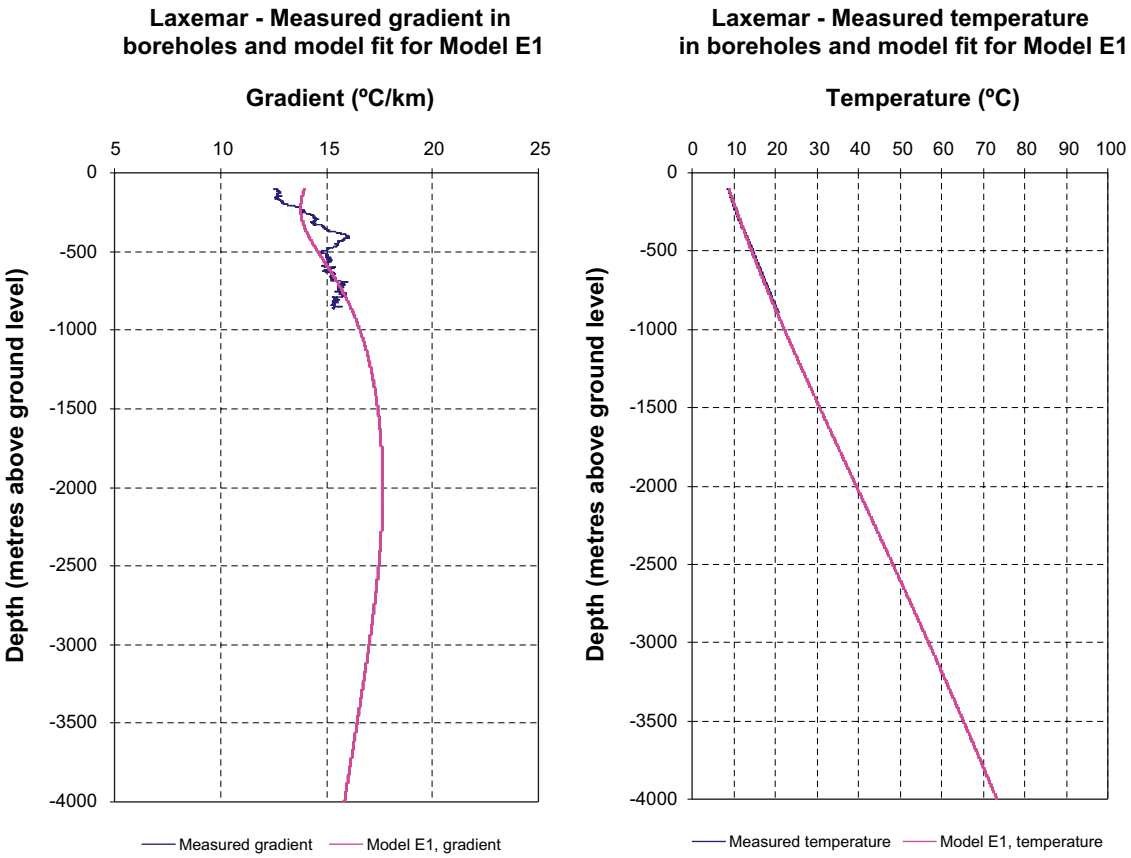

Figure A3-4. *Model E1, 4,000 meters downwards instead of 1,000 m.*

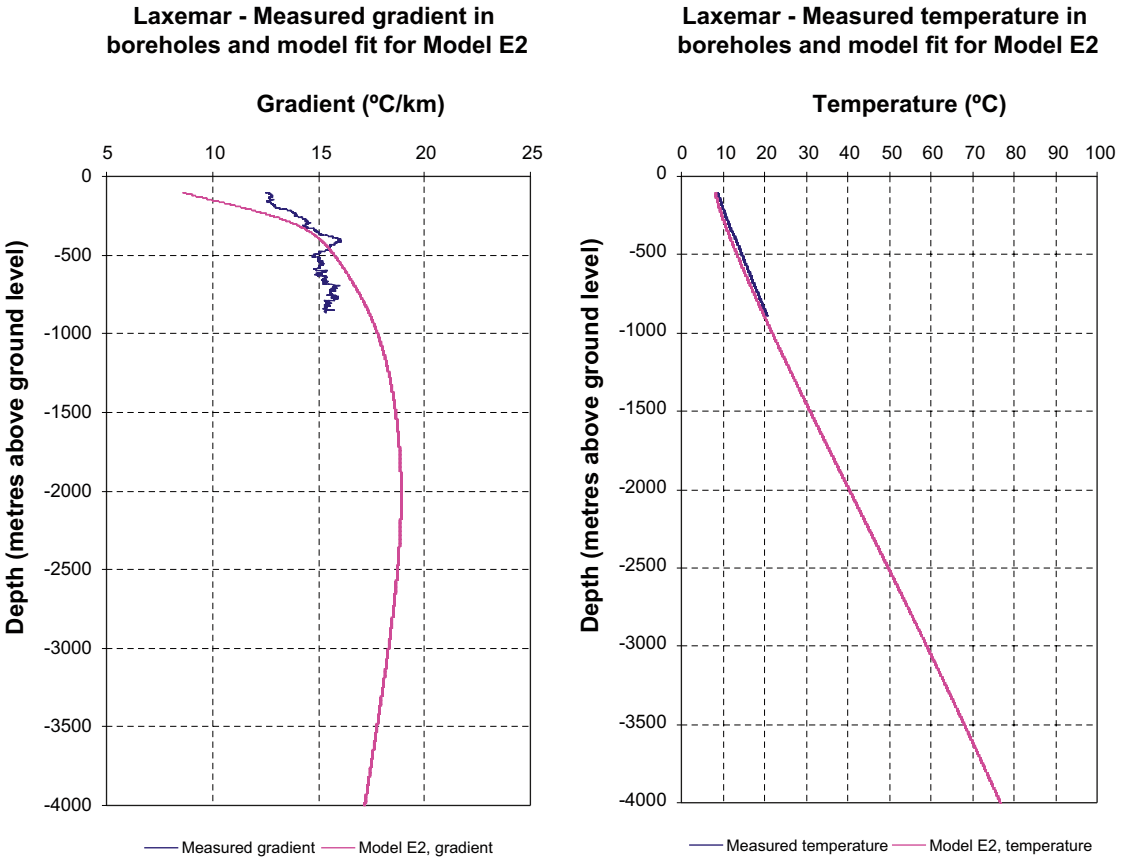

Figure A3-5. *Model E2, 4,000 meters downwards instead of 1,000 m.*

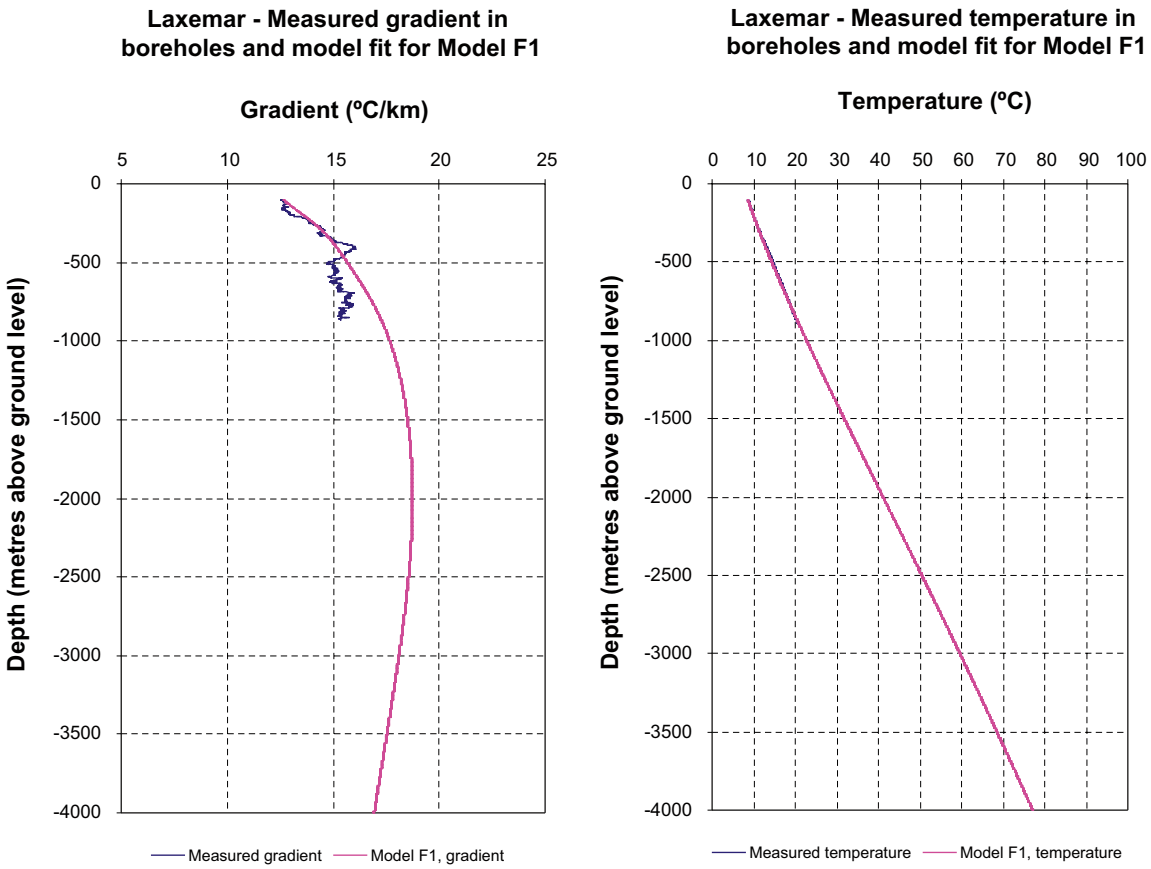

Figure A3-6. *Model F1, 4,000 meters downwards instead of 1,000 m.*

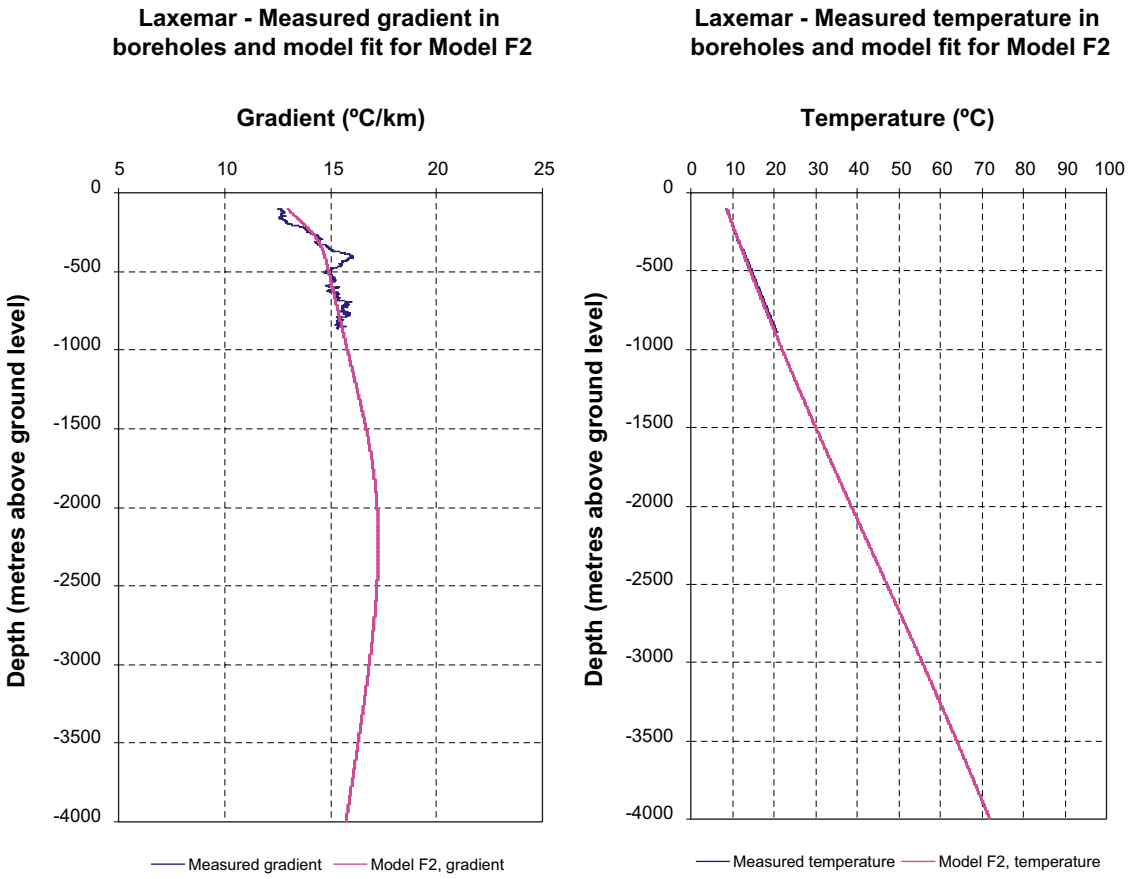

Figure A3-7. *Model F2, 4,000 meters downwards instead of 1,000 m.*

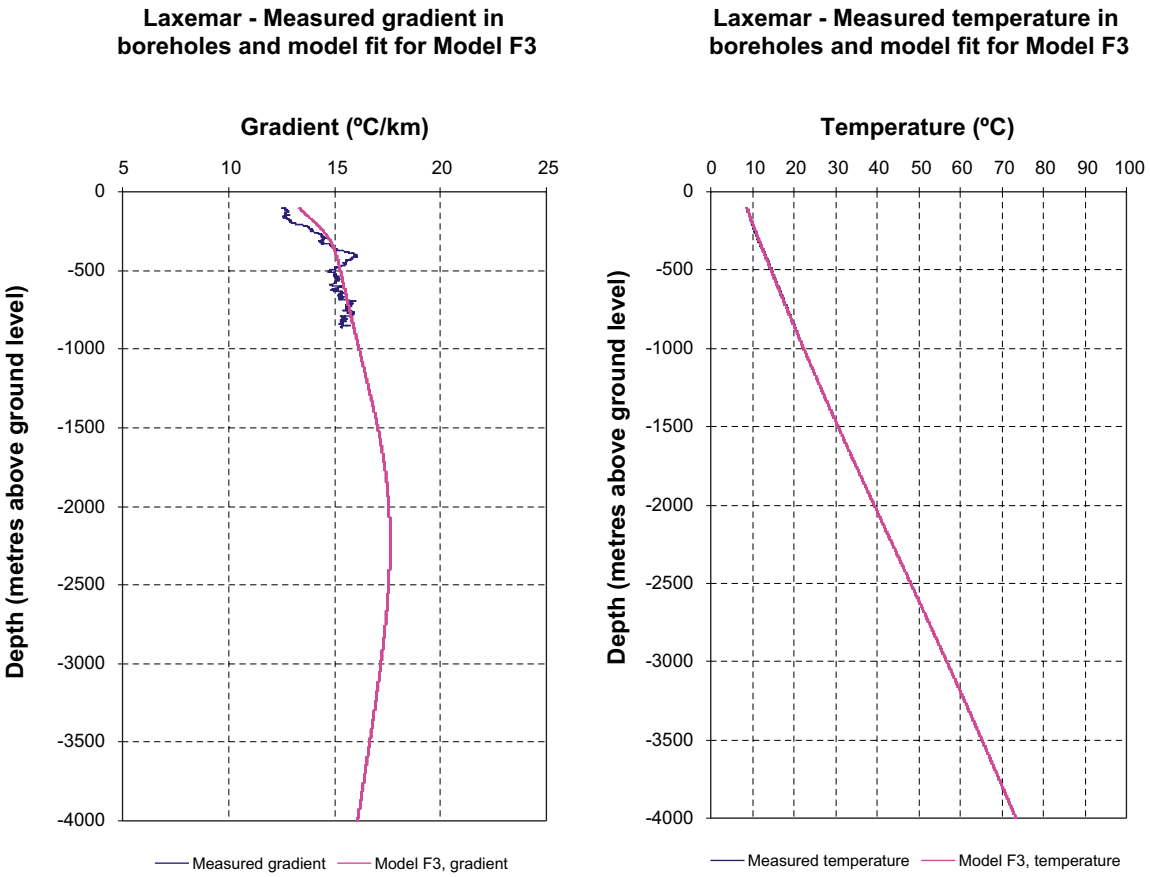

Figure A3-8. *Model F3, 4,000 meters downwards instead of 1,000 m.*

Appendix 4

Location of boreholes

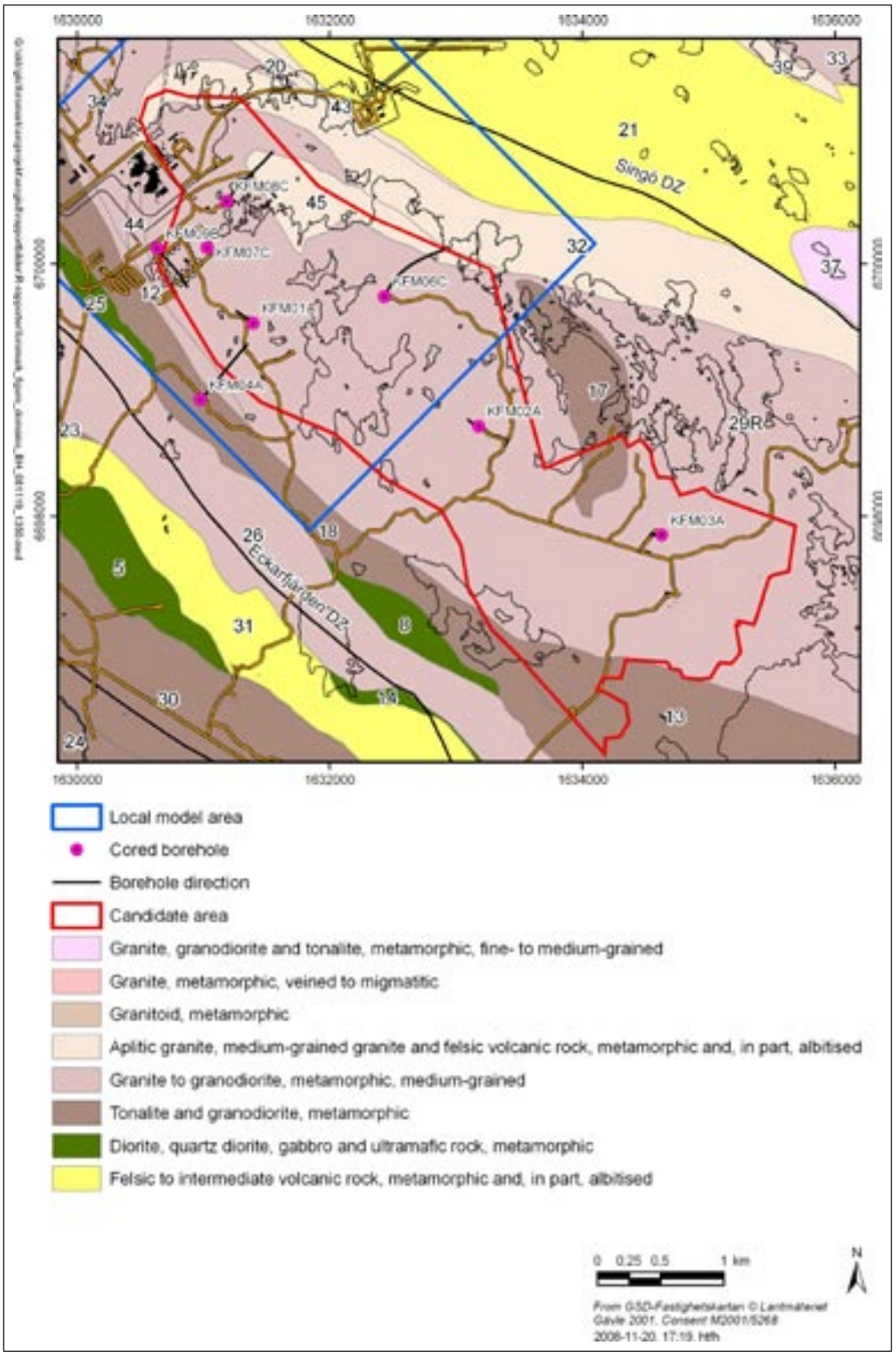

Figure A4-1. *Geological map over the Forsmark area together with approved boreholes.*

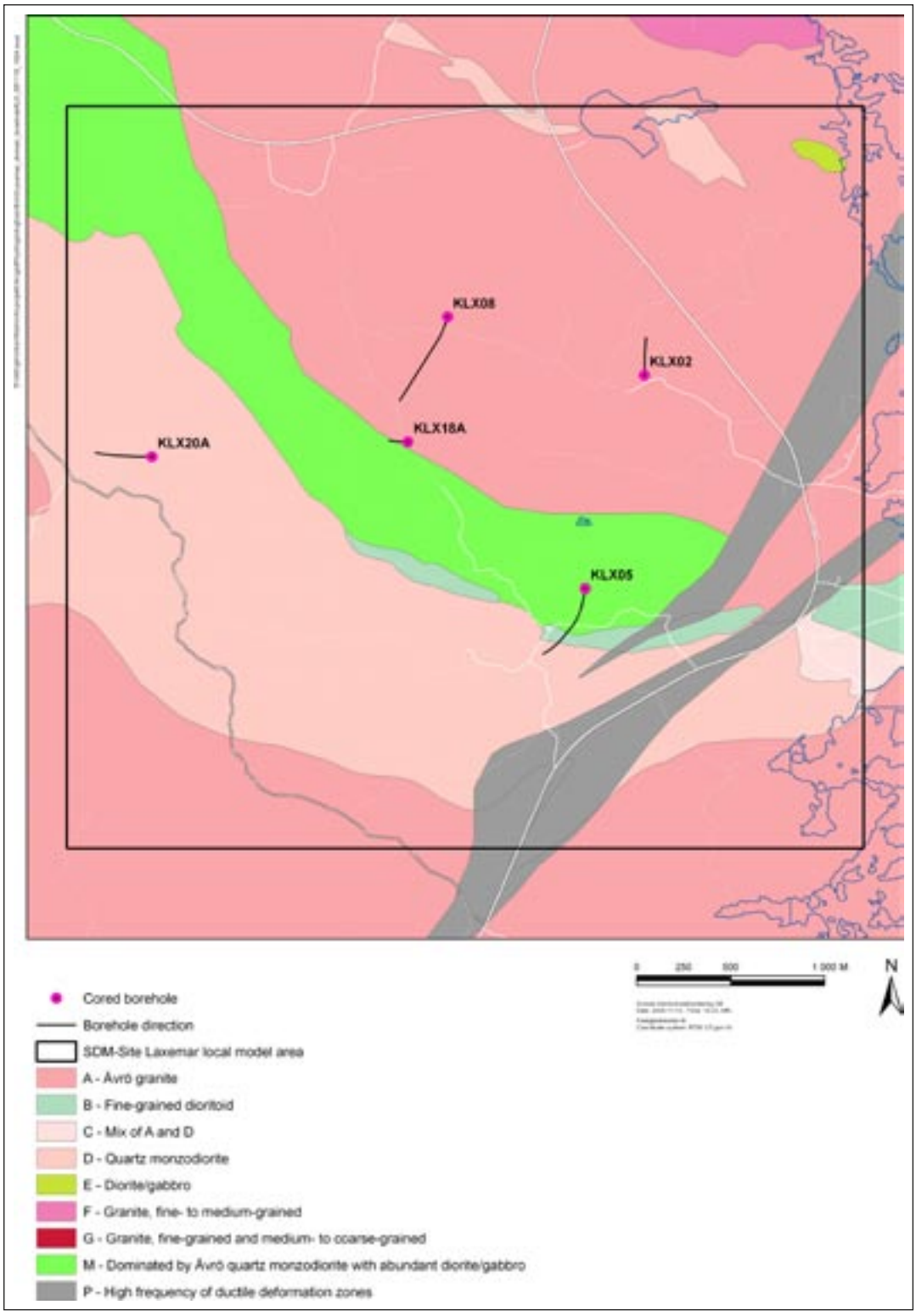

Figure A4-2. *Geological map over the Laxemar area together with approved boreholes.*

Appendix 5

Reconstruction of the Eemian period of the palaeotemperature record

During the Eemian interglacial, it is likely that both Forsmark and Laxemar were submerged by the Baltic sea due to the deglaciation of the large Saalian ice sheet. In line with this, the paleotemperature curves used as input to the permafrost simulations were adjusted to reflect this. According to /Björk et al. 2000/ the Eemian interglacial period starts at 127 kyrs BP and ends at 116 kyrs BP, resulting in an 11 kyrs long period. Other studies define the start of the Eemian at 133 and 130 kyrs BP. The length of the Eemian in the GRIP ice core is more than 15 kyrs, although with poor dating /Dansgaard et al. 1993/. It can be concluded that the length and timing of the Eemian period is uncertain.

The following steps were conducted to adjust the temperature curve:

1. The length of Eemian submerged periods was first assumed to be similar to the length in the Holocene period.
2. The same temperature as for reconstructed Holocene submerged periods (+4°C) /SKB 2006/ were used for the submerged Eemian periods.
3. The ground level temperature for the period *after* submerged conditions was set to the Eemian annual air temperatures as reconstructed for the last warm phase of the Eemian from the GRIP data (taken from /SKB 2006/), that is +8°C for Forsmark, and 8.7°C for Laxemar. The *length* of the non submerged periods was set to the same as unsubmerged periods of the reconstructed Holocene (see comment below).
4. Based on that the Saalian glaciation was more severe than the Weichselian, most probably with a thicker ice sheet, it was assumed that the sites were submerged for 1,000 year longer than in the Holocene reconstruction (10.5 kyrs in Holocene for Forsmark and 11 kyrs for Laxemar /SKB 2006/), i.e. 11.5 kyrs for Forsmark and 12 kyrs for Laxemar. The longer period of submerged conditions were placed at the start of the Eemian.

The resulting timing of the reconstructed simplified Eemian period is 129–114 kyrs BP for Laxemar and for 126.5–114 kyrs BP Forsmark. It should be noted that this is a crude reconstruction of the Eemian for the two sites, both in terms of timing, length and prevailing conditions. Nevertheless it provides a coarse estimate of the conditions at the sites during the previous interglacial period.

If comparing Forsmark and Laxemar, submerged conditions prevail in the Eemian reconstruction for a longer time at Forsmark than at Laxemar, in line with the Holocene reconstruction. In this reconstruction, the Eemian ends 2000 years later than in /Björck et al. 2000/, at 114 kyrs BP. This is due to that we have chosen to continue to use the GRIP temperature data and time scale for the unsubmerged periods ending the Eemian. There is no reason to prolong the unsubmerged periods of the Eemian since it would be difficult to say by how much, and because this would give even longer period compared to /Björck et al. 2000/.

One result of including, the very likely, submerged conditions for the main part of the Eemian interglacial is that not much of the warm Eemian temperatures are seen in the resulting ground temperature curves (Figure 5-3 and 5-4).

The Eemian reconstruction was made by Jens-Ove Näslund, SKB.

Appendix 6

Modelling of KLX02

Introduction

In the main report, concerning Laxemar, the measured reference profile stopped shortly after 870 m due to lack of data. Of all the boreholes used in the modelling, only KLX02 has thermal data down to 1,434 m below ground. Because of the uncertainty this lack of data resulted in, that deeper section remained unused.

It is however of interest to conduct a separate modelling concerning borehole KLX02 alone, in order to include a larger depth in the analysis.

Climate model

The same climate model as in the main modelling of Laxemar was used, see Figure 5-4.

Geothermal gradient and temperature

There are two sets of temperature data available concerning KLX02, one from 2003 and one from 1993. Data from 2003 spans between 0–1,023 m below ground surface. The corresponding interval for 1993 data is 200–1,434 m below ground, see Figure A6-1 (left).

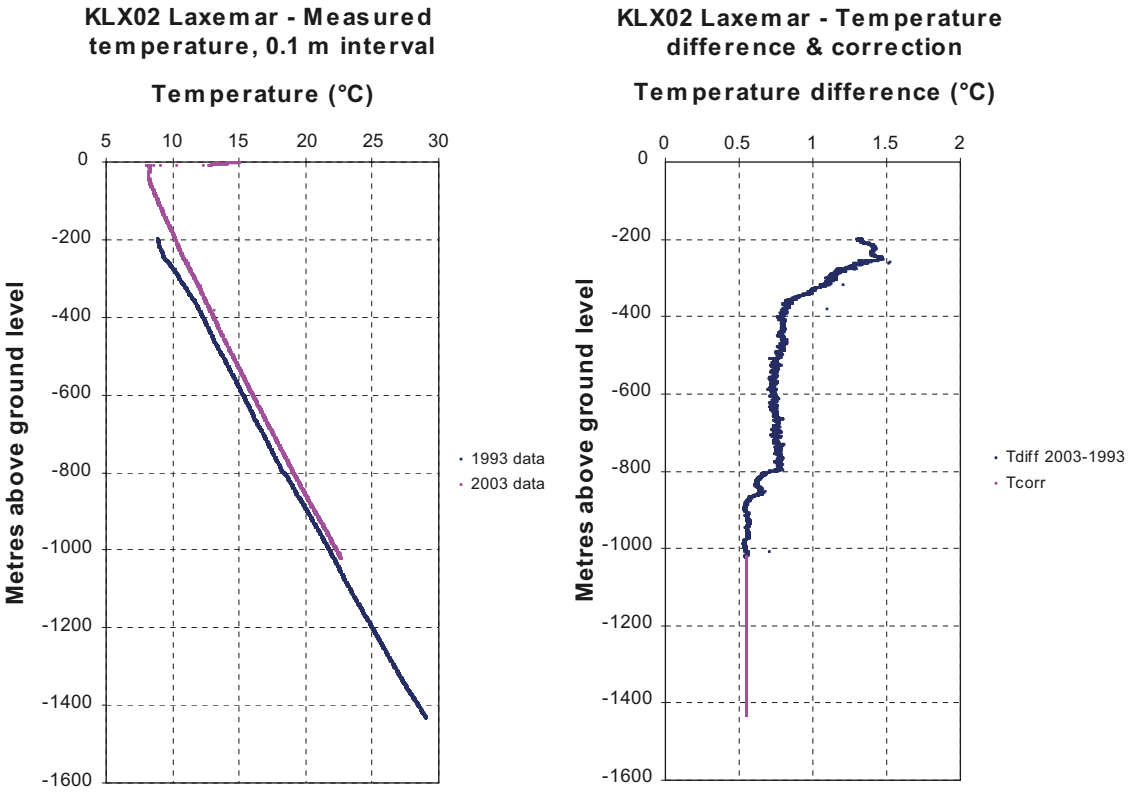

Figure A6-1. *Comparison of 1993- and 2003- temperature loggings, 0.1 m intervals (left). Temperature difference between the 2003 profile and the 1993 profile (blue line). The pink line is the average difference for the last 100 m and is the amount added to the 1993 temperature profile, 0.1 m intervals (right).*

As can be seem, there is a continuing difference in temperature between the two loggings. Data from 2003 is considered more reliable than data from 1993. In order to make best use of the data, the two loggings can be combined, using 2003 data down to 1,023 m below ground and 1993 data below that point. In order to prevent a notch in the temperature profile, the 1993 profile is displaced by 0.56°C. This number is the average difference of the two profiles for the last 100 m above 1,023 m, see Figure A6-1 (right).The resulting combined and modified temperature profile can be seen in Figure A6-2.

The temperature profile in 0.1 m intervals is transformed into 2 m intervals, as seen in the right graph in Figure A6-2. In order to let the analysis be unaffected by very recent air temperature fluctuations, the data between 0 and 252 m below ground is discarded prior to the modelling.

Concerning the gradient, there was only available 2003 data down to 1,018 m below ground. This gradient data had been calculated from 2003 temperature loggings, using Equation 2-3. By using the new combined and modified temperature profile in Figure A6-2 (0.1 m scale), calculating the gradient for the remaining depth was possible by using the least-square method.

Figure A6-3 presents the calculated gradient for KLX02 in 0.1 m intervals. The left figure is non-smoothed while the right is smoothed over a ± 48 m moving average.

The smoothed gradient profile is then transformed into 2 m intervals, see Figure A6-4.

This gradient profile is then used together with the temperature profile as a reference during the modelling.

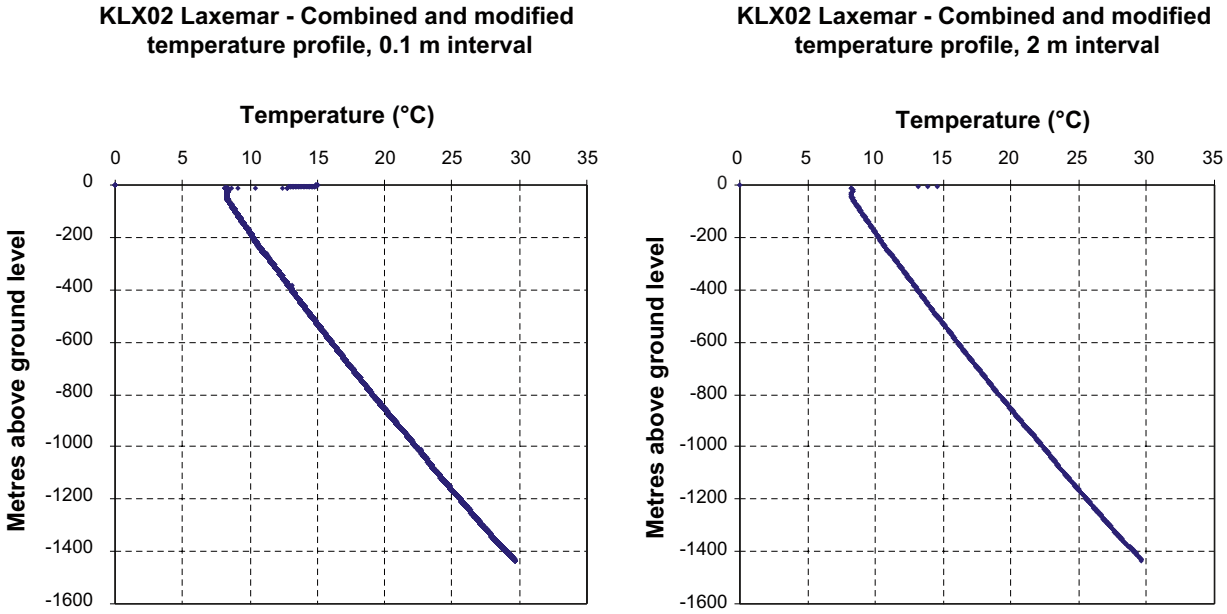

Figure A6-2. *Combined and modified temperature profile, 0.1 m intervals (left) and 2 m intervals (right).*

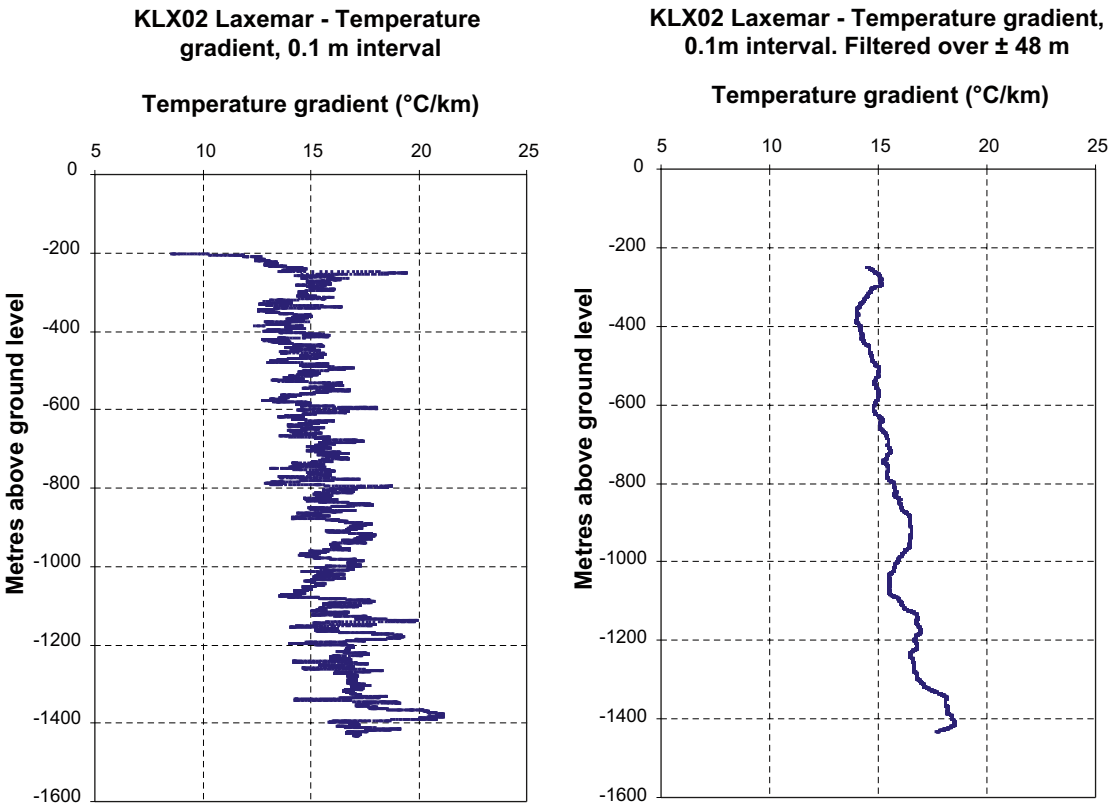

Figure A6-3. *Calculated gradient profile for KLX02 in 0.1 m intervals. Non-smoothed (left) and smoothed over a ± 48 m moving average (right).*

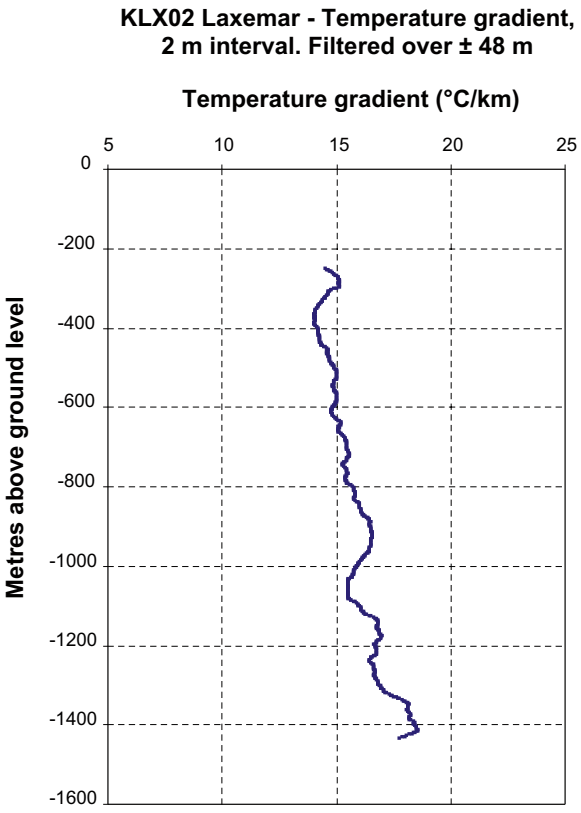

Figure A6-4. *2 m interval gradient profile for KLX02 smoothed over a ± 48 m moving average.*

Current surface temperature

The current surface temperature was extrapolated from temperature data on larger depths using a linear model. The result differed depending on the range used in the extrapolation, see Table A6-1.

The average 7.58°C was used as surface temperature in the modelling. This is 0.31°C higher than what was used in Section 7.1.2 (based on all boreholes).

Thermal conductivity, diffusivity, internal heat generation and surface heat flow

The values for thermal conductivity, heat capacity and internal heat generation was calculated from the average value for each rock code and the proportions of the latter in KLX02 using a weighted average. The thermal diffusivity was then calculated from the thermal conductivity and heat capacity. The thermal conductivity, internal heat generation, and thermal diffusivity was calculated to 2.85 W/(m·K), 2.03 μW/m^3, and 1.32 mm^2/s respectively.

The average thermal conductivity and heat capacity values for each rock code were taken from /Sundberg et al. 2008b/. Concerning that reference, it should be clarified that the values were taken from mean values listed in the histograms in Chapter 5.6.2. These values differ slightly from the values presented in Table 5-2 in the same report. This is due to the fact that the former is based on de-clustered data while the latter is not. Since no values for rock code 501061 were available, values for 511058 were used.

The adjustment for anisotropy was then applied. The thermal conductivity and diffusivity in the vertical direction was decreased due to the anisotropy with approximately 3%, see Appendix 6.1. The vertical components of thermal conductivity and thermal diffusivity were thus 2.76 W/(m·K) and 1.28 mm^2/s respectively after adjustments for anisotropy.

The heat generation values for each rock type were taken from Table 7-3. This table does not present any values for rock code 501046 and 501056. This is because they both originate from rock code 501044, which was subdivided into these two rock codes. Therefore, the heat generation value for 501044 has been used for both 501046 and 5101056.

The start value on the surface heat flow was chosen to 58 mW/m^2.

Model calculations

The purpose of the model calculations is to study the effects of closer specifications concerning data from site models, and effects from changes in climate. Table A6-2 presents the input data to the different model and Figure A6-5 clarifies the time periods.

Model 1 represents the input values listed in the previous section.

Model 2 experiments with a lowered surface heat flow from 58 to 56 mW/m^2.

In Model 3, the temperature of the whole climate data curve (except T2) is raised 1.88°C, i.e. the difference between the current ground temperature for Laxemar in /SKB 2006/ and the extrapolated current surface temperature used in Model 1 and 2. The heat flow is adjusted to 54 mW/m^2.

Table A6-1. Extrapolated current ground surface temperature – Sensitivity to extrapolation range.

	Extrapolated surface temperature (T_2), °C		
	202–102m	252–102m	302–102m
KLX02	7.58	7.60	7.54

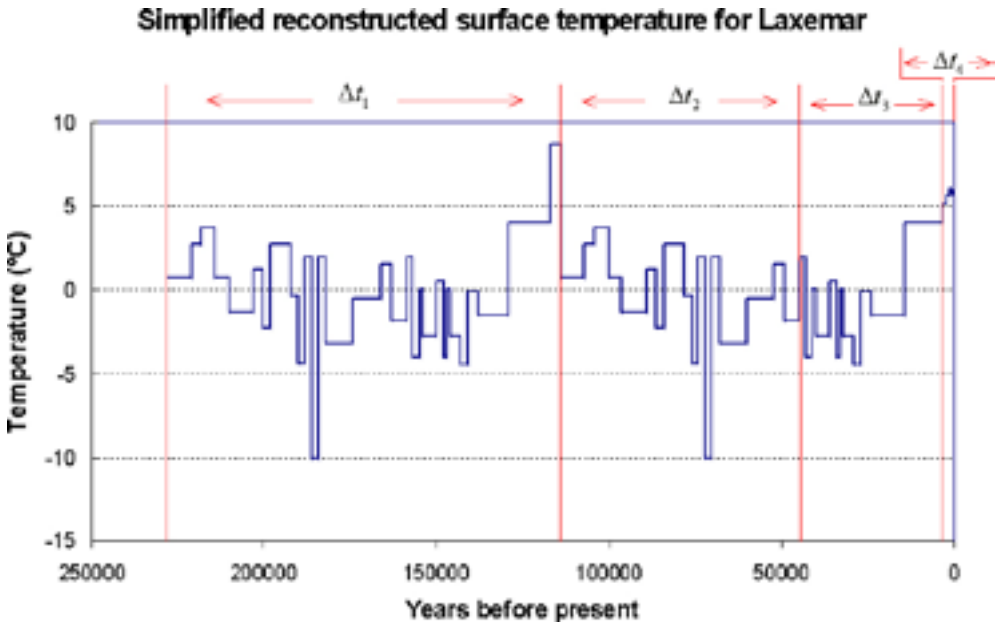

Figure A6-5. *Clarification of the time periods Δt_1, Δt_2, Δt_3, and Δt_4 corresponding to ΔT_1, ΔT_2, ΔT_3, and ΔT_4.*

Table A6-2. Parameters for the models at Laxemar KLX02. Data used for the model calculations for KLX02. κ = thermal diffusivity, λ = thermal conductivity, Q_0 = heat flow at ground level, A = radiogenic heat production, T_0 = ground temperature 228 kyrs BP, T_1 = ground temperature 14–3.1 kyrs BP, T_2 = ground temperature 300–0 yrs BP, ΔT_1 = ground temperature change 228–114 kyrs BP, ΔT_2 = ground temperature change 114–44.5 kyrs BP, ΔT_3 = ground temperature change 44.5–3.1 kyrs BP, ΔT_4= ground temperature change 3,100–300 yrs BP.

Model	κ [mm²/s]	λ [W/(m·K)]	Q_0 [mW/m²]	A [μW/m³]	T_0 [°C]	T_1 [°C]	T_2 [°C]	ΔT_1 [°C]	ΔT_2 [°C]	ΔT_3 [°C]	ΔT_4 [°C]
1	1.28	2.76	58	2.03	0.7	4	7.58	0	0	0	0
2	1.28	2.76	56	2.03	0.7	4	7.58	0	0	0	0
3	1.28	2.76	54	2.03	2.58	5.88	7.58	1.88	1.88	1.88	1.88

Table A6-3 presents curve fitting statistics for the models. An explanation to r^2 and RMSD can be found in the corresponding section for Forsmark (6.2.2).

Model 2 and 3 have the factor in common that they both experiment with changes of heat flow. Figure A6-9 below present how RMSD is affected by changes in heat flow for these models.

Neither Model 1 nor 2 results in very good fits to measured data. The best result was obtained from Model 3, which uses a heat flow of 54 mW/m².

Table A6-3. Results for the models at Laxemar KLX02. Model fit of gradient and temperature to measurements.

Model	Model fit of gradient		Model fit of temperature	
	r^2	RMSD [°C/km]	r^2	RMSD [°C/km]
1	0.664275	1.47	0.999857	0.882
2	0.664275	1.016	0.999823	1.366
3	0.78564	0.594	0.999884	0.111

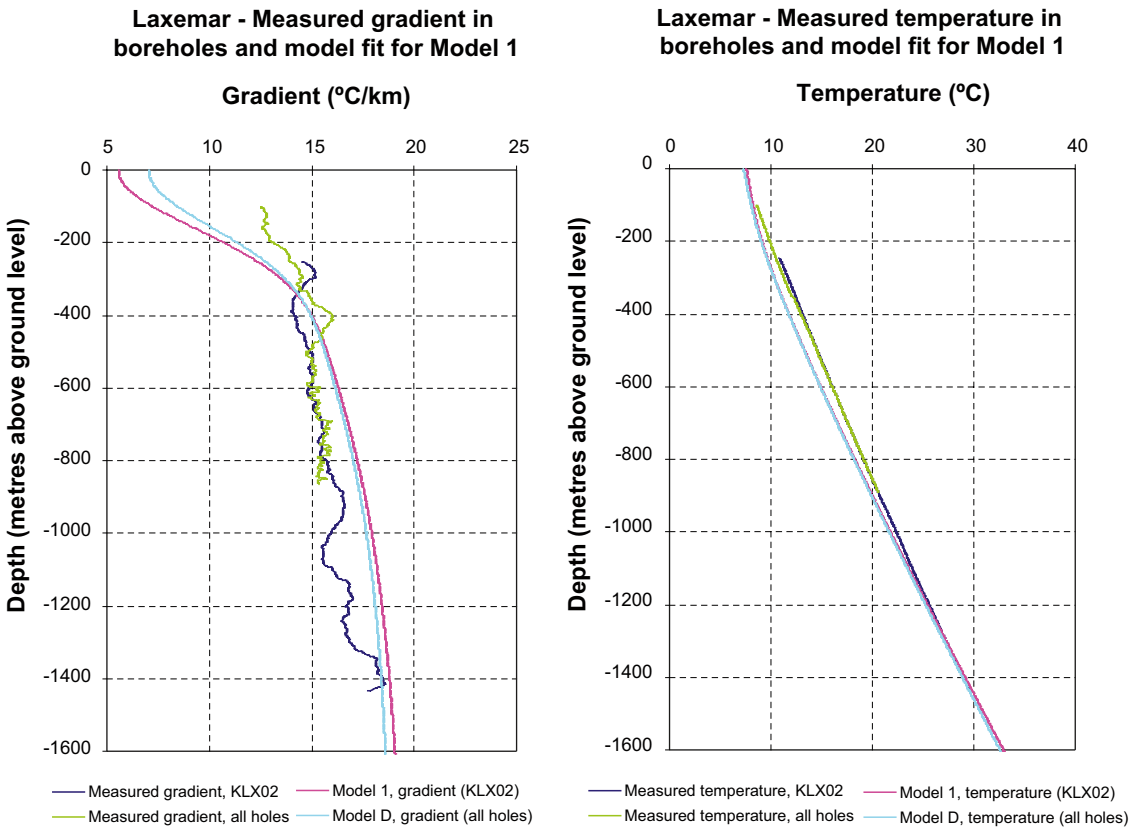

Figure A6-6. *Comparison between Model 1 and measurements: temperature gradient (left) and temperature (right). The measured profiles from all holes and Model D are also displayed.*

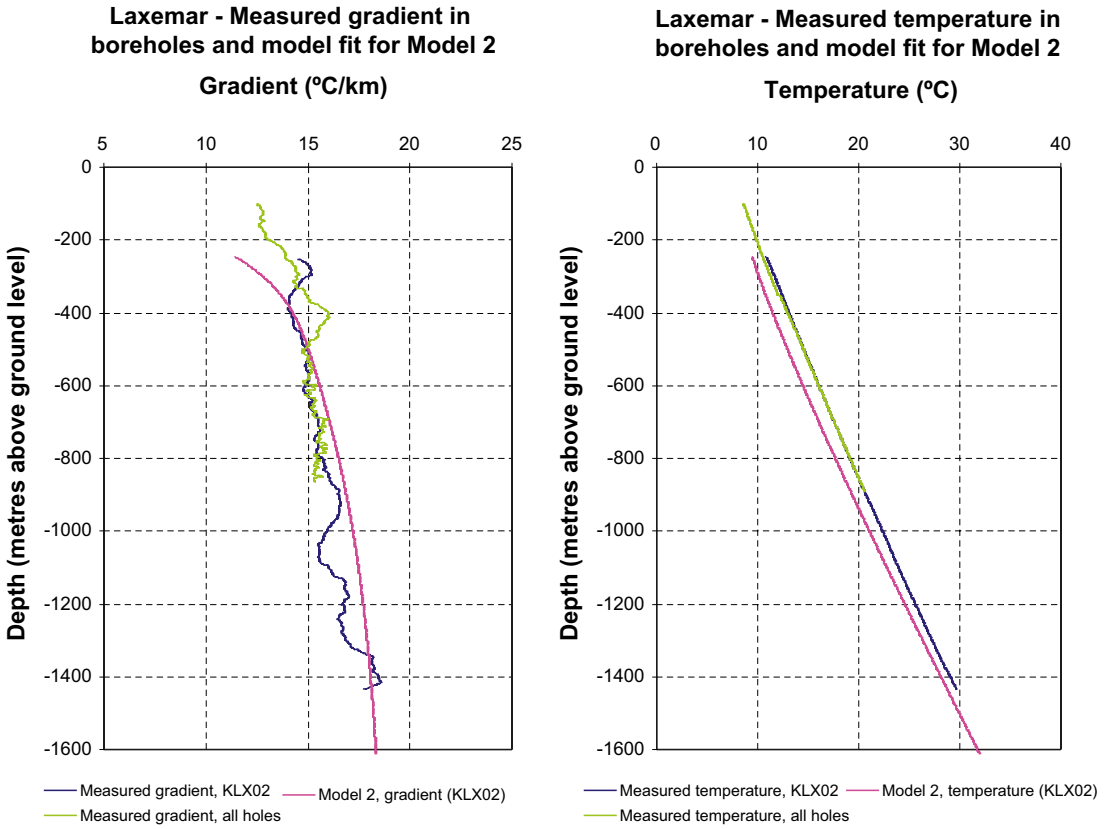

Figure A6-7. *Comparison between Model 2 and measurements: temperature gradient (left) and temperature (right). The measured profiles from all holes are also displayed.*

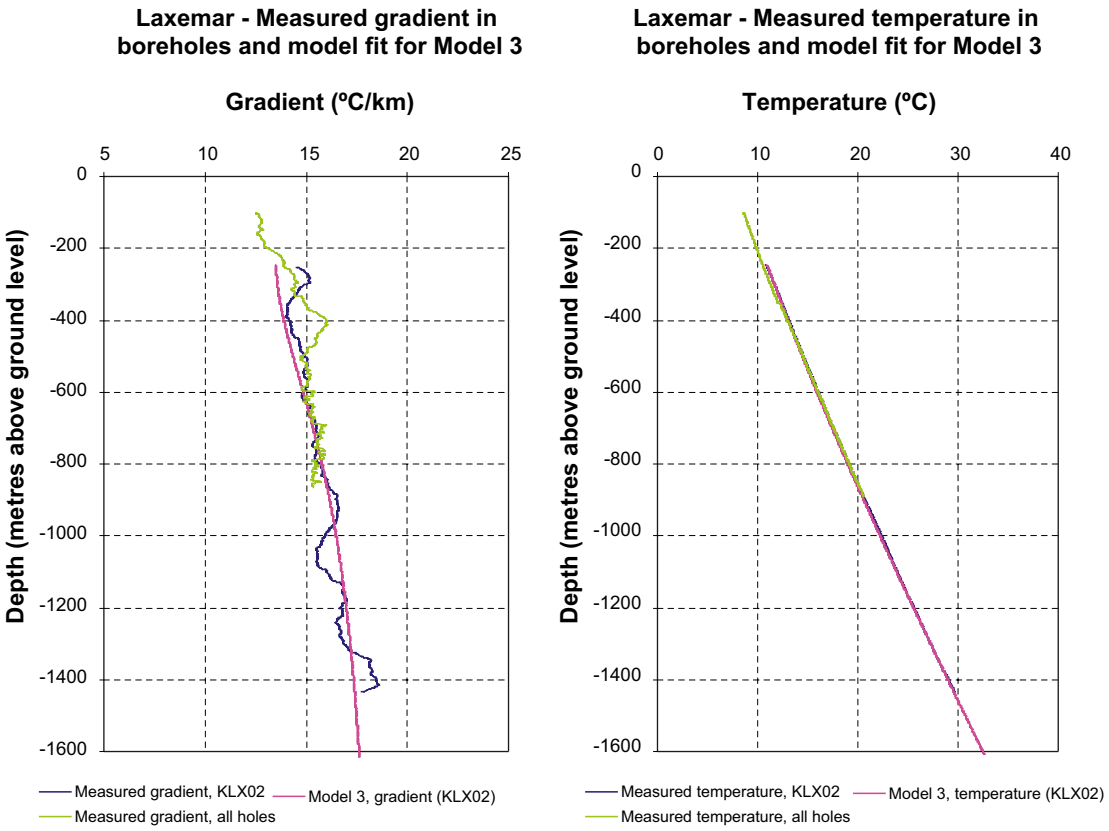

Figure A6-8. *Comparison between Model 3 and measurements: temperature gradient (left) and temperature (right). The measured profiles from all holes are also displayed.*

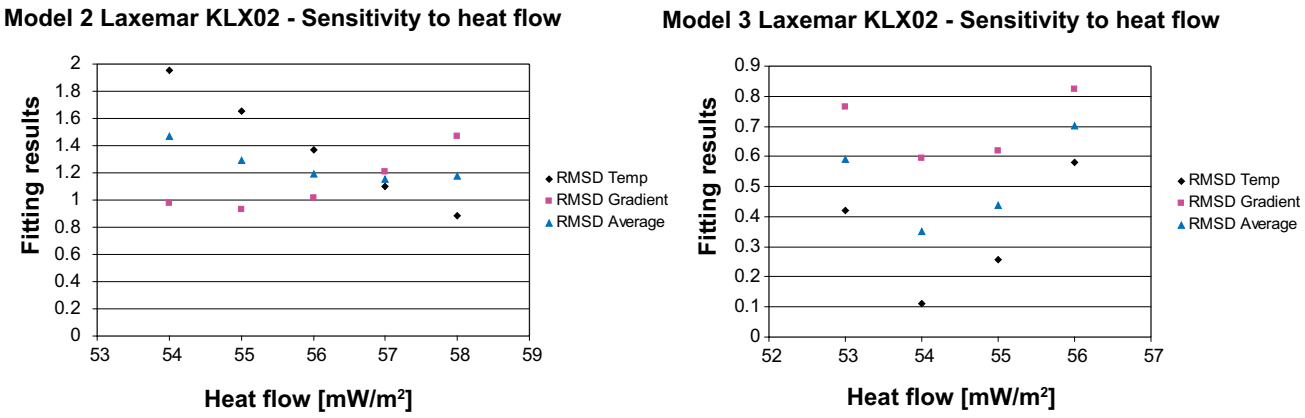

Figure A6-9. *Heat flow impact on RMSD for Model 2 and 3. The RMSD average represents an average between the two other RMSD values.*

Conclusions

General conclusions

- The best fit to measured data considering this borehole alone was obtained with a heat flow of 54 mW/m^2.
- The dip of the foliation plane is based on very few measurements and is therefore uncertain. Also the local anisotropy factor is uncertain. These uncertainties are transferred to the calculation of the thermal conductivity in the vertical direction, which in turn is strongly related to the calculation of the heat flow.
- The current ground surface temperature extrapolated from KLX02 temperature loggings is 7.58°C, i.e. 0.31°C higher than in the overall Laxemar simulations, and nothing in the modelling suggests another value.
- After examining local KLX02 data, both concerning rock type distribution and the dip of foliation plane, the thermal conductivity and diffusivity for KLX02 was increased with 0.4% and 2.4% respectively in comparison to the overall Laxemar simulations.
- Heat generation was lowered from 3 µW/m^3 in the overall Laxemar simulations to 2 µW/m^3 in the KLX02 specific modelling.

Model conclusions

- Model 1 does not fit very well to measured data, neither temperature nor gradient. The modelled temperature profile deviates from the measured profile. The deviation ranges from –1.4°C (around 400 m depth) to +0.1°C (around 1,100 m depth).
- Model 2 experiments with a lowered heat flow, the gradient fit is slightly better than before, the temperature fit is far worse.
- Model 3 modifies the climate data by increasing the whole climate history curve except the current temperature by 1.88°C. This is equal to the difference between the current ground temperature for Laxemar in /SKB 2006/ and the extrapolated current surface temperature used in Model 1 and 2. It also adjusts the heat flow to 54 mW/m^2. This results in a very good fit for the gradient and especially for the temperature.

Model 3 clearly resulted in the best fit to measured data. Raising the whole climate curve (except T_2) with the difference between the current ground temperature for Laxemar in /SKB 2006/ and the extrapolated current surface temperature used in Model and adjusting the heat flow top 54 mW/m^2 proved to be a good choice.

APPENDIX 6.1 Calculation of impact from anisotropy in the vertical direction

Because of the anisotropy, the thermal conductivity is higher parallel to the foliation than perpendicular to it. It is thus possible to calculate the impact from anisotropy on the thermal conductivity and diffusivity in the vertical direction if the anisotropy factor and the dip of the foliation plane can be approximated.

The anisotropy factor is approximated to 1.15 /Sundberg et al. 2008b/, i.e. the thermal conductivity is 15% higher in the direction parallel to the foliation plane than perpendicular to it.

Only two separate measurements regarding the dip of the foliation plane have been conducted in the KLX02 surroundings (15° and 40° /Boremap data in SICADA database/). While the uncertainty thus can be concluded to be large, a dip of 30° was decided to be used in the calculations.

According to /Kappelmeyer and Haenel 1974/, the thermal conductivity in the direction of an optional angle α with respect to an anisotropy plane, is:

$$\lambda_{optional} = \lambda_{par} \cdot \cos^2(\alpha) + \lambda_{per} \cdot \sin^2(\alpha) \qquad \text{Equation A6.1-1}$$

where

λ_{per} Thermal conductivity perpendicular to the anisotropy plane

λ_{par} Thermal conductivity parallel to the anisotropy plane

$\lambda_{par} = 1.15 \cdot \lambda_{per}$

It is assumed that the thermal conductivity measurements are taken in random directions and thus can be seen as the geometric mean between the thermal conductivity parallel and perpendicular to the foliation plane.

Thus

$$\lambda_m = (\lambda_{par} \cdot \lambda_{per})^{0.5} = (1.15\lambda_{per} \cdot \lambda_{per})^{0.5} = 1.15^{0.5}\, \lambda_{per} \qquad \text{Equation A6.1-2}$$

where

λ_m Measured thermal conductivity

This implicates that

$\lambda_{per} = (1.15)^{-0.5}\lambda_m = 0.933\, \lambda_m$

$\lambda_{par} = 1.15\lambda_{per} = 1.15 \cdot (1.15)^{-0.5}\lambda_m = 1.072 \cdot \lambda_m$

Since the angle between a vertical plane and the foliation plane is 60° (90°–30°), the vertical thermal conductivity component λ_v due to anisotropy can then be calculated:

$\lambda_v = \lambda_{par} \cdot \cos^2(60°) + \lambda_{per} \cdot \sin^2(60°) \Rightarrow$

$\lambda_v = 0.967\, \lambda_m$

It can thereby be concluded that the thermal conductivity (and diffusivity) in the vertical direction is approximately 3.3% lower than the measured. However, the uncertainty both related to the dip and the local anisotropy factor is large.

ISSN 1404-0344
CM Gruppen AB, Bromma, 2009